Use of the cyanobacterial lectin, microvirin-N, for specific detection of the tuberculosis biomarker mannose-capped lipoarabinomannan

By

Megan van der Horst

Dissertation

Submitted to the Faculty of the

Graduate School of Vanderbilt University

In partial fulfilment of the requirements

for the degree of

DOCTOR OF PHILOSOPHY

in

Chemistry

August 13, 2021

Nashville, Tennessee

Approved:

David W. Wright, PhD

Brian O. Bachmann, PhD

David E. Cliffel, PhD

Mark R. Denison, PhD

Copyright © 2021 by Megan van der Horst
All Rights Reserved

Acknowledgements

A simple “thank you” cannot describe how grateful I am for all the help and encouragement I have received in my journey to this point. I would not be where I am today without the many amazing people who have supported me.

First and foremost, I must thank Dr. David Wright. Early in my career at Vanderbilt, David told me, “You learn by doing, not by reading.” This advice may have led some bad experiments, but I can honestly say I learned from each of them. David, thank you for allowing me the freedom to fail and to learn from my mistakes. In your lab, I’ve learned to think critically and independently, but I’m so grateful to have had you as a sounding board when I need one. Lastly, thank you for allowing me to pursue experience outside of the lab during my time in graduate school. My internships have helped me so much, and I am grateful to have a mentor who understood their importance. Thank you also to my committee members, Dr. Brian Bachmann, Dr. David Cliffel, and Dr. Mark Denison, who have provided essential guidance throughout my time at Vanderbilt.

To my fellow lab members, thank you for guiding me and listening to me. To Dr. Carson Moore, I owe you everything. Graduate school would have been so much worse without you by my side. I don’t know what I would have done without your scientific knowledge, editing skills, and sulfuric acid ;). But more importantly, I don’t know what I would have done without your friendship and generosity. Now I just need to convince you to move to Washington D.C.! To Dr. Andrew Kantor, thank you for your thoughtful consideration of my project. It wasn’t always easier being the only TB researcher in the lab, but you always took the time to understand the science behind

my project to offer the best guidance. Also, thank you for helping me look on the bright side and find the best in other people. Your kindness inspires me to be a better person. To Dr. Jenna DeSousa, I am so glad you joined our lab. Your dedication is inspiring and your sense of humour makes every day more fun. To Micaella and Kelly, good luck with everything and know I always be just a text away.

I owe so much to the past Wright lab members and Haselton lab members, as well. Wes, thank you for teaching me everything I know. I'm honestly not sure I would even be able to pipette without your mentorship. Lesh, thank you for everything. Technically, you aren't a Wright lab member but you've helped me so much, that you should be. You taught me how to write a scientific paper and have always been there when I have a question, even when I ask the same question over and over again ;). Christine, thank you for your all your guidance and support. In particular, thank you for all you recent and past help with statistics. Mindy, thank you for teaching me PCR and helping me troubleshoot whenever it didn't work. Nick, thank you for helping me brainstorm ideas and for helping me waste time by talking about running ;). Stephanie, thank you for all your help expressing and characterizing MVN. I can't wait to see how your project turns out. Dalton, thank you so much the OB-ELISA video and for calming me down when I was fully panicking about graduation. I know you are going to be so successful. Megan, thank you for your experimental guidance and positivity when nothing seemed to be working. Lastly, Rick, thank you for being a second mentor to me by sharing your lab space and wisdom with me.

I am so grateful for my internship mentors, as well. Sindy, I'm so thankful for everything you've taught me so much, all the opportunities you've given me, and for always making time for me in your busy schedule. You've helped me discover my

passion for making science more inclusive and I am so excited to continue this work. Denise, thank you for all your guidance and support. I must also thank my international collaborators who are continuing this work: Dr. Emmanuel Moreau and the rest of the FIND team, Dr. Jonathan Blackburn and Dr. Fezile Khumalo at the University of Cape Town, and the entire RePort-Brazil team. I am so excited to see your results!

I am so so so grateful for my family and friends. Taylor, I still can't believe how lucky I am to have met you. If I listed every thank you, it would be longer than my dissertation. So, I'll simply say thank you for it all, but especially for always bring me dessert. I'm so excited to start this new adventure with you by my side! To my mom, dad, and sister, thank you all for your constant love and support. I am so lucky to have such am amazing family around me, and I can't wait for us all to be together again. My cats can't read, but I owe them a thank you, as well. Roxi, thank you for waking up every morning excited to see me. Callie, thank you for keeping me company while I worked from home this year.

I was so lucky to make many wonderful friends in Nashville. Lauren, thank you taking a chance and living with me, it was a lot of fun. Katya, thank you for being my first non-graduate school friend. I'm so grateful for all our fun times. Also, thank you for showing me the importance of having my nails done ;). Chris, thank you for all the hours we've spent running together and talking about everything from science to life. If you read this, I promise to do the Marine Corps 50K with you! Jenna, thank you for being my entire pandemic pod. I'm so grateful for your friendship and advice, as well as your dessert and cocktail knowledge. Thank you to the rest of my running friends, as well: Alex, Joanna, Joey, Megan, Nicole, and so many more. I was extremely fortunate to have one of my best friends from college move to Nashville for a year –

Sara, thank you for inspiring me to go after what I deserve in every area of my life. Lastly, I am so grateful to the rest of my friends who have given me their support long-distance: Brian, Calvin, Hannah, Ivy, Jess, and Tricia.

Table of Contents

Page

Acknowledgements iii

List of Tables x

List of Figures xi

List of Abbreviations xv

Chapter

I. **The tuberculosis diagnostic landscape** 1

TB is a public health crisis 1

Diagnostic tests for TB 3

LAM in urine 6

The structure of LAM 9

First-generation ManLAM detection tests 11

Second-generation ManLAM detection tests 13

Microvirin-N 15

Scope of this work 17

II. **Microvirin-N is a novel molecular recognition element for the tuberculosis biomarker lipoarabinomannan** 19

Introduction 19

Materials and Methods 22

Expression and purification of MVN 22

Bioconjugation procedures 23

Binding characterization of molecular recognition elements by BLI 24

Binding pair evaluation by BLI 26

Stability test of MVN by BLI 27

Results 27

Discussion 32

Conclusions 35

Acknowledgements 36

III. Development of a specific lipoarabinomannan detection assay using microvirin-N 37
Introduction 37
Materials and Methods 38
Bioconjugation procedures 38
MVN-based plate ELISA 39
OB-ELISA 40
Alere LFAs 43
Antibody-based plate ELISA 43
Results 44
Discussion 58
Conclusions 63
Acknowledgements 63
IV. Detection of the lipoarabinomannan mannose capping motif in clinical urine with microvirin-N 65
Introduction 65
Materials and Methods 67
Clinical subjects and samples 67
Urine sample preparation and testing 69
Statistical analysis 70
Results 71
Discussion 79
Future Work 83
Conclusions 89
Acknowledgements 90

Appendix

I. **Progress toward development of a low-resource diagnostic test for multidrug-resistant tuberculosis** 91
Introduction 91
Materials and Methods 96
Silica condensation reactions 96

Sulfo-SMCC conjugation with NMR quantification 96
Oligonucleotides 97
Ligation and PCR reactions 98
Results 98
Discussion 110
Conclusions 113
Acknowledgements 115

References 115

List of Tables

Table		Page
1.	Cascade of care analyses for TB in India and South Africa	3
2.	Diagnostic tests for TB	6
3.	Binding epitopes of antibodies that target the mannose cap	15
4.	Binding epitopes of anti-LAM antibodies	21
5.	Dissociation constants of MVN and anti-LAM antibodies to *M. tb* ManLAM, *M. leprae* ManLAM, and *M. smegmatis* PILAM	29
6.	Study population characteristics by TB- and HIV-status	68
7.	Mann Whitney test p values for TB-positive samples versus TB-negative samples	76
8.	OB-ELISA diagnostic performance	79
9.	Oligonucleotide sequences	97
10.	Conjugation of sulfo-SMCC linker to G4 polyamidoamine dendrimers	100
11.	Cycle threshold values for the validation of the oligonucleotide ligation and PCR system	104

List of Figures

Figure		Page
1.	Three potential hypotheses for the origin of urinary ManLAM	8
2.	Depiction of ManLAM, PILAM, and AraLAM	10
3.	Size of MVN in comparison to streptavidin and immunoglobulin	16
4.	PyMOL rendering of the resolved crystal structure for MVN bound to the Manα-(1,2)-Man structure	20
5.	BLI workflow	26
6.	BLI binding curve showing that MVN binds to ManLAM	28
7.	Formation of an orthogonal ManLAM binding pair with MVN and the anti-LAM antibody Ab28	30
8.	MVN stability study at room temperature and 4°C	31
9.	MVN-based OB-ELISA workflow	42
10.	Optimization of MVN and detection antibody concentration for MVN-based plate ELISA	44
11.	MVN-based plate ELISA performed with and without MVN capture	46
12.	Exploring blocking agent and type of immunoassay plate with the MNN-based plate ELISA	48
13.	Investigating depletion methods with blocked wells and beads	49

14. Optimization of detection antibody concentration and number of MVN-functionalized magnetic beads for the OB-ELISA in buffer 50

15. LODs of OB-ELISA for ManLAM and PILAM in buffer 51

16. Optimization of capture and detection format, detection antibody concentration, and loading density of MVN-functionalized magnetic beads for the OB-ELISA in urine 53

17. LODs of OB-ELISA for ManLAM and PILAM in pooled human urine 54

18. Alere LFA test line area for standard curves of ManLAM and PILAM in pooled human urine 55

19. Optimization of capture and detection antibody concentrations and blocking buffer for the antibody-based plate ELISA 56

20. LODs of antibody-based plate ELISA for ManLAM and PILAM in pooled human urine 57

21. OB-ELISA on large-volume mock samples of ManLAM in pooled human urine 58

22. Training video of MVN-based OB-ELISA procedure with urine pre-concentration 70

23. LOD of the MVN-based OB-ELISA on concentrated mock urine samples 72

24. OB-ELISA normalized absorbance values for clinical samples 74

25. Box-and-whisker plots by HIV-status and country of origin of the clinical samples 76

26. OB-ELISA results by sex and age 77

27. Receiver operating characteristic curve for the OB-ELISA 78

28. Workflow for a membrane urine filtration system 85

29. Subset of the LAM motifs that will be tested as part of a glycan array study 86

30. Study design for OB-ELISA testing in Brazil 88

31. Schematic of the dendrimer nucleotide probe 93

32. Schematic of the oligonucleotide ligation assay with colorimetric and PCR detection 95

33. Proof-of-concept experiment to validate the silica condensation system 99

34. Quantification of ability of G4 and G5 polyamidoamine dendrimers to precipitate silica 101

35. Proof-of-concept experiment to validate the oligonucleotide ligation system with PCR detection 103

36. Investigation of ligation temperature 106

37. Investigation of cycling between ligation and melting during the oligonucleotide ligation reaction 108

38. Time study of the oligonucleotide ligation reaction 109

39. Optimization of ligation time, melt time, and total time for the oligonucleotide ligation reaction 110

List of Abbreviations

Word	Acronym
1. Tuberculosis	TB
2. Multidrug-resistant tuberculosis	MDR-TB
3. Mycobacterium tuberculosis	*M. tb*
4. Lipoarabinomannan	LAM
5. Mannose-capped lipoarabinomannan	ManLAM
6. Phosphate-inositol lipoarabinomannan	PILAM
7. Uncapped lipoarabinomannan	AraLAM
8. 5-Deoxy-5-methylthio-xylofuranose	MTX
9. Microvirin	MVN
10. Bio-layer interferometry	BLI
11. Enzyme-linked immunosorbent assay	ELISA
12. On-bead enzyme-linked immunosorbent assay	OB-ELISA
13. Lateral flow assay	LFA
14. Nuclear magnetic resonance	NMR
15. Polymerase chain reaction	PCR
16. Limit of detection	LOD
17. Phosphate-buffered saline (with Tween 20)	PBS (PBST)
18. Bovine serum albumin	BSA
19. Horseradish peroxidase	HRP
20. 3,3′,5,5′-Tetramethylbenzidine	TMB
21. Sulfosuccinimidyl-4-(N-maleimidomethyl)cyclohexane-1-carboxylate)	Sulfo-SMCC

Chapter I

The tuberculosis diagnostic landscape[a]

TB is a public health crisis

TB is an infectious disease caused by *M. tb* that primarily affects the lungs. Broadly, there are three stages of TB: exposure, latent disease, and active disease. Not everyone who is exposed to the bacteria becomes infected. Transmission depends on many factors, including: the immune status of the exposed individuals, the strength of the infectious source (i.e. a cough that produces droplets), the infectiousness of the person with TB (i.e. how many TB bacteria they are expelling into the air), and environmental factors (i.e. duration, frequency, and proximity of exposure).[1] It is estimated that approximately 25% of the world's population is latently infected with the *M. tb* bacteria.[2] It's important to note that people with latent TB are not symptomatic and are not capable of transmitting the disease.[3] Of people with latent TB, about 3-10% develop the active disease, which resulted in about 10 million incident cases in 2019.[4-6] Symptoms of TB include persistent cough, coughing up blood or sputum, chest pain, fatigue, weight loss, loss of appetite, fever, chills, and night sweats.[7] Although TB is both treatable and curable, over 1.4 million people still die from TB every year.[5]

One of the contributing factors to this high mortality rate is that the causative agent, *M. tb*, is the most common opportunistic infection in HIV-positive patients.[8]

[a] Portions of this chapter were reproduced from Ref. 105 with permission from the Royal Society of Chemistry.

People infected with HIV are approximately 21 times more likely to develop active TB and have a 2 times higher fatality rate compared to people without HIV.[8,9] Reasons for comparatively poor outcomes for HIV-positive TB patients stem from late diagnosis and delays in starting antiretroviral therapy and/or TB treatment.[9] These diagnostic and treatment failures can be further explored by performing a care cascade analysis to determine the patient retention at each step in TB care.[10]

Subbaraman, *et al.* studied the cascade of care of TB in India to determine why there are so many fatal cases of TB (**Table 1**).[11] They found that only 72% of people with active TB reached a TB diagnostic center, and 16% of those patients did not receive a diagnosis, despite making it to a center.[11] Further, only approximately half of people with active TB registered for TB treatment, and nearly 14% of those who registered for treatment did not complete it.[11] This drastic loss is likely due to the lengthy standard treatment for TB, consisting of a regimen of isoniazid, rifampin, pyrazinamide, and ethambutol for two months, plus isoniazid and rifampin for an additional four months.[12] In addition to the long-term dosage requirements, many side effects have been reported for these antibiotics. Overall, Subbaraman found that only 39% of people with active TB had recurrence-free survival.[11] Further, this failure to diagnose and treat individuals with active TB has a strong effect on the health of other people. On average, people with untreated active TB can infect 10-15 people per year, starting the entire cycle over again.[13] Naidoo, *et al.* studied a similar cascade of care in South Africa and found a 5% loss of patients prior to test access, a 13% loss at diagnosis, a 12% loss at the start of treatment, and a 17% loss at treatment completion (**Table 1**).[14]

Table 1. Cascade of care analysis for India and South Africa showing losses for accessing a diagnostic test, receiving a diagnosis, initiating treatment, and completing treatment.[11,14]

	India[11]		South Africa[14]	
	Number	**Percentage**	**Number**	**Percentage**
Number of cases	2,700,000	100	532,005	100
Accessed diagnostic	1,938,027	72	504,514	95
Received diagnosis	1,629,906	60	435,483	82
Registered for treatment	1,417,838	53	372,577	70
Completed treatment	1,221,764	45	279,816	53

Diagnostic tests for TB

A clear solution to this problem is to improve access to and receipt of diagnosis of TB, which combined represent the largest gap in the care cascade for both India and South Africa.[11,14] Broadly, diagnostic tests for tuberculosis can be divided into radiography, microscopy, bacterial culture, nucleic acid amplification tests, and biomarker-based tests.[15] Chest radiography, or chest x-ray, is used to identify abnormalities in the lungs that indicate TB.[16] Radiography has a high sensitivity for pulmonary TB, but a low specificity as many lung abnormalities can be non-specifically indicative of other diseases.[11] Further, radiography is unable to detect extrapulmonary TB, which is estimated to account for 30% of TB cases.[16,17] Other drawbacks include exposing the patient to radiation, requiring trained personnel and specialized equipment, and high costs to patients.[16]

Traditional sputum smear microscopy uses Ziehl-Neelson acid-fast staining to identify *M. tb* bacteria in a sputum sample.[18] In some cases, this technique has been replaced with fluorescence sputum smear microscopy, which uses an acid-fast fluorochrome dye and an intense light source.[19] However, conventional sputum smear microscopy is used more frequently in low- and middle-income countries and will be the focus of this discussion, since these countries are where the majority of TB cases occur.[19] Sputum smear microscopy has low sensitivity and high specificity.[19] Like radiography, it has poor performance at detecting extrapulmonary TB. Additionally, performance is compromised in patients co-infected with HIV and in children.[20] However, it is still widely used due to its affordability and speed.[20]

Mycobacterial culture from a sputum sample is considered the gold standard for TB diagnosis due to its high sensitivity and specificity.[21] Traditionally, mycobacterial culture has been performed on Lowenstein-Jensen medium (solid agar), but the Mycobacteria Growth Incubator Tube (MGIT) system (liquid culture) is becoming the norm and will likely be used moving forward.[22] The biggest drawback to mycobacterial culture is the length of time required to achieve a result with the slow-growing *M. tb*; solid culture requires four to six weeks to see mycobacterial growth while liquid culture only requires 1-2 weeks.[15] Further, the length of time for a negative result to be reported is even longer with an average time of 8 weeks for solid culture and 6 weeks for liquid culture.[23] Another concern with mycobacterial culture is the risk of cross-contamination between samples, which is even greater for liquid culture than solid agar.[21] Lastly, mycobacterial culture has high-resource requirements and is costly, although solid culture is slightly more affordable than liquid culture.[21]

Nucleic acid amplification tests amplify and detect *M. tb* DNA through PCR,

typically from a sputum sample. These tests are highly sensitive and specific.[24] Additionally, they are much faster than culture.[24] The most common nucleic acid amplification test is Cepheid's Gene Xpert MTB/RIF assay.[25] This system uses single-use cartridges that integrate sample processing and PCR-based detection to simultaneously detect *M. tb* and resistance to rifampin, which can be used as a marker for MDR-TB.[26] This system will be discussed in more detail in Appendix I, but overall, this technology is easy to use, despite requiring specialized equipment and laboratory infrastructure.[26] However, it is quite costly, with each cartridge costing approximately $10 in addition to the cost of the instrument.[27]

Biomarker-based diagnostic tests for tuberculosis most commonly detect LAM, a glycolipid found in the cell wall of mycobacteria such as *M. tb.*[28] Biomarker tests are fast and affordable, but lack sensitivity and specificity.[29] However, they are still a good option for initial testing where speed and cost are more important factors.[29] Importantly, these tests use urine samples, rather than sputum, which has additional benefits.[30] Conventional sputum smear microscopy, bacterial culture, and nucleic acid amplification tests, such as GeneXpert MTB/RIF, all require biohazardous *M. tb*-infected sputum samples to yield a positive diagnosis of TB.[31] Yet, it is difficult for many patients with active TB to produce sputum samples, especially those co-infected with HIV, people with diabetes, and children.[31] Further, urine analysis obviates the biohazards associated with sputum handling and can be easily collected from all patients.[30,32] Overall, the benefits of biomarker tests outweighs the drawbacks, and considerable research effort is dedicated to improving them further.[33] The performance characteristics of the TB diagnostic tests are summarized in **Table 2**

Table 2. There are multiple types of diagnostic tests for TB that vary in sensitivity, specificity, cost, and resource requirements.

Diagnostic method	Sensitivity	Specificity	Cost	Resource requirements
Chest radiography[16]	High	Low	High	High
Sputum smear microscopy[19]	Low	High	Low	High
Mycobacterial culture[21]	High	High	High	High
Nucleic acid amplification test[24]	High	High	High	High
Biomarker-based test[29]	Low	Low	Low	Low

LAM in urine

As previously mentioned, one of the main advantages to TB biomarker tests is detection of LAM in urine.[34] However, initially urinary LAM detection was limited to individuals who were co-infected with HIV.[32] Several hypotheses were proposed to explain this phenomenon (**Figure 1)**.[35] One possibility is that as LAM is shed from the surface of the mycobacteria, it binds to antibodies or high-density lipoprotein, and the resulting complexes are too large to be filtered through the renal glomerular membrane.[36-39] In the case of HIV co-infection, glomerular dysfunction could result in the presence of LAM in urine; however, the absence of a correlation between urinary LAM and proteinuria lessens this hypothesis.[40] A second hypothesis is that LAM enters urine only in the case of renal or disseminated TB, which is more common in patients with HIV.[35] Lastly, it is hypothesized that free LAM is filtered by the kidneys and secreted into urine with a higher concentration of detectable LAM in HIV-positive individuals. This is due to a higher overall TB burden in HIV-positive patients, while a

lower TB burden and resulting decreased concentration of LAM in HIV-negative individuals falls below the detection limit.[41] Paris, *et al.* was able to show that LAM could be detected in 96% of TB-positive HIV-negative patients by concentrating the urine prior to analysis.[41] The sample preparation method used in this study will be discussed in more detail in Chapter IV, but it was found that HIV-negative patients had a much lower concentration of LAM in urine compared to HIV-positive patients. Specifically, they found that the concentration of LAM in the urine of TB-infected, HIV-negative individuals varies from approximately 10 to 1000 pg/mL.[41] Higher LAM concentrations are reported in HIV-positive individuals, up to 100 ng/mL, due to a higher overall bacillary load.[41] This study, as well as other recent research reports, support the third hypothesis that concentration of LAM in HIV-negative individuals is simply below the LOD for most methods.[41,42] Now, the focus has shifted to understanding the structure of LAM in more detail with the goal of improving molecular recognition elements for LAM and, thus, detection tests for LAM.[43]

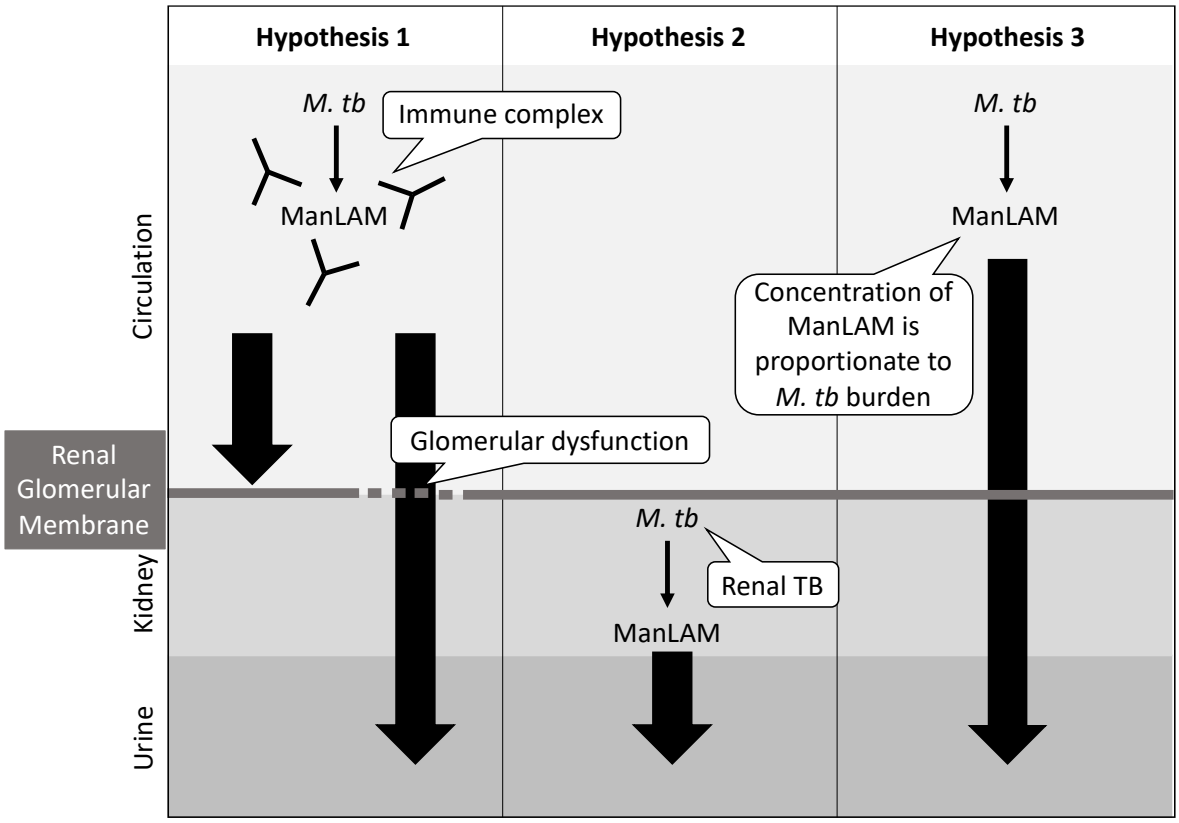

Figure 1. Three potential hypotheses have been proposed to explain urinary ManLAM in HIV-positive and HIV-negative cases. The first hypothesis is that antibodies bind to ManLAM forming an immune complex that is too large to be filtered through the renal glomerular membrane, except in cases of glomerular dysfunction which is possible in HIV co-infection. A second hypothesis is that urinary ManLAM is the result of renal TB, which is more common with HIV co-infection. The third hypothesis is that free ManLAM is present in urine in all cases but that the concentration is dependent on the *M. tb* burden, which is typically higher for HIV-positive individuals compared to those who are HIV-negative. Figure adapted from Ref. 35.

The structure of LAM

LAM has three structural domains: (1) a mannosyl-phosphatidyl-*myo*-inositol linker, (2) a polysaccharide backbone composed of a D-mannan core and D-arabinan branches, and (3) a capping motif on the terminal ends of the D-arabinan branches (**Figure 2)**.[44] The linker and backbone are conserved in all LAM variants, while the capping motif differs depending on the species of mycobacterium.[44,45] There are three classifications of LAM based on variations in their capping motif: (1) ManLAM, which is capped with mannose, (2) PILAM, capped with phospho-*myo*-inositol, and (3) AraLAM, which is devoid of capping motifs.[44,46] PILAM and AraLAM are found in the cell wall of fast-growing, non-pathogenic mycobacteria. In contrast, ManLAM is unique to the surface envelope of slow-growing, pathogenic mycobacteria, such as *M. tb, M. bovis* and *M. leprae*.[47]

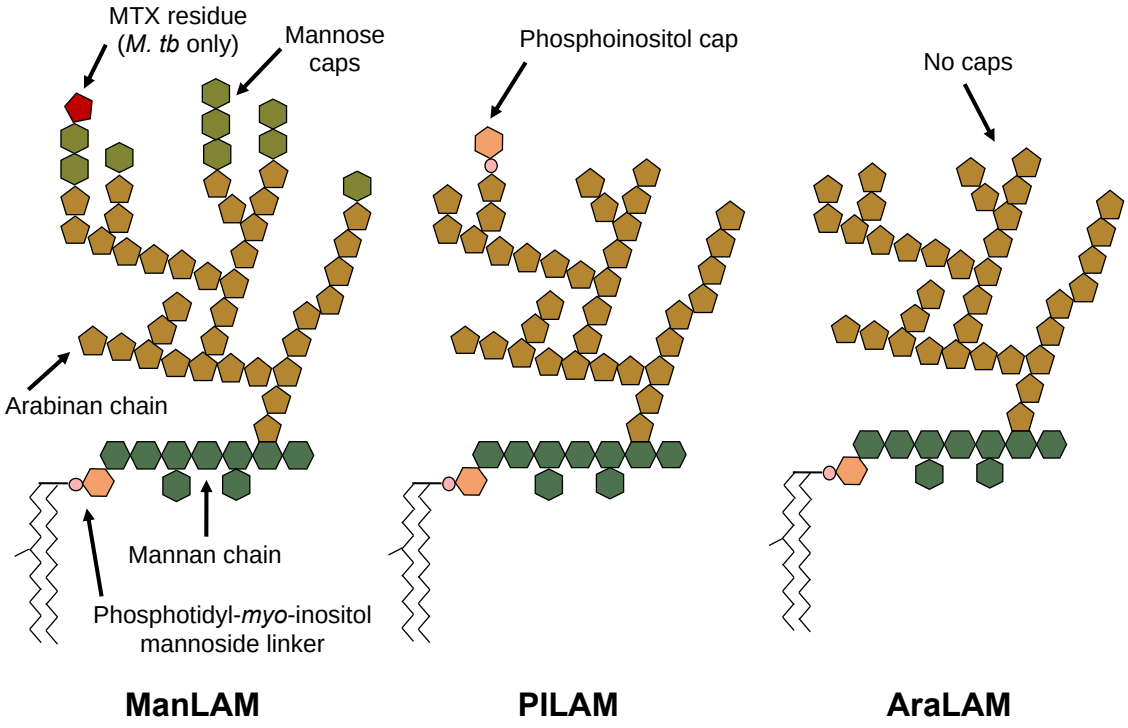

Figure 2. Schematic showing the similarities and differences between the three types of LAM: ManLAM is capped with mannose residues, PILAM is capped with phosphoinositol, and AraLAM is devoid of capping residues. Throughout this work, the specific variant of LAM (ManLAM, PILAM, or AraLAM) will be used where applicable and LAM will be used generally to discuss conserved features, shared properties, and non-specific interactions. Figure adapted from Ref. 43.

A great deal of heterogeneity exists within each variant of LAM, as well as from a single source of LAM.[48] For example, the mannose caps can take one of three forms: (1) a single mannose residue, (2) α-(1,2)-linked di-mannosyl residues, or (3) α-(1,2)-linked tri-mannosyl residues.[49] Generally, *M. tb* ManLAM is capped with di-mannosyl residues.[50] In contrast, ManLAM from *M. avium,* a different pathogenic mycobacteria, is preferentially capped with mono-mannose motifs.[50] Additionally, the total number of

mannose caps per ManLAM molecule varies.[50] *M. tb* and *M. bovis* ManLAM express the highest number of mannose capping residues (seven to nine per ManLAM molecule), whereas *M. leprae* ManLAM averages only two mannose caps per ManLAM molecule.[51,52] This makes the abundance of mannose caps on *M. tb* ManLAM an especially attractive target for new capture and detection agents.[53] An additional unique feature of *M. tb* ManLAM is the presence of MTX substituents on the terminal mannose capping motifs.[54,55] Lastly, studies have reported differences in the structure of *in vitro* ManLAM – ManLAM isolated from mycobacterial culture – and *in vivo* ManLAM – ManLAM that is found in TB-patients, posing further complications for the development of diagnostic test. [43]

First-generation ManLAM detection tests

ManLAM has been studied as a biomarker for TB in diagnostic tests since 1997; however, a commercial test was not available until 2003 with the development of the Clearview TB ELISA assay from Inverness. [42,56] The Clearview TB ELISA was developed to detect ManLAM in urine through the use of polyclonal antibodies that bind to the conserved backbone.[57] A study of the sensitivity of the ELISA showed that it displayed higher sensitivity in people co-infected with HIV and with advanced immunosuppression.[58] In 2010, Inverness re-branded to Alere and the Clearview ELISA was replaced by the Alere Determine TB LAM Ag LFA, which utilizes the same polyclonal antibodies to detect ManLAM, in a format suitable for point-of-care testing.[34,42,59] Similarly to the Clearview ELISA, the Alere LFA was found to have higher sensitivity in people infected with HIV and with very low CD4 counts (<100 CD4

cells/μL), and thus was recommended for use in these populations by the World Health Organization.[60]

However, implementation of the Alere LFA has been limited largely due to its variable sensitivity and specificity. Results from clinical studies and a meta-analysis present pooled sensitivities for the Alere LFA between 34% and 60% depending on the reference standard.[58] Increased sensitivity was correlated to the severity of patient immune suppression, as the concentration of ManLAM in urine is thought to depend on the patient's immunocompetence, reflecting increased bacillary load, dissemination of *M. tb,* and potentially also renal involvement of TB disease in such patients.[58] Similarly, although most studies have reported high positive predictive values, there remains unexplained variability in specificity, with individual studies reporting values ranging from 79% to 100%.[58] While poor specificity may reflect the shortcomings of individual assays, it is also possible that false-positive results are due to cross-reactivity with LAM molecules expressed by non-tuberculous mycobacteria, or related bacteria of the *Actinomycetales* order, particularly as the Alere LFA relies on anti-LAM antibodies that bind to the common polysaccharide backbone of all LAM variants.[30,32,61,62]

Cross-reactivity with LAM variants is well-established in the literature.[63] One study showed that disseminated non-tuberculosis mycobacterial infections, specifically *M. avium*, *M. kansasii*, and *M. intracellilare,* can generate a false-positive response on the Alere LFA.[64] Another study observed false positive Alere LFA results due to *M. leprae* in Brazilian patients.[65] Notably, these mycobacteria are all considered slow-growing pathogenic mycobacteria, which are known to display ManLAM.[49] However, Boehme, *et al.* observed cross-reactivity with LAM from rapid-growing, non-pathogenic mycobacteria – both the PILAM and AraLAM subtypes – with the

Clearview ELISA, which utilizes the same antibodies as the Alere LFA.[34,61] This cross-reactivity has severe implications on the clinical usefulness of the Alere LFA.

Clinically, non-tuberculosis mycobacterial infections are most common in cases of severe immune deficiency, such as HIV and cancer.[66,67] However, reports have indicated that non-TB mycobacterial infections are increasing in prevalence in people who are not immune-compromised.[68] Yet, information on the prevalence of non-tuberculosis mycobacteria infections is lacking, particularly in TB-endemic countries where the chance of misdiagnosis is high.[69] A further complication factor is that different species of non-tuberculosis mycobacteria vary in their disease manifestations and clinical relevance.[70] However, it is obvious that assays capable of distinguishing the variant of LAM are needed, both for proper treatment and for improved surveillance.

Second-generation ManLAM detection tests

Recently, the focus has shifted to an investigating ManLAM substructures in urine, notably the mannose caps and MTX residues which distinguish ManLAM from other variants of LAM. [43,53,71] Researchers utilized the MTX-specific antibody, S4-20 (referred to as MoAb1 in early studies), to develop a novel immunoassay for ManLAM, the FujiLAM assay.[72] The FujiLAM assay was found to be 70% sensitive, versus a sensitivity of 42% displayed by the Alere LFA with the same cohort.[72] This increase in sensitivity is partially due to the silver amplification step, which produces a 100-fold increase in the size of the colloidal gold used for detection.[72] Unlike the Alere LFA, the FujiLAM assay displays no cross-reactivity with other variants of LAM because of the

distinct targeting of the MTX epitope, which is present only on *M. tb* ManLAM.[72,73] However, in comparison to the mannose capping residues, the MTX capping residue is present in low abundance on *M. tb* ManLAM; typically only one MTX residue is present per ManLAM molecule versus seven to nine mannose capping residues.[54] Therefore, MTX may be a suboptimal moiety to target on *M. tb* for diagnostic purposes.

Another method of improving the specificity of ManLAM detection assays is to target the mannose caps unique to the pathogenic variant. Several antibodies have been developed that are specific for this epitope, including My2F12, G3, and P30B9.[53,74] All three antibodies were found to bind binds strongly to di-mannose capped tetra-arabinoside and hexa-arabinoside structures with variations in their weak binding interactions to other mannose capped structures (**Table 3**).[74] Notably, none of these antibodies were able to bind to structures that contained an MTX motif.[74] Despite the similar binding patterns of these three antibodies, their applications and uses differ. Unfortunately, P30B9 has not yet been used in further studies, but future work will be of great interest. Sigal, *et al.* found that G3 was not capable of binding ManLAM in clinical samples, despite demonstrating a strong affinity for *in vitro Man*LAM.[73] They hypothesized that this was due to an increased number of MTX residues, which block binding of G3, on *in vivo* ManLAM versus *in vitro* ManLAM; however, Chan, *et al.* developed a ManLAM detection assay utilizing My2F12 that was able to detect *in vivo* ManLAM in urine.[53] This assay was reported to have a sensitivity of 26.6 – 46.7% in HIV-negative individuals, which leaves room for improvement.[53]

Table 3. A glycan array was used to identify the mannose structure specificity of three antibodies that target ManLAM mannose caps.[74] All three antibodies had strong binding interactions with di-mannose capping motifs, but the antibodies varied in their weak interactions. [74] In the glycan array study, G3 was referred to as MoAb2, but the more recently used (and more distinct name) was chosen to be used for this discussion.[73]

	Mannose capping motif		
Antibody	**Mono-**	**Di-**	**Tri-**
My2F12		Strong	Weak
G3 / MoAb2	Weak	Strong	Weak
P30B9	Weak	Strong	

Microvirin-N

MVN, a 14.3 kDa lectin, was first identified in *Microcystis aeruginosa in* 2005 by Kehr, *et al* (**Figure 3**).[75] *M. aeruginosa* is the most common cyanobacteria found in freshwater lakes, forming dense water blooms with an unpleasant smell and toxic metabolic products.[76] The presence of mannose-binding lectins in members of the *Microcystis* genus has been documented in the literature, including the *M. viridis* lectin MVL and the *M. aeruginosa* lectin MAL.[77-79] In this first study of MVN, a glycan array was used to determine the carbohydrate specificity of MVN.[75] Based on 33% sequence homology to cyanovirin-N, a mannose-binding lectin isolated from *Nostoc ellipsosporum* that displayed promising anti-HIV activity, a microarray consisting of eight derivatives of high-mannose structures was used to probe the binding of

MVN.[75,80] Cyanovirin-N has been shown to display high affinity for the high-mannose branched oligosaccharides, Man_8 and Man_9, found on the HIV surface envelope glycoprotein, gp120.[81] The results of the glycan array demonstrated that MVN binds to Man_9, as well as sub-structures consisting of the D1 and D3 arms of Man_9, all three of which contain Manα-(1,2)-Man linkages.[75] Additionally, structures without Manα-(1,2)-Man linkages showed no signal for binding, providing further evidence that MVN specifically binds to this linkage.[75] Furthermore, a later study tested the specificity of MVN with a glycan array of almost 400 sugars, with a much greater diversity in structure than the previous array, and confirmed that MVN is specific for Manα-(1,2)-Man linkages.[82]

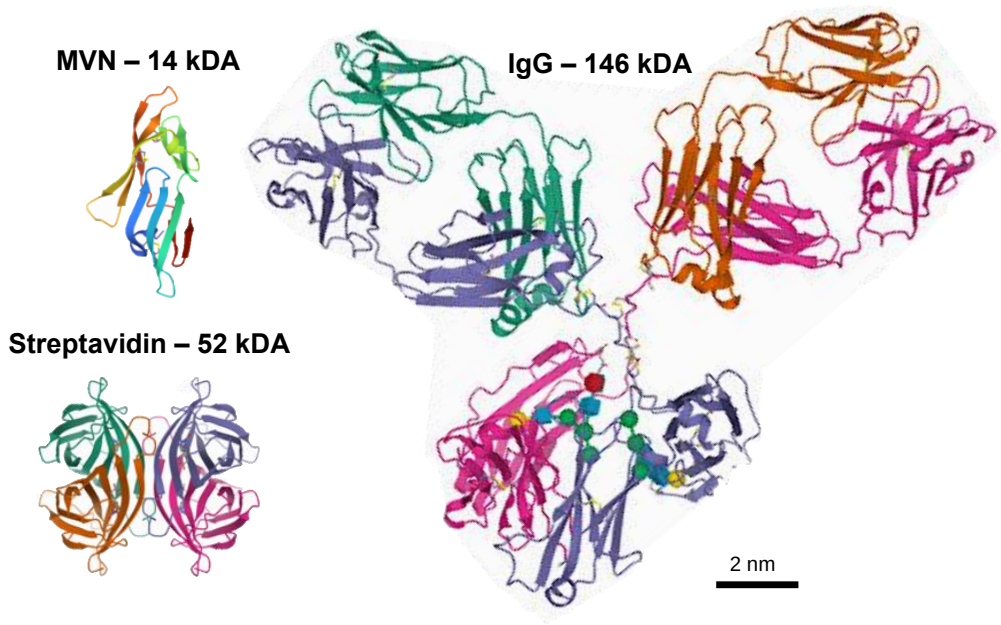

Figure 3. The lectin MVN (14 kDa) is shown in comparison to streptavidin (52 kDa) and an immunoglobulin (IgG) antibody (146 kDa).[82-87]

Following this report of the discovery of MVN, Huskens, *et al.* studied the anti-HIV activity of MVN.[88] In contrast to cyanovirin-N, MVN was shown to be active against the HIV-1 M subtype, but not the HIV-1 O subtype or HIV-2.[88] Moreover, MVN was shown to have a much higher safety profile than cyanovirin-N.[88] Subsequent studies have further explored the anti-HIV activity of MVN.[89-93] Additionally, MVN was shown to exhibit antiviral activity against hepatitis C, which has a cell envelope that contains many high-mannose glycans.[94,95] Notably, MVN has not been tested with *M. tb* by other research groups, but cyanovirin-N was shown to bind to ManLAM which contains the same Manα-(1,2)-Man linkages as HIV Man_9.[96] The goal of this project is to utilize MVN to bind *in vivo* ManLAM, as antibodies specific for the mannose caps were shown to have mixed results for binding to ManLAM in urine.[73] It is reasoned that MVN may have different results due to its small size and high degree of carbohydrate specificity.

Scope of this work

New approaches for TB control and care are urgently needed. Accurate diagnosis is one of the cornerstones of TB control, therefore considerable research effort has been dedicated to the development of new testing formats to enable well-timed diagnosis, guide the appropriate treatment, and curb the transmission and unacceptably high number of deaths due to this otherwise curable disease.[31,60,] The goal of this project is to utilize the lectin MVN as a novel molecular recognition element for ManLAM. It has been established that MVN binds to Manα-(1,2)-Man linkages, which are present in the mannose caps of ManLAM.[75,88] In Chapter II, the binding of MVN to ManLAM and other variants of LAM will be investigated using BLI. In Chapter III, a MVN-based OB-ELISA will be developed that allows *in vitro* ManLAM to be

detected in urine. In Chapter IV, clinical urine samples will be tested with the MVN-based OB-ELISA to determine whether MVN is capable of binding to mannose caps on *in vivo* ManLAM. As a result, this work represents a critical advance in TB diagnostic technology, opening many avenues for further study.

Chapter II

Microvirin-N is a novel molecular recognition element for the tuberculosis biomarker lipoarabinomannan[b]

Introduction

The discovery of MVN, a highly specific Manα-(1,2)-Man binding lectin, was reported in 2005 by Kehr *et al.*[75] Since then, it has been investigated for anti-HIV-1 activity and as a neutralizing agent for hepatitis C viral infections.[88,94,97] A solution structure of MVN bound to an α-(1,2) di-mannose shows that binding occurs through a single site.[82] The binding site for the reducing mannopyranose is located in a deep groove formed by two β-turns **(Figure 4**).[82] Binding is governed by hydrophobic interactions and van der Waals forces.[82] However, the binding site for the terminal mannose is more shallow and formed of the hinge linker and a helix structure.[82] Six hydroxyl groups of this residue are proposed to form hydrogen bonds with MVN.[82] MVN displays remarkable specificity to Manα-(1,2)-Man linkages as demonstrated by a binding experiment with a glycan array of almost 400 sugars.[82] As previously mentioned, *M. tb*, as well as other slow-growing, pathogenic mycobacteria species, express ManLAM which contains Manα-(1,2)-Man linkages; in contrast, non-pathogenic mycobacteria, such as *M. smegmatis* and *M. chelonae,* express PILAM

[b] Portions of this chapter were reproduced from Ref. 105 with permission from the Royal Society of Chemistry.

and AraLAM, respectively, which express non-mannose caps.[44] Therefore, the use of MVN to target the mannose caps that make ManLAM distinct would enhance the specificity of detection.

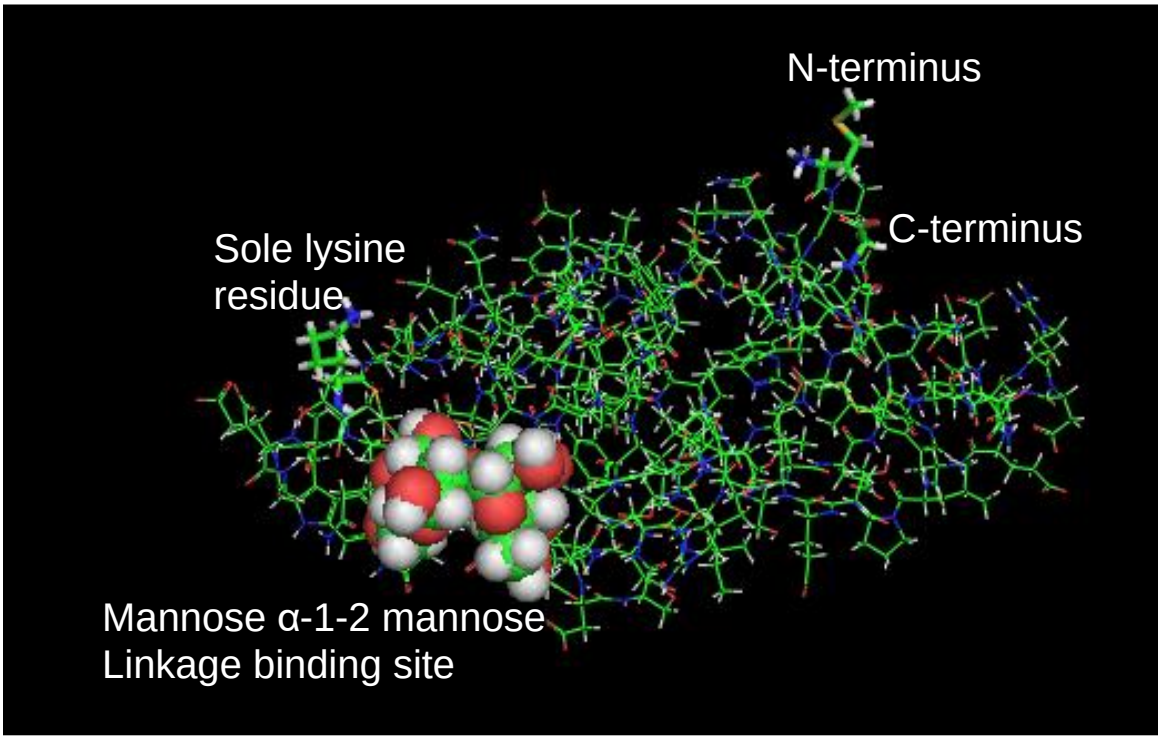

Figure 4. A PyMOL rendering shows the resolved crystal structure for MVN bound to the Manα-(1,2)-Man structure. MVN has a N-terminal hexa-histidine affinity tag for purification and a single intrinsic lysine residue which allows for simple bioconjugation procedures.

Current ManLAM detection tests employ either polyclonal or monoclonal antibodies. Polyclonal antibodies raised against ManLAM are more likely to recognize multiple antigenic epitopes compared to monoclonal antibodies, but carry the risk of

batch-to-batch variation and cross-reactivity.[98] Although monoclonal antibodies target a single epitope, the majority of monoclonal antibodies generated against ManLAM target the conserved arabinan branches.[74,99-102] Broadly, they target capped or uncapped tetra-arabinoside or hexa-arabinoside motifs, with some antibodies displaying additional specificity (**Table 4)**. However, none of these antibodies are capable of distinguishing between the variants of LAM, leading to cross-reactivity and high false-positive detection rates.[103] Recently, new antibodies have been developed that are specific for ManLAM, either by binding to the mannose caps (My2F12, G3, and P30B9) or the MTX residues (S4-20), underscoring the need for ManLAM-specific capture agents to improve the specificity of *M. tb* diagnostic assays.[53,71]

Table 4. Binding epitopes of the anti-LAM antibodies tested in this study as determined by glycan array (Ara4 = linear tetra-arabinoside, Ara6 = branched hexa-arabinoside, Any Man Cap = any mannose capping structure with or without MTX, ManX = mannose capping structure consisting of X mannose residues).[74]

Antibody	Binding epitope
FIND Ab25	Ara6 ± Any Man Cap
FIND Ab28	Ara6 ± Any Man Cap
FIND Ab170	Ara6 ± Any Man Cap
FIND Ab194	Ara4, Ara6 ± Man1 Cap
FDX01	N/A
CS35	Ara4, Ara6 ± Any Man Cap
CS40	Ara4, Ara6 + Man1 Cap ± MTX

In this chapter, the high affinity and exceptional specificity of MVN, a small cyanobacterial lectin, toward *M. tb* H37Rv ManLAM using BLI is demonstrated. BLI is an optical technique that uses biosensors functionalized for highly specific binding of target molecular recognition elements which can then interact with the biomarker of interest.[104] White light is directed down the biosensor towards two layers – a biocompatible layer on surface of the tip and an internal reference layer – which reflect the light.[104] As molecules bind to the surface of the biosensor, a molecular layer is formed that increases in thickness, widening the distance between the two planes and changing the interference pattern between the two beams of light.[104] The change in interference pattern is representative of molecular binding.[104] This technique was used to study the binding of MVN and anti-LAM antibodies to ManLAM, as well as variants of LAM expressed by non-pathogenic mycobacteria.

Materials and Methods

Expression and purification of MVN

MVN expression and purification was performed by the Vanderbilt Antibody and Protein Resource Core. Briefly, competent *E. coli* BL21-DE3 bacteria were transformed with the MVN-pET15b plasmid (190 ng plasmid per 100 μL competent bacteria) by heat shock. The plasmid-transformed bacteria were plated onto LB Agar plates containing ampicillin (100 μg/mL). Colonies were selected from the plates and stored as a glycerol stock. A 50 mL aliquot of LB medium containing 100 μg/mL ampicillin was inoculated with MVN-pET15b transformed BL21-DE3 bacteria as a starter culture, and allowed to grow at 37°C, 22 rpm overnight (~16-18 hours). 1 L sterilized TB Broth was inoculated with overnight starter culture until the OD_{600} reading

reached ~0.1. Ampicillin was then added to a final concentration of 100 μg/mL. The culture was allowed to grow at 37°C, 22 rpm until the OD_{600} reading reached ~0.6-0.8. The culture was cooled to 18°C and isopropyl β-D-1-thiogalactopyranoside was added to final concentration of 1 mM. Cultures were further incubated overnight (~16-18 hours) at 18°C, 22 rpm. Bacterial cells were harvested via centrifugation and either used fresh or stored frozen.

Cell pellets were resuspended in 150 mL phosphate buffer (25 mM NaH_2PO_4, 500 mM NaCl, 10% glycerol, pH 8) containing 2 μg/mL lysozyme (Sigma: Cat. No. L6876), 1 mL protease cocktail (Sigma: Cat. No. P8849), and powdered DNase I (Sigma: Cat. No. DN25). The cell suspension was then passed through an Emulsiflex-C3 High Pressure Homogenizer (Avestin) three times maintaining lysis pressure at 15,000 psi. The lysate was centrifuged and the resulting supernatant was clarified by filtering through a 0.22 μm filter. The clarified lysate was loaded onto a 5 mL HisTrap HP column (GE: 17-5248-02) and purified by FPLC. MVN was eluted with a linear imidazole gradient from 0-500 mM. Fractions containing MVN were pooled and dialyzed against PBS overnight at 4°C. Protein concentration was determined by quantification gel – Invitrogen NuPAGE 4-12% gradient gel run in 1x MES buffer with densitometry performed using the Image Studio Lite Version 5.2 software.

Bioconjugation procedures

Anti-LAM antibodies Ab25, Ab28, Ab170, Ab194, and FDX01 were procured from the Foundation for Innovative New Diagnostics (FIND) and conjugated to biotin with a 20x molar equivalence of EZ-Link NHS-PEG_4-Biotin (Thermo Scientific: Cat.

No. 21329) in DI water. Following a 30-minute incubation step at room temperature, the antibody-biotin conjugates were purified from excess biotin reagent using 7k MWCO Zeba desalting columns (Thermo Scientific: Cat. No. 89883). The concentration of the resulting antibody-biotin conjugates was determined by micro-volume analysis using a BioTek Take3 plate with the IgG setting.

Binding characterization of molecular recognition elements by BLI

Anti-LAM antibodies CS35 and CS40 were procured from the Biodefense and Emerging Infections Research Resources Repository (BEI Resources). MVN and all anti-LAM antibodies were subjected to binding experiments on the ForteBio Octet RED96 to determine binding affinity to *M. tb* H37Rv ManLAM, *M. leprae* ManLAM, and *M. smegmatis* PILAM.[18] Dip and Read Ni-NTA biosensors (ForteBio: Cat. No. 18-5101) were used to determine the binding affinity of MVN-His_6. Dip and Read Streptavidin biosensors (ForteBio: Cat. No. 18-5019) were used for the binding experiments with biotinylated Ab25, Ab28, Ab170, Ab194, and FDX01. Dip and Read Anti-Mouse Fc capture biosensors (ForteBio: Cat. No. 18-5088) were used for the binding experiments with CS35 and CS40.

For the Streptavidin and Anti-Mouse Fc capture biosensors, the biosensors were first introduced to a biosensor buffer (0.1% BSA (Fisher: BioReagents: Cat. No. BP9706100), 0.02% Tween 20 in PBS (Fisher BioReagents: Cat. No: BP337100) for a 300 second equilibration step in a black 96-well plate. The biosensors were then transferred to wells containing biotinylated antibody (0.5 μg/mL) for 400 seconds (**Figure 5A**). The loaded biosensors were moved to wells containing biosensor buffer

for a 60 second baseline step and then transferred to sample wells containing a two-fold serially diluted range of *M. tb* ManLAM, *M. leprae* ManLAM, or *M. smegmatis* PILAM with a buffer reference well for a 400 second association step. The two-fold serial dilution began at an initial concentration of LAM such that the starting concentration of LAM was at least 10x higher than the expected K_D and the lowest concentration was 2x lower than the expected K_D.[19] Lastly, the biosensors were moved back to the baseline buffer wells for a 900 second dissociation step.

The same procedure was used with Dip and Read Ni-NTA biosensors to determine the binding affinity of MVN-His_6, except the biosensor buffer was 0.02% Tween 20 in PBS and MVN-His_6 was loaded onto the biosensor at 0.5 μg/mL (**Figure 5B**). Inside the ForteBio software, a global 1:1 fit model was selected to derive the kinetic (k_{on}, k_{off}) and equilibrium (K_D) data.

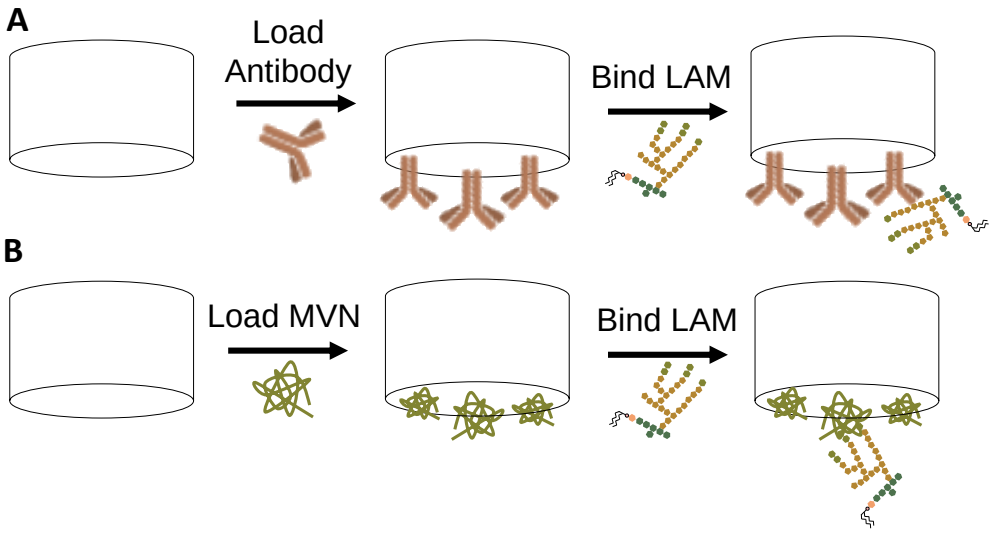

Figure 5. Schematic showing the abbreviated workflow for BLI. **A)** First, anti-LAM antibodies were loaded onto streptavidin biosensors. Then, the biosensors were moved to solutions of LAM to measure the interaction between LAM and the antibody. **B)** This process was repeated with MVN, with the exception that Ni-NTA biosensors were used to bind to the His_6-tag on MVN.

Binding pair evaluation by BLI

The binding pair evaluation was run on the Octet RED96, equipped with Dip and Read Ni-NTA sensors. The biosensors were first introduced to a biosensor buffer (0.02% Tween 20 in PBS) for a 300 second equilibration step, followed by a loading step where the biosensors were transferred to wells containing 0.7 μg/mL MVN-His_6 for 400 seconds. The loaded biosensors were transferred to wells containing biosensor buffer for a 60 second baseline step and then transferred to sample wells containing 0.325 μg/mL *M. tb* H37Rv ManLAM for a 400 second association step. The biosensors were returned to the baseline wells for a 60 second baseline step and then

transferred to wells containing 12 μg/mL non-conjugated Ab28 for another 400 second association step. Lastly, the biosensors were returned to the baseline buffer wells for a 900 second dissociation step.

Stability test of MVN by BLI

MVN-His_6 was stored at either 4°C or RT. Repeated binding experiments at set time points were performed on MVN-His_6 to determine changes in its binding affinity toward *M. tb* H37Rv ManLAM over time as a representation of stability. For the batch stored at 4°C, measurements were made on days 0, 1, 2, 3, 4, 8, 12 (excluded by outlier test), 16, 22, 29, 36, 43, 49 (measured twice using two batches of ManLAM and averaged), 63, 77, 91, and 105. For the batch stored at RT, aliquots were moved from the freezer to RT on days 0, 1, 2, 3, 4, 5, 6, 8, 10, 12, and 14; binding experiments were performed with each aliquot on the last day. The binding experiments were performed in the same manner as outlined previously.

Results

To evaluate the binding of MVN to ManLAM, MVN was subjected to BLI experiments with *M. tb* H37Rv ManLAM. For these experiments, Ni-NTA functionalized biosensors were used to bind the His-tag on MVN. MVN loading onto the biosensor can be visualized by an increase in the binding shift (**Figure 6a**). The biosensor tips were then moved to wells with solutions of *M. tb* ManLAM spiked into buffer to allow *M. tb* ManLAM to bind to MVN on the biosensor tip. It is clear that *M. tb*

ManLAM binds to MVN as indicated by the increase in the binding shift (**Figure 6b**). Lastly, the dissociation of the MVN-ManLAM complex was measured to assess the stability of the complex (**Figure 6c**). The dissociation constant (K_D) was determined by taking the ratio of the rate of dissociation to the rate of association for a range of concentrations, with lower K_D values indicating a higher binding affinity. For the interaction between MVN and *M. tb* ManLAM, the dissociation constant was calculated to be less than 1 pM (**Table 5**).

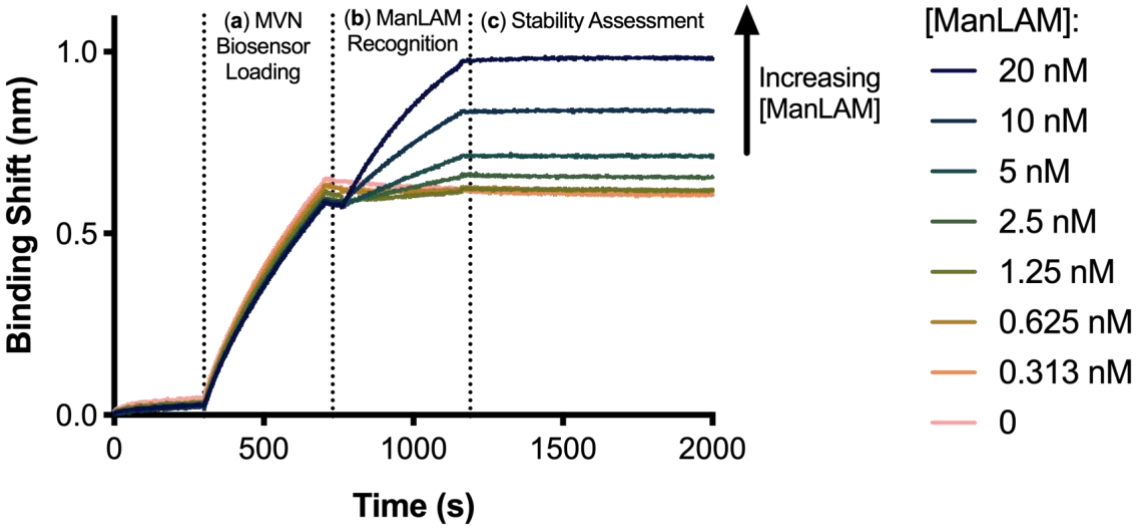

Figure 6. BLI binding curve showing MVN binding to ManLAM. (**a**) First, MVN was loaded onto the biosensor which is shown by an increase in binding shift. (**b**) Then, the binding of MVN to ManLAM at a range of concentrations was measured. (**c**) Lastly, the MVN-ManLAM complex was allowed to dissociate to assess the stability of the complex.

BLI experiments were repeated with *M. leprae* ManLAM and *M. smegmatis* PILAM to study the interaction of MVN to non-TB LAM. It was found that MVN bound to *M. leprae* ManLAM but did not exhibit binding to *M. smegmatis* PILAM (**Table 5**). Lastly, the binding of seven different anti-LAM antibodies to these three variants of LAM was measured. It was found that the antibodies were not capable of discriminating between the variants of LAM (**Table 5**). Therefore, it can be concluded that MVN displays a specificity for ManLAM that is not observed with the anti-LAM antibodies tested in this study. Furthermore, when comparing the strength of binding to ManLAM, MVN was observed to have an equally strong or stronger interaction than the antibodies.

Table 5. Dissociation constants of MVN and anti-LAM antibodies to *M. tb* ManLAM, *M. leprae* ManLAM, and *M. smegmatis* PILAM, calculated from BLI experiments. MVN displays a specificity for ManLAM that is not observed with these anti-LAM antibodies.

	Dissociation Constant (K_D) to Antigens		
	***M. tb* ManLAM**	***M. leprae* ManLAM**	***M. smegmatis* PILAM**
MVN	< 1 ± 9 pM	74.4 ± 0.5 nM	N.B.
FIND Ab25	1320 ± 16 pM	967 ± 11 pM	817 ± 18 pM
FIND Ab28	16.5 ± 0.4 nM	10.7 ± 0.14 nM	5.76 ± 0.11 nM
FIND Ab170	636 ± 11 pM	118 ± 2 pM	< 1 ± 2 pM
FIND Ab194	873 ± 20 pM	2.52 ± 0.02 nM	19.7 ± 0.003 nM
FDX01	870 ± 20 pM	Not tested	Not tested
CS35	< 1 ± 110 pM	< 1.0 ± 60 pM	< 1 ± 80 pM
CS40[c]	8740 ± 60 pM	Not tested	113 ± 0.8 nM

[c] Courtesy of Dr. Westley Bauer.

BLI was also used to study the formation of orthogonal binding pairs with ManLAM. After the formation of the MVN-ManLAM complex, the biosensor tip was moved to a solution of an anti-LAM antibody to determine if the antibody is capable of orthogonal binding to the complex. Non-specific binding was observed between MVN and CS35, as well as MVN and CS40. Orthogonal binding pairs were observed with Ab25, Ab28, Ab170, Ab194, and FDX01 with BLI (**Figure 7**).

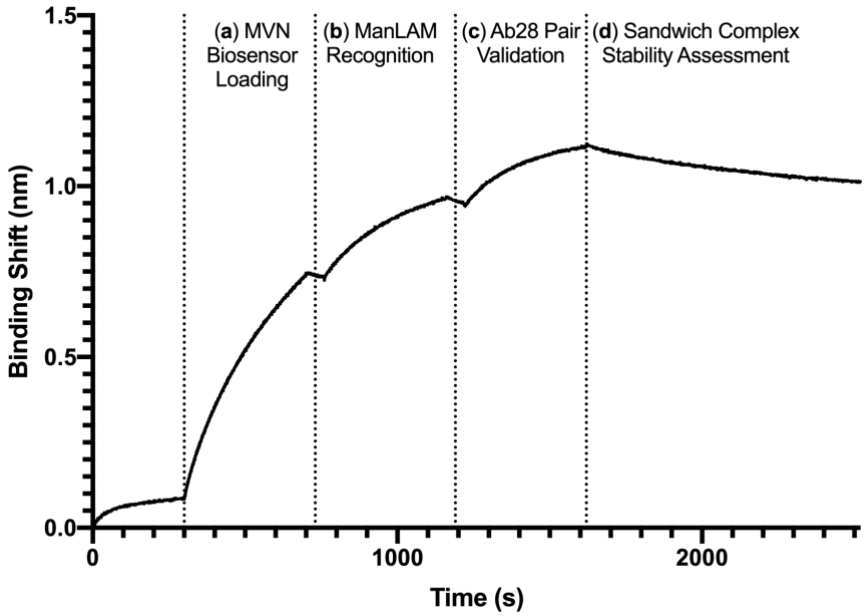

Figure 7. Representative BLI data showing the formation of an orthogonal ManLAM binding pair with MVN and the anti-LAM antibody Ab28. Binding pairs were also formed with Ab25, Ab170, Ab194, and FDX01.

Lastly, BLI was used to assess the stability of MVN over time. The dissociation constant of MVN, stored at room temperature and at 4°C, was measured against H37Rv *M. tb* ManLAM over time, as a measure of stability. MVN remained stable at 4°C for over 100 days with minimal decreases in binding affinity after 70 days (**Figure 8A**). Furthermore, MVN that was stored at RT for two weeks showed no evidence of degradation during the course of the experiment (**Figure 8B**).

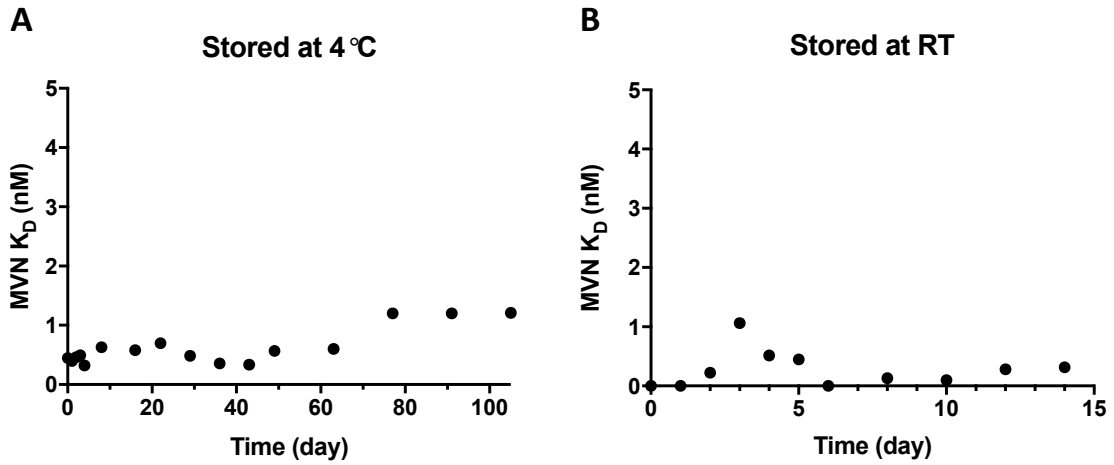

Figure 8. A) MVN stability study where binding experiments were performed for 100+ days on MVN stored at 4°C. Binding affinity starts to decrease after 70 days. **B)** MVN stability study performed for 2 weeks on MVN stored at room temperature (RT). No decrease in binding affinity is observed over this time period.

Discussion

Antibodies, both polyclonal and monoclonal, are the foundation of biomarker-based assays for TB; however, shortcomings exist with both types of antibodies. Previous work has shown no appreciable binding to ManLAM for anti-LAM polyclonal antibody matrices when tested with BLI.[105] This could be caused by the immobilization of non-specific antibodies on the biosensor, which would skew the global binding data. Further, this observation substantiates the argument that polyclonal antibodies are not ideal for employment in quality-controlled assays for the detection of ManLAM. In this work, seven monoclonal antibodies were tested for binding to *M. tb* ManLAM, *M. leprae* ManLAM, and *M. smegmatis* PILAM. The BLI results indicate that none of the antibodies were capable of specifically distinguishing between the different variants of LAM. This result is in agreement with studies that have mapped binding of the anti-LAM antibodies to the polysaccharide backbone of the LAM molecules, which is conserved between the different variants.[74,102]

In contrast, MVN was found to bind to *M. tb* and *M. leprae* ManLAM, but not to *M. smegmatis* PILAM. This result was expected as MVN is known to bind selectively to Manα-(1,2)-Man linkages, which are present in the mannose caps of ManLAM.[97] The difference in binding affinity of *M. tb* ManLAM versus *M. leprae* ManLAM is attributed to variation in the number of mannose capping residues. *M. tb* and *M. bovis* ManLAM express seven to nine mannose caps per ManLAM molecule, while *M. leprae* ManLAM averages only two.[51,52]

Additionally, the high affinity and specificity of MVN to ManLAM affords the ability to discriminate between pathogenic mycobacteria, which express ManLAM on the surface of the bacteria, and non-pathogenic mycobacteria, which express either

PILAM or AraLAM.[44] Therefore, non-TB pathogenic mycobacterial species, such as *M. bovis* and *M. leprae*, would also be detected by MVN, although *M. leprae* ManLAM is detected at a lower affinity as discussed above.[53] However, this binding would not limit the use of MVN in a diagnostic test. Coupling symptomatic investigation with a MVN-based diagnostic would allow medical staff to differentiate between pathogenic mycobacterial infections as most ManLAM-presenting pathogenic bacteria either cause cutaneous infection or pulmonary TB (lung infection).[53] Mycobacteria that cause cutaneous infections, such as *M. leprae*, induce illness that can be differentiated from *M. tb* empirically based on signature skin sores or lesions; therefore, they can be readily diagnosed without the need for ManLAM tests.[53] Additionally, it is unnecessary to differentiate between pulmonary TB causing species, such as *M. bovis*, because they have the same or very similar treatment strategies to *M. tb* infection.[106] Hence, screening tests would not need to further differentiate between pathogenic mycobacteria infections to permit proper treatment and avoid subjecting non-TB infected individuals to long durations of anti-TB therapy that can cause a host of potential side effects.

In traditional “sandwich” style *in vitro* assays, like ELISAs and LFAs, orthogonal binding pairs are employed to capture and detect biomarkers of interest. Pairing MVN with an orthogonal, high-affinity ManLAM capture element is therefore needed to detect ManLAM in these formats. BLI was used to screen the seven monoclonal antibodies to identify an orthogonal binding pair with MVN. It was found that Ab25, Ab28, Ab170, Ab194, and FDX01 were capable of acting as an orthogonal ManLAM binding agent in the binding pair, while CS35 and CS40 were eliminated due to non-specific binding between the antibodies and MVN. MVN was not investigated as a self-binding pair (i.e. using MVN as both capture and detection elements) as MVN is known

to bind to HIV-1.[75] A MVN self-binding pair could display cross-reactivity with HIV-1, which would compromise the assay's specificity and sensitivity for *M. tb* ManLAM due to the high co-morbidity of HIV with TB.[97] Alternatively, when using MVN in a binding pair with an anti-LAM capture antibody, the antibody would provide specificity for the LAM backbone thereby eliminating cross-reactivity with HIV, while MVN would detect only ManLAM molecules among the captured LAM variants.

Lastly, MVN has several advantageous biophysical properties for use in an analytical tool; it was expressed with a N-terminal hexa-histidine affinity tag and has a single intrinsic lysine residue, which lends itself to facile bioconjugation techniques. Conjugating biotin to this residue enables the immobilization of MVN to any streptavidin coated substrate.[75,107] Further, previous results have shown that conjugation to biotin does not block ManLAM-binding by MVN.[105] Stability is an important parameter for the utility of protein-based capture reagents. Importantly, the thermal stability of MVN at room temperature will limit the need for cold-chain transportation of MVN-based point-of-care tests to remote clinic sites in developing countries, further improving the accessibility of MVN-based point-of-care diagnostic tests. Another practical advantage to using MVN is that, like *in vitro* monoclonal antibody production, MVN can be produced via vector-based expression in *E. coli*, which can be readily scaled up in industrial bacterial bioreactors and is resistant to batch-to-batch variation. Furthermore, the stable expression of MVN in *E. coli*, a bacterium that multiplies every 20 minutes and easily tolerates incubation and protein expression at lower temperatures (e.g., 18°C), means that MVN can be produced in large quantities at a significantly lower cost than recombinant proteins that have to be expressed in mammalian cells. In turn, the lower cost of production of MVN will

translate to a lower cost per assay, which is crucial to ensuring the successful rollout in developing countries.

Conclusions

Point-of-care diagnostic tests for the detection of the TB biomarker ManLAM in urine play an increasingly important role in TB detection. The lectin MVN was employed as the molecular recognition element to selectively probe the structure of ManLAM versus other variants of LAM. Previous reports detail this lectin's high affinity and specificity for the Manα-(1,2)-Man linkages, but this is the first report that exploits this binding for the detection of the TB biomarker ManLAM. BLI experiments showed that MVN has sub-picomolar binding affinity against ManLAM and stringent selectivity as it was shown that MVN does not bind PILAM, a variant of LAM found on non-pathogenic mycobacteria. In contrast, the employment of anti-LAM antibodies that bind to the polysaccharide branches of both ManLAM and PILAM leads to cross-reactivity. Taken together with the other advantageous properties of MVN (ability to form an orthogonal binding pair with anti-LAM antibodies, ease of production, and long-term stability at 4°C), MVN is an ideal molecular recognition element for the development of analytical tools to study the structure of ManLAM.

Acknowledgements

I am so grateful for Dr. Westley Bauer and Dr. Leshern Karamchand who began this work and were essential to its advancement. I would also like to thank Dr. Carole Bewley (Laboratory of Bioorganic Chemistry, NIDDK, National Institutes of Health) who kindly provided the MVN-pET15b plasmid, the Vanderbilt Antibody Protein Resource Core for the expression of MVN, Stephanie Pearlman for assistance with the characterization of MVN, and the Foundation for Innovative New Diagnostics for supplying the anti-LAM antibodies. This chapter is based on work supported by the "A Prototype Diagnostic Device for Rapid, Sensitive and Direct Identification and Quantification of Mycobacterium Tuberculosis at Point-of-Care in Low Resource Settings" grant from the University of Cape Town/South African Medical Research Council, the National Science Foundation Graduate Research Fellowship program under Grants DGE-1445197 and DGE-1937963, and the National Research Foundation of South Africa (NRF) under Grant SFP150729132726 and Grant 64760.

Chapter III

Development of a specific lipoarabinomannan detection assay using microvirin-N[d]

Introduction

Conventional TB diagnostic tests rely on resource-intensive nucleic acid amplification, such as the Xpert MTB/RIF test, or technologies that lack specificity and sensitivity, such as sputum smear microscopy and chest radiography. Moreover, the diagnostic accuracy of these techniques is further impaired in patients with HIV coinfection, many of whom cannot produce the required sputum sample.[8,15,108] Globally, the use of biomarker-based diagnostic testing for TB is increasing and many countries are phasing out the use of smear microscopy and chest radiography. Typically, these tests are lab-based, such as ELISAs, or point-of-care, such as LFAs. In an ELISA, a molecular recognition element is first immobilized to a solid support (typically a microplate).[109] Then, the sample is added, and the biomarker binds to the immobilized molecular recognition element.[109] Lastly, an orthogonal molecular recognition element with a detection moiety, often HRP, is added.[109] If the biomarker of interest is not present in the sample, the orthogonal molecular recognition element cannot bind and no signal is generated.[109]

[d] Portions of this chapter were reproduced from Ref. 105 with permission from the Royal Society of Chemistry.

In a LFA, the sample flows down a cellulose membrane and first encounters a conjugate pad, which contains the detection element. This detection element is typically a gold nanoparticle conjugated to a molecular recognition element specific to the biomarker of interest.[110] The sample flows laterally along the nitrocellulose strip until it reaches the test line, where an orthogonal molecular recognition element simultaneously binds to the biomarker, following the classic sandwich assay format described above.[110] The aggregation of gold nanoparticles at the test line creates a visual signal that is indicative of a positive result.[110] Lastly, the sample reaches the control line, where the gold nanoparticle conjugate binds directly - regardless of the presence of biomarker - as a test control.[110] LFAs are simpler and faster than ELISAs, but are not capable of quantitation to the same degree as ELISAs.

In this study, MVN was utilized in a ManLAM detection test to specifically bind the Manα-(1,2)-Man linked mannose caps of ManLAM with sub-picomolar binding affinity.[75,82,88] By developing a “sandwich” pairing of MVN with a monoclonal antibody that binds an orthogonal hexa-arabinoside motif located in the branches of LAM, a highly specific detection test for ManLAM was developed. The detection limit and cross-reactivity of the resulting assay were compared to the Alere LFA and an in-house antibody-based ELISA.

Materials and Methods

Bioconjugation procedures

MVN (1.36 mg/mL) was conjugated to biotin using a 20x molar equivalence of EZ-Link NHS-PEG$_4$-Biotin (Thermo Scientific: Cat. No. 21329) in DI water. Following

a 30-minute incubation step at room temperature, the MVN-biotin conjugate was purified from excess biotin reagent using a 7k MWCO Zeba desalting column (Thermo Scientific: Cat. No. 89883). The concentration of the resulting MVN-biotin conjugate was determined by micro-volume analysis using a BioTek Take3 plate on a BioTek Synergy H4 plate reader with the lysozyme setting.

FIND Ab25 and Ab28 were conjugated to HRP using EZ-Link Plus Activated Peroxidase (Thermo Scientific: Cat. No. 31489). The single-use aliquot was dissolved in DI H_2O and the resulting solution was added to each antibody, followed by sodium cyanoborohydride. The reactions were incubated for 1 hour at room temperature. Quenching buffer was added and allowed to react for 15 minutes. The resulting antibody-conjugates were transferred to an Amicon Ultra-0.5 mL Centrifugal Filter Ultracel - 100K spin filter (Millipore Sigma: Cat. No. UFC510024) and centrifuged for 10 minutes at 14,000 x*g*. The spin filters were washed three times with PBS then inverted into new collection tubes and centrifuged for 2 minutes at 1,000 x*g*. The concentration of the antibody-conjugate was determined by microvolume analysis using a BioTek Take3 plate with the IgG setting.

MVN-based plate ELISA

Solutions (100 μL) of 1.3 μg/mL MVN were added to an Immulon 2HB clear flat-bottomed 96-well plate (ThermoFisher: Cat. No. 3455), sealed, and shook for 1 hour at room temperature. Wells were washed three times with PBST (PBS, 0.1% Tween 20). 5**%** BSA PBST (235 μL) was added to the wells and allowed to incubate for 2 hours, followed by 3 washes with PBST. Next, ManLAM or PILAM spiked into buffer

(100 μL) was added to the wells, and the plate was allowed to incubate for 2 hours, followed by 4 washes with PBST. A solution (100 μL) of 0.5 μg/mL detection antibody Ab25 conjugated to HRP (conjugation described above) was added to the wells and allowed to incubate for 1 hour, followed by 5 washes with PBST. An aliquot of TMB One (100 μL , Promega: Cat. No. G7431) was added to each well and the plate was incubated on a shaker for 10 minutes while protected from light. Lastly, 2 M H_2SO_4 (100 μL) was added to each well to stop the reaction and the signal was measured by absorbance at 450 nm to the thousandths place on a microplate reader. All measurements were made in triplicate and outliers were removed by a Grubbs' test.

OB-ELISA

First, Dynabeads MyOne™ Streptavidin T1 beads (Invitrogen: Cat. No. 65601) were functionalized with MVN-biotin conjugate. MVN was conjugated to biotin as described above. The streptavidin beads were washed three times with PBS using a magnetic separation rack (Invitrogen: Cat. No CS15000). The MVN-biotin conjugate was added at a ratio of either 60 μg MVN per 1 mg beads (Bead 1, for experiments in buffer) or 30 μg MVN per 1 mg beads (Bead 2, for experiments in urine). The resulting mixture was incubated for 30 minutes at room temperature. The beads were then washed three times with PBS and blocked with excess D-biotin in PBS for 30 minutes. Lastly, the beads were washed three times with PBS and re-suspended in PBST (PBS, 0.1% Tween 20).

Solutions (100 μL) of ManLAM or PILAM in 0.1% BSA PBST or pooled human urine (Innovative Research: Cat. No. IRHUURE1000ML) were placed in a clear

uncoated flat-bottom 96-well plate. Then, 20 μg of Bead 1 or 40 μg of Bead 2 MVN-functionalized magnetic Dynabeads were added to each well, and the plate was sealed and incubated on a shaker for 30 minutes (**Figure 9A**). The beads were magnetically separated from the supernatant using a 96-well magnetic separation rack (EdgeBio: Cat. No. 57624) and washed three times with PBST. An equal volume of 1 μg/mL Ab25 conjugated to HRP in 0.5% BSA PBST (for experiments in buffer) or 2 μg/mL Ab28 conjugated to HRP in 0.5% BSA PBST (for experiments in urine) was added to the wells. The plate was incubated on a shaker for 30 minutes, followed by three washes with PBST. An aliquot of TMB One (100 μL) was added to each well containing beads and the plate was incubated on a shaker for 10 minutes while protected from light. Lastly, 2 M H_2SO_4 (100 μL) was added to each well to stop the reaction, and the signal was measured by absorbance at 450 nm to the thousandths place on a microplate reader. When capture and detection were performed simultaneously, the detection antibody was added to the samples prior to adding the magnetic beads (**Figure 9B**). Following a 30-minute incubation on a shaker, the beads were washed three times with PBST and TMB was added. The rest of the procedure was followed as described above. When larger volumes of urine were tested, the entire procedure was scaled accordingly.

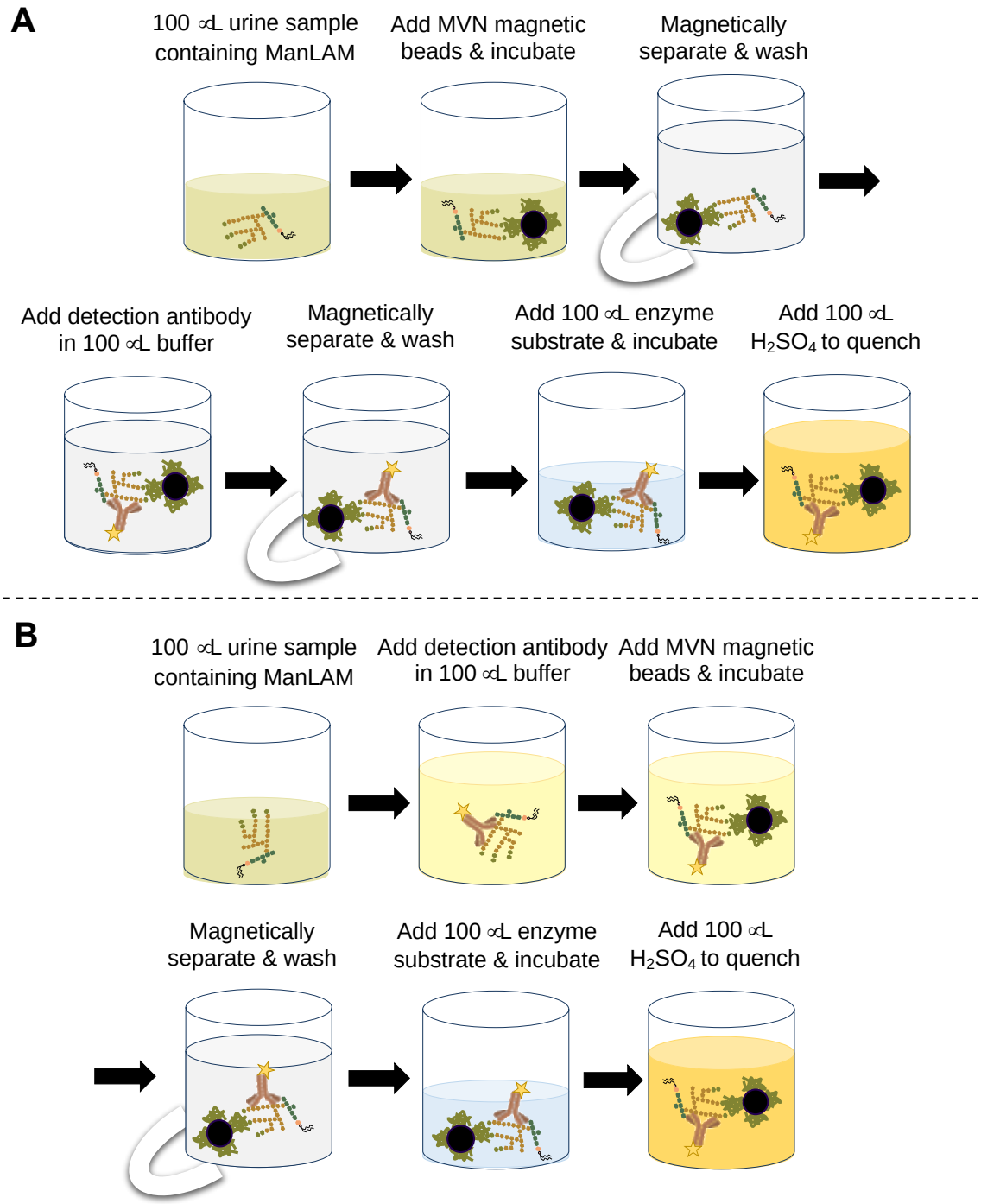

Figure 9. The MVN-based OB-ELISA can be performed with (**A**) sequential or (**B**) simultaneous capture and detection steps.

All measurements were made in triplicate and outliers were removed by a Grubbs' test. For measurements made in urine, the average signal of the blank was subtracted from raw absorbance values to correct for background. The LODs were calculated as $3SD_{blank}$/slope.

Alere LFAs

Alere LFAs were performed according to the manufacturer's instructions – ManLAM or PILAM (60 μL) spiked into pooled human urine was applied to the Alere LFAs (Lot No. 170423) in triplicate. After 25 minutes, the LFAs were read visually and on the Qiagen ESEQuant LFR – Lateral Flow Reader to determine the test line area. LODs were based on visual interpretation of test lines.

Antibody-based plate ELISA

This assay was performed with the same procedure as the MVN-based plate ELISA with the following changes: 4 μg/mL Ab170 was used for the capture reagent, mock samples were made with ManLAM or PILAM spiked into pooled human urine, and 0.5 μg/mL Ab28 conjugated to HRP was used for the detection reagent. All measurements were made in triplicate and outliers were removed by a Grubbs' test. The LODs was calculated as $3SD_{blank}$/slope.

Results

Initially, a classic plate ELISA was developed to utilize the high affinity and specificity of MVN for ManLAM as demonstrated by BLI (Chapter II). In this assay, MVN was used as the capture agent and the anti-LAM antibody Ab25, conjugated to HRP, was used for detection due to literature precedent for the use of lectins as capture agents and the ubiquitous use of antibodies for detection.[111,112] Using solutions of ManLAM (at 32.5 ng/mL) spiked into buffer, the ELISA was optimized for the concentration of MVN used for capture and the concentration of anti-LAM antibody for detection. For MVN, it was found that a concentration of 1.3 μg/mL resulted in the highest signal-to-noise (**Figure 10A**). For the antibody, a concentration of 0.5 μg/mL produced marginally better results and was used moving forward (**Figure 10B**).

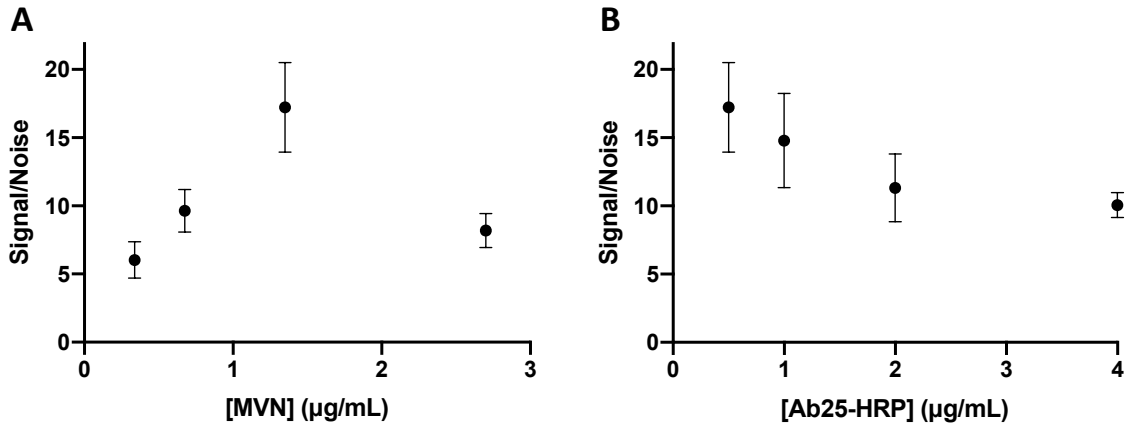

Figure 10. A) MVN concentration was optimized for the plate ELISA and 1.3 μg/mL was selected. **B)** Detection antibody concentration was optimized and 0.5 μg/mL was chosen.

However, early results showed that PILAM displayed strong signal on the MVN-based plate ELISA. This result contradicted the BLI results which indicated that PILAM does not bind to MVN and prompted further investigation. The plate ELISA was performed with and without MVN to determine if the signal was the result of PILAM binding to MVN or if it was non-specific signal. The results showed that PILAM (at 6.5 μg/mL) displayed signal regardless of the presence of MVN indicating that the signal was non-specific (**Figure 11**). Further, the signal-to-noise was increased when MVN was not present. On the other hand, ManLAM (at 65 ng/mL) only displayed signal in the presence of MVN, indicating a specific interaction.

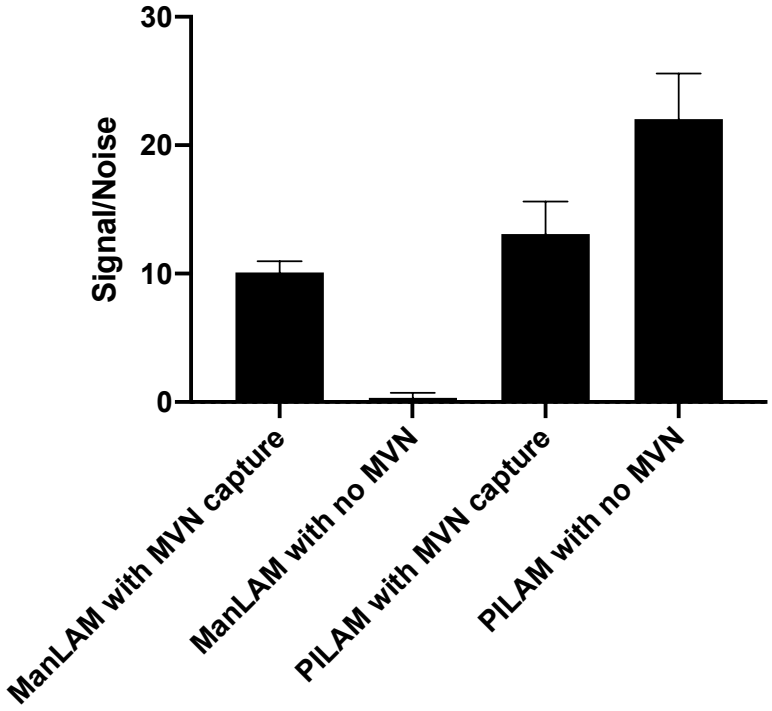

Figure 11. Results of MVN-based plate ELISA performed with and without MVN capture to determine if PILAM signal was due to specific capture by MVN or non-specific binding. With ManLAM, signal was only observed with MVN capture. For PILAM, signal was observed independent of whether a capture agent was used, indicating that PILAM binds non-specifically.

The conditions of the MVN-based plate ELISA were changed with the goal of decreasing the non-specific binding of PILAM. First, the blocking agent was changed from BSA to casein (both at 5% in PBST). Although this modification did result in a decrease of non-specific PILAM signal (at 6.5 μg/mL), it also resulted in a decrease in ManLAM signal (at 65 ng/mL) and, therefore, was not sufficient (**Figure 12A**). Next, different types of passive binding immunoassay plates were tested with the plate ELISA and the new blocking conditions. The assay had previously been performed

using the Immulon 2HB plate, which is considered a “slightly hydrophilic” plate.[113] A different “slightly hydrophilic” plate, MediSorp, was tested for comparison, as well as hydrophobic plates, Immulon 1B and PolySorp, and plates with a greater degree of hydrophilicity, Immulon 4HBx and MaxiSorp.[113] It was found that hydrophobic plates reduced the ManLAM signal while increasing the non-specific PILAM signal (**Figure 12B**). On the other hands, hydrophilic plates reduced the PILAM non-specific signal while increasing the ManLAM signal. Although this result marked a positive change, the ManLAM signal-to-noise was still lower than it had been when BSA and Immulon 2HB plate were used so other methods were pursued without implementing either of these changes.

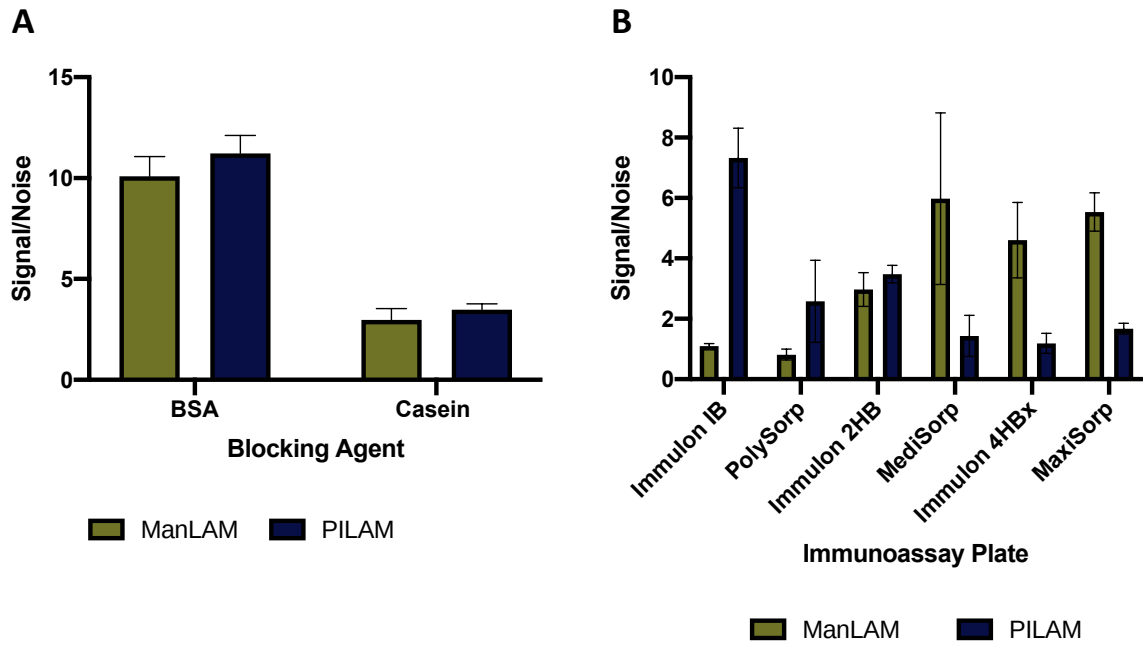

Figure 12. A) BSA and casein blocking were compared in the MVN-based plate ELISA. Casein was found to reduce both ManLAM and PILAM signals and, therefore, was not sufficient. **B)** The type of immunoassay plate was also explored to reduce non-specific PILAM signal. Previously, Immulon 2HB plates had been used. It was found that increasing the hydrophobicity of the plate (Immulon 1B and PolySorp) increased the degree of non-specific PILAM binding while increasing the hydrophilicity (Immulon 4HBx and MaxiSorp decreased the non-specific binding PILAM binding.

Following unsuccessful attempts to decrease non-specific PILAM signal with assay optimization, sample preparation methods to deplete PILAM were investigated. First, a standard curve of PILAM in buffer was pre-incubated in BSA-blocked wells and then the signal was assessed with the MVN-based ELISA. In this experiment, pre-incubation was not found to have a significant effect on the PILAM signal (**Figure 13A**).

Then, beads of different surface chemistries, including amine beads, carboxylate beads, Co-NTA beads, and silane beads, were explored for PILAM depletion by incubating solutions containing PILAM with beads and then assessing signal with the MVN-based plate ELISA. It was found that there was no significant difference in PILAM signal (at 13 μg/mL) for any bead type (**Figure 13B**).

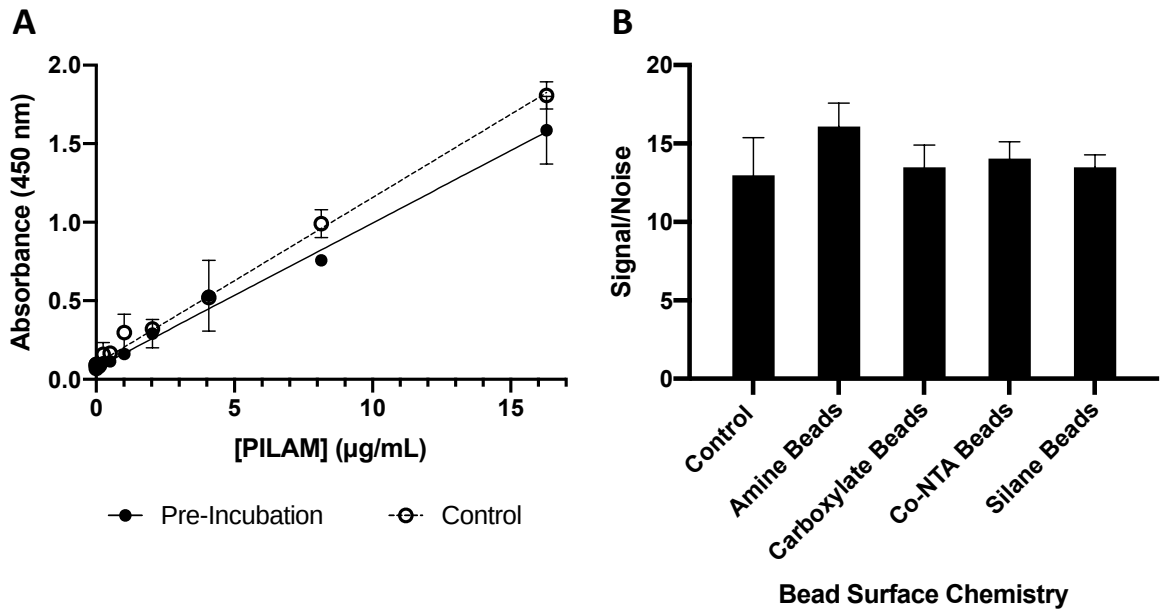

Figure 13. A) Pre-incubating in blocked wells had no significant effect on non-specific PILAM signal in the MVN-based plate ELISA. **B)** Depletion methods with beads were also unsuccessful in reducing non-specific PILAM signal.

The realization that PILAM does not bind to beads led to the development of an OB-ELISA using MVN-functionalized streptavidin beads to specifically capture ManLAM, followed by on-bead detection using an anti-LAM antibody. Initially, the OB-ELISA was developed using mock samples of ManLAM (at 65 ng/mL) spiked into

buffer. In this matrix, the concentration of detection antibody and the number of MVN-functionalized magnetic beads (loading density of 60 μg MVN-biotin per 1 mg beads) were optimized for the highest signal-to-noise when tested. For the detection antibody, it was found that there was no significant difference between 0.5, 1.0, and 2.0 μg/mL (**Figure 14A**). Future experiments were performed with 1.0 μg/mL detection antibody as it represents a moderate concentration with low variation and sufficient signal to noise. For the number of beads, it was found that 20 μg of beads resulted in the highest signal-to-noise (**Figure 14B**).

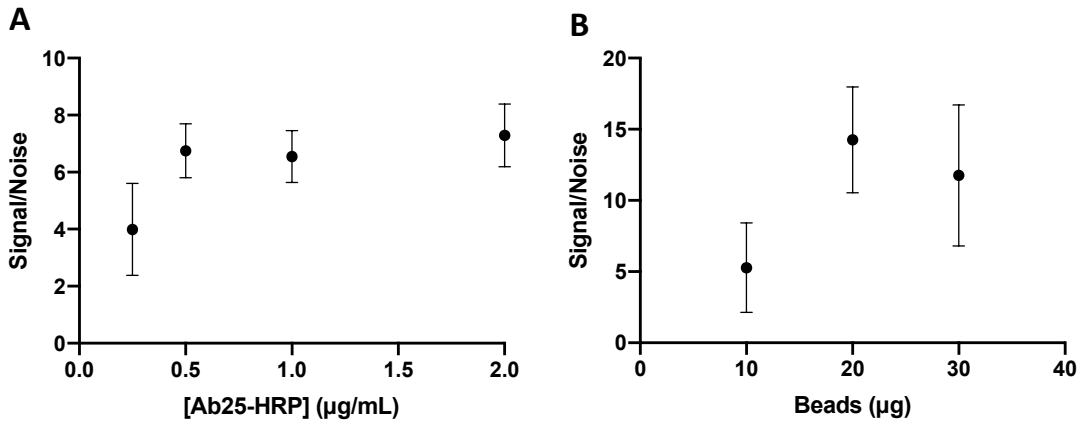

Figure 14. A) Detection antibody concentration was optimized for the OB-ELISA and 1.0 μg/mL was selected. **B)** Number of MVN-functionalized beads was optimized and 20 μg was chosen.

The optimized OB-ELISA was then tested with standard curves of ManLAM (n=15) or PILAM (n=8) spiked into buffer to determine the LOD for each biomarker. When tested with ManLAM, the OB-ELISA was found to have a LOD of 1.02 ng/mL

(**Figure 15A**). When tested with PILAM, the OB-ELISA was found to exhibit no signal for all concentrations tested (**Figure 15B**). In addition to the improvement in specificity with the OB-ELISA, the overall assay time was considerably shortened from ~7 hours to ~1.5 hours, in comparison to the plate ELISA.

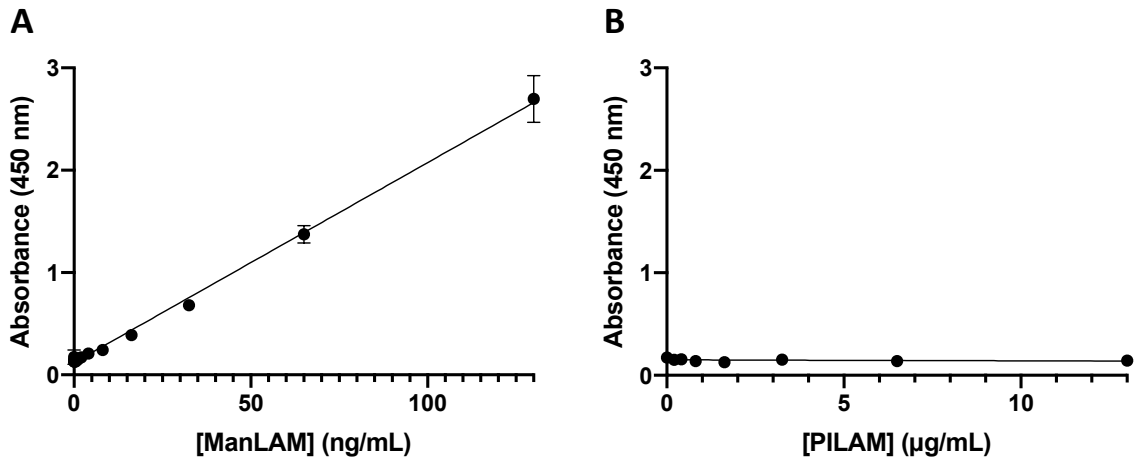

Figure 15. A) The LOD of the OB-ELISA was determined to be 1.02 ng/mL ManLAM in buffer. **B)** The OB-ELISA exhibited no signal with PILAM concentrations up to 13 μg/mL.

Following optimization in buffer, the OB-ELISA was tested with mock patient samples of *in vitro* ManLAM spiked into pooled human urine. The urine was pooled from multiple healthy donors and purchased from Innovative Research. Initial results were unsatisfactory compared to the performance of the OB-ELISA in buffer. Therefore, further optimization was performed. This included testing different assay formats, re-optimizing the detection antibody concentration, and exploring the interactions between bead mass, the loading density of MVN on the bead, and the

PEG spacer length for the biotin moiety on MVN. It should be noted that for the remainder of the experiments in this chapter, Ab28 was used for detection, rather than Ab25, due to supply constraints. First, an “all-in-one” OB-ELISA format was employed because it shortened overall assay time by 30+ minutes, bringing the overall assay time to under 1 hour, when compared to sequential capture and detection steps. Furthermore, the “all-in-one” format exhibited a slight improvement on the signal-to-noise ratio (at 65 ng/mL ManLAM) (**Figure 16A**). In parallel, the concentration of anti-LAM antibody was optimized for the highest signal-to-noise ratio and 2 μg/mL was chosen (**Figure 16B**). Lastly, the number of beads used, MVN loading density, and PEG spacer length were investigated simultaneously. Two different PEG spacers were investigated: PEG_4 and PEG_{12}. Bead 1 (previously used) was functionalized with 60 μg MVN-PEG_4-biotin per 1 mg beads and Bead 2 was functionalized with 30 μg MVN PEG_4-biotin per 1 mg beads. Beads 3 and 4 were functionalized at the same loading density as Beads 1 and 2, respectively, but with MVN-PEG_{12}-biotin. The interaction between loading density and number of beads was explored by using twice as many beads that were functionalized at 50% loading density (Beads 2 and 4). It was found that PEG_{12} reduced the ManLAM signal-to-noise (at 12.5 ng/mL) for both conditions tested (**Figure 16C**). Ultimately, 40 μg of Bead 2 was selected as it produced a high signal-to-noise ratio and low variability.

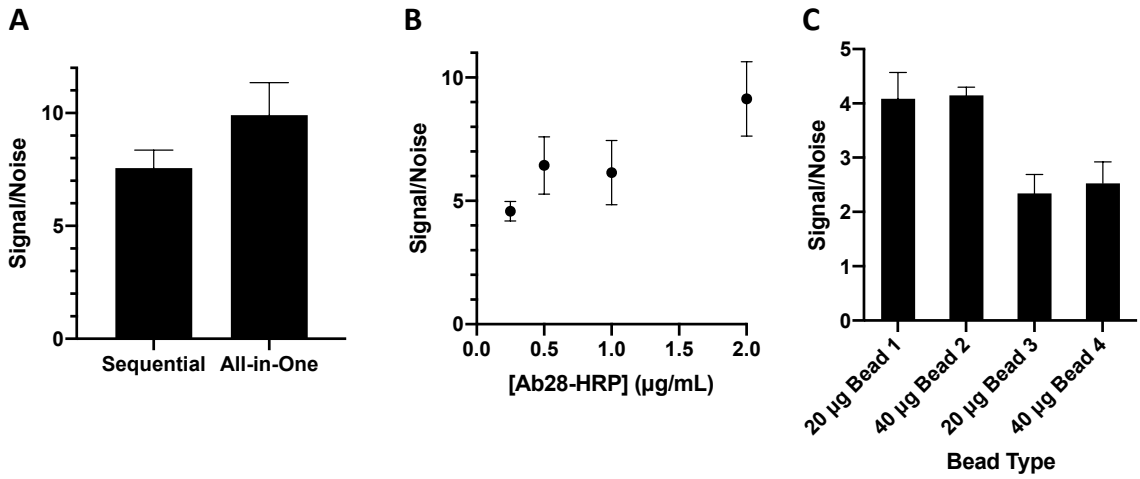

Figure 16. A) A sequential capture and detection format was compared to an all-in-one OB-ELISA format in mock samples made of pooled human urine. The all-in-one format was used moving forward as it had a slight improvement in signal-to-noise and reduced the assay time by 30+ minutes. **B)** Detection antibody concentration was re-optimized for the new matrix and 2 μg/mL was selected. **C)** The amount of beads used, MVN loading density, and PEG spacer length were investigated and 40 μg of Bead 2 (functionalized with 30 μg MVN PEG_4-biotin per 1

LOD experiments were performed for the OB-ELISA with the mock patient samples. A standard curve of *in vitro* ManLAM spiked into pooled human urine (n=7) was generated and the LOD was found to be 1.14 ng/mL (**Figure 17**). Importantly, no signal was observed when mock samples containing PILAM were tested, which demonstrates the specificity of our MVN-based assay exclusively toward ManLAM. Increased background noise was observed with the urine matrix so background-corrected data was used when plotting absorbance.

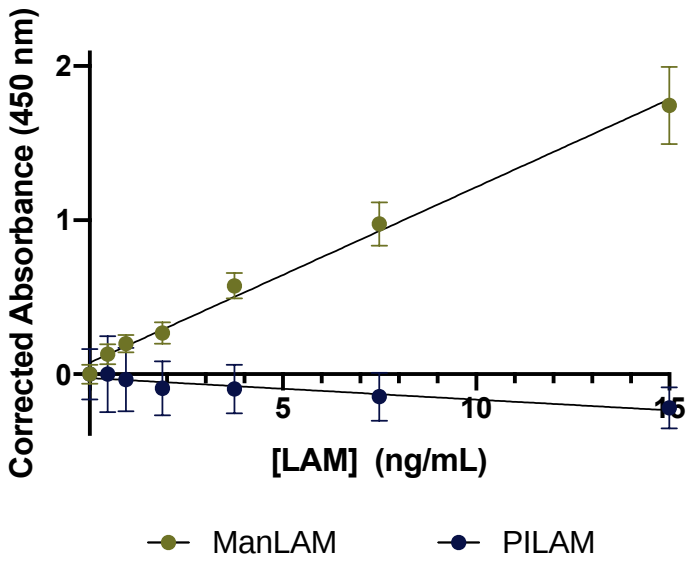

Figure 17. The LOD of the OB-ELISA was determined to be 1.14 ng/mL ManLAM in pooled human urine. No signal was produced when tested with PILAM.

The sensitivity and specificity of the OB-ELISA were compared to the Alere LFA by testing the LFA with mock samples consisting of *in vitro* ManLAM or PILAM spiked into pooled human urine. Both mock samples of ManLAM and PILAM produced noticeable test line signal, indicating that the Alere LFA is cross-reactive with PILAM, as expected based on the use of non-specific anti-LAM antibodies. The visual LODs were determined to be 1.25 ng/mL ManLAM and 0.625 ng/mL PILAM. Interestingly, more intense test lines (greater test line area signal) and a lower LOD were observed when the Alere LFAs were tested with PILAM (**Figure 18**).

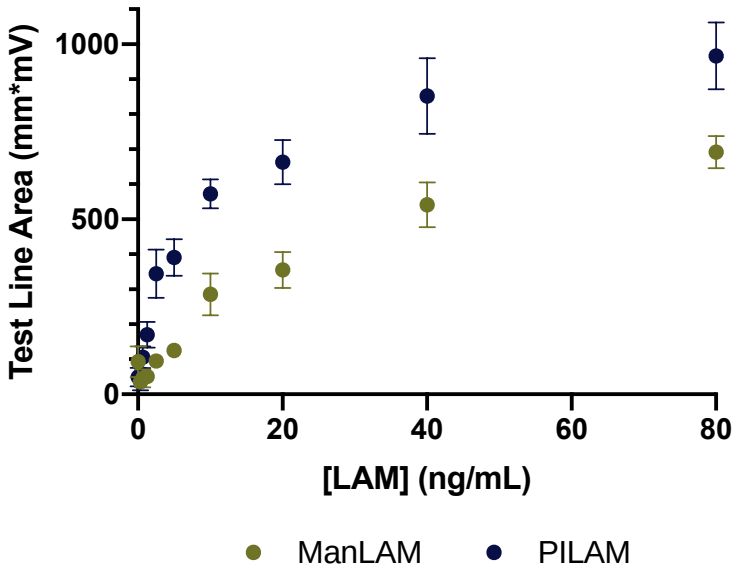

Figure 18. Standard curves of ManLAM or PILAM spiked into pooled human urine were tested on the Alere LFA and the intensity of the resulting test line was measured with a Lateral Flow Reader. Both ManLAM and PILAM produced detectable test lines on the Alere LFA, with PILAM producing a more intense test line at all concentrations tested.

For further comparison, a plate ELISA was developed that uses anti-LAM antibodies for both capture and detection. The conditions of the antibody-based plate ELISA were optimized, including the concentrations of the capture antibody, blocking agent, and the detection antibody. First, the concentration of the capture antibody Ab170 was varied (at 130 ng/mL ManLAM) and 4 μg/mL was chosen (**Figure 19A**). Secondly, the percentage of BSA in the blocking buffer was optimized (at 20 ng/mL ManLAM) and 1.25% was selected (**Figure 19B**). Lastly, the concentration of detection antibody Ab28 conjugated to HRP was optimized (at 20 ng/mL ManLAM) and 0.5 μg/mL was chosen (**Figure 19C**).

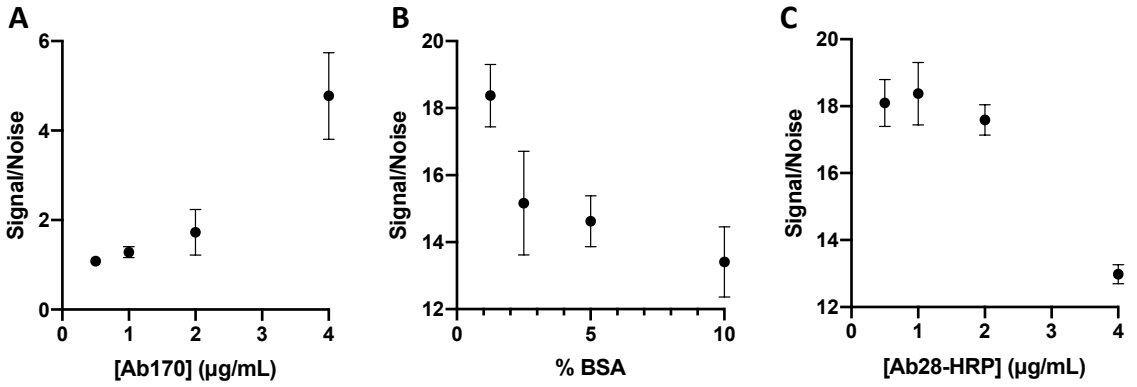

Figure 19. A) Capture antibody concentration was optimized for the antibody-based plate ELISA and 4 μg/mL was chosen. **B)** Percentage of BSA in the blocking buffer was optimized and 1.25% was selected. **C)** Detection antibody concentration was optimized and 0.5 μg/mL was chosen.

Standard curves of *in vitro* ManLAM and PILAM spiked into pooled human urine (n=8) were used to determine the LODs to be 729 pg/mL and 360 pg/mL, respectively (**Figure 20**). In line with the results of the Alere LFA, the antibody-based plate ELISA was found to be more responsive to PILAM than ManLAM.

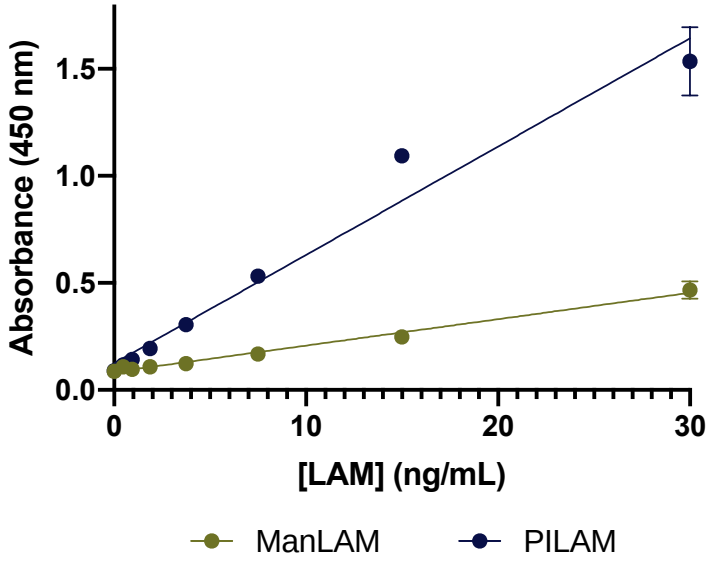

Figure 20. The LODs the antibody-based plate ELISA were determined to be 729 pg/mL ManLAM and 360 pg/mL PILAM in pooled human urine.

Lastly, larger urine sample volumes (250, 500 μL) were explored with the OB-ELISA to show that the signal (at 750 pg/mL ManLAM) can be increased through volumetric enrichment by increasing the amount of biomarker available (**Figure 21)**. However, the background signal increased with the sample volume, limiting the sensitivity of the assay for large-volumes. Clearly, this platform is capable of tolerating large volumes, but further work is required to realize the full potential due to the complex nature of urine.

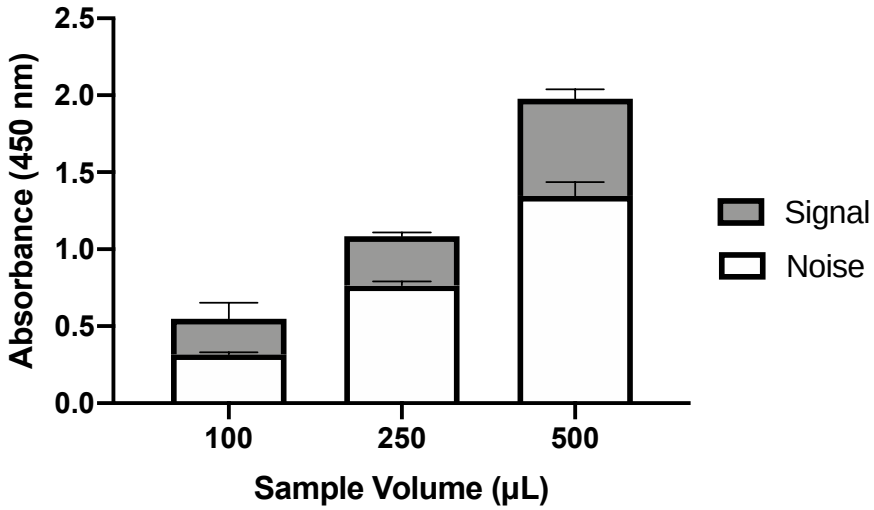

Figure 21. A) Larger urine sample volumes in the OB-ELISA increased the resulting signal; however, the noise increased as well. The area in gray represents the background corrected absorbance for each volume.

Discussion

An ELISA was developed to showcase the high-affinity ManLAM-binding of the novel molecular recognition element MVN. The sub-picomolar binding affinity of ManLAM to MVN made MVN an ideal capture reagent, while the ubiquity of antibodies as detection conjugates in ELISAs prompted the selection of an anti-LAM antibody as the detection conjugate.[112,114] Throughout this work, the specific anti-LAM antibody used for detection varied depending on the clone that could be procured.

Initial work focused on the development of a plate ELISA; however, this assay was found to display non-specific binding with the non-pathogenic PILAM variant, despite the observed specificity of MVN for ManLAM versus PILAM by BLI. Reassuringly, experimental evidence showed that PILAM bound non-specifically on

the plate ELISA, regardless of the presence of the capture agent MVN. This result relieved doubts regarding the specificity of MVN and prompted the re-optimization of the assay to reduce the non-specific PILAM binding. It was hypothesized that PILAM was interacting with either the blocking agent or the immunoassay plate as PILAM signal increased when MVN was not present. However, any modifications to either of these variables that was successful in reducing the PILAM non-specific signal was found to simultaneously decrease the specific binding of ManLAM. Interestingly, PILAM signal was found to decrease with more hydrophilic plates, contradicting the general trend of glycan binding increasing as hydrophilicity increases.[113] One possible explanation for this is that the blocking agents were able to immobilize more effectively to hydrophilic plates to prevent binding of PILAM, as the strength of immobilization of water-soluble proteins is known to increase with increasing hydrophilicity.[113]

Depletion approaches also failed to significantly reduce the non-specific PILAM signal. It should be noted that the PILAM concentration used for these experiments was extremely high in an effort to demonstrate the specificity of MVN for ManLAM by testing with 100-fold greater concentrations of PILAM. However, the high PILAM concentration may have been the reason why the depletion approach failed. Results indicated that PILAM must bind to either the blocking agent or immunoassay plate, but pre-incubation in blocked wells did not reduce background signal. It is possible that the blocked well was saturated with the high concentration of PILAM and, therefore, a significant decrease in signal was not observed.

The failure of bead-based depletion approaches prompted the development of an OB-ELISA for the specific detection of ManLAM. As with the plate ELISA, MVN was selected as the capture agent, and an anti-LAM antibody was used for detection. The

capture bead was generated by loading streptavidin magnetic Dynabeads with biotinylated MVN.[21] It is noteworthy that MVN has an approximately 10-fold lower molecular weight than IgG antibodies, which could result in a higher overall loading density of MVN. Further, for an equivalent bead surface loading density, the surface-bound MVN molecules would experience less steric hinderance and, hence, lower impairment on ManLAM-binding than the surface-bound anti-LAM IgG antibodies.

The OB-ELISA was successfully able to detect ManLAM spiked into buffer at a detection limit of 1.02 ng/mL and showed no signal when tested with PILAM, fulfilling the promised specificity of MVN based on BLI results. Notably, no signal was observed with 13 μg/mL PILAM, twice the concentration used to explore non-specific binding in earlier experiments. Clinical concentrations of ManLAM range from 10 to 1000 pg/mL for HIV- individuals and up to 100 ng/mL for HIV+ individuals.[41] Therefore, the assay was likely capable of detecting ManLAM in some HIV+ individuals with high bacillary loads but the sensitivity of the assay would need to be improved to be capable of detecting ManLAM in HIV- individuals. However, as these results were in a proof-of-concept matrix of spiked buffer, it was decided to switch to a more realistic matrix before undertaking further optimization to improve the sensitivity.

With this in mind, the OB-ELISA was tested with *in vitro* ManLAM or PILAM spiked into pooled human urine. Additional optimization was performed to improve the sensitivity of the assay in this matrix. Notably, the format was changed from sequential capture and detection steps, separated by bead washing with buffer, to a simultaneous all-in-one capture and detection step. This format was demonstrated by Markwalter, *et al.* for the simultaneous capture and detection of two malaria biomarkers on magnetic beads.[115] The simultaneous capture and detection format had a slight

increase in signal-to-noise but decreased both the assay time and number of wash steps by 50%. Additionally, the detection antibody concentration was doubled and twice as many beads with a 50% loading density of MVN were used to improve signal and decrease variability, respectively. These changes resulted in a LOD of 1.14 ng/mL for ManLAM.

For comparison, standard curves of ManLAM or PILAM spiked into pooled urine were tested on the Alere LFA, the only available ManLAM assay at the time. The visual LOD was determined to be 1.25 ng/mL ManLAM and 0.625 ng/mL PILAM, which are similar to the reported values of 500-1000 pg/mL.[116,117] The LOD of the OB-ELISA (1.14 ng/mL) falls in this range indicating it is equally sensitive. Importantly, the Alere LFAs detect both the pathogenic variant ManLAM and the non-pathogenic variant PILAM, while the OB-ELISA is specific for ManLAM. In fact, this non-specificity is described in the product literature from the Alere LFA, which states that the test "does not differentiate between the various species of mycobacteria."[118]

For further comparison, an antibody-based plate ELISA was developed to contrast the use of traditional molecular recognition elements (i.e., antibodies) to MVN. In this assay, anti-LAM antibodies were used for both capture and detection. As expected based on BLI results, this assay was capable of detecting both ManLAM and PILAM spiked into pooled human urine with LODs of 729 pg/mL and 360 pg/mL, respectively. It is hypothesized that the antibody-based plate ELISA is capable of detecting lower concentrations of PILAM than ManLAM due to the greater affinity of the anti-LAM antibodies for PILAM versus ManLAM as indicating by the BLI results in Chapter II. Further, this result is in agreement with the results of experiments with the Alere LFAs, which showed greater test line intensity and lower LODs for PILAM versus

ManLAM. Of note, the antibody-based assay displayed a slightly lower LOD for ManLAM (729 pg/mL) than the MVN-based OB-ELISA (1.14 ng/mL). This is attributed to the greater number of binding sites on the ManLAM arabinan branches for an anti-LAM antibody compared to the number of mannose cap binding sites for MVN. However, the MVN-based OB-ELISA has markedly improved specificity as no signal is observed when tested with PILAM.

As the LOD of the OB-ELISA still did not meet the goal of detecting ManLAM in the urine of HIV- individuals (with an upper range of 1 ng/mL), larger urine sample volumes (250, 500 μL) were investigated to determine whether the signal can be increased through volumetric enrichment by proportionally increasing the amount of biomarker available.[41,119] Large-volume urine samples are easily acquired - unlike other sample types (i.e. blood, sputum) - therefore, it would be feasible to use larger volumes of urine to improve the LOD of the OB-ELISA.[120] An increase in signal was observed with increasing sample volume; however, the background signal increased asl well. Thus, the maximum theoretical enhancement factor was not met at large sample volumes; when a 250 μL sample was used, the corrected absorbance was enhanced by a factor of 1.4 compared to a theoretical enhancement of 2.5 and when a 500 μL sample was used, the corrected absorbance showed enhancement by a factor of 2.7 compared to the theoretical enhancement of 5. This is likely due to the complexity of urine as a sample matrix. Investigating large volume samples using this method has been shown to have potential for further increasing the sensitivity of this assay, but has also proven to have some unexpected challenges. Further investigations will be reserved for future work, as it remains outside of the scope of the current project.

Conclusion

In this chapter, an OB-ELISA was developed that demonstrates the utility of MVN to selectively detect *in vitro* ManLAM in urine samples. As expected based on the BLI results, the assay exhibited a clear specificity for ManLAM compared to PILAM, with a LOD of 1.14 ng/mL ManLAM. This value falls between the LODs of an in-house antibody-based plate ELISA (729 pg/mL) and the commercially-available Alere LFA (1.25 ng/mL). It is important to highlight that the plate ELISA and Alere LFA lack specificity for ManLAM and detect all variants of LAM while the OB-ELISA is specific for ManLAM only. Additionally, the sample volume for the OB-ELISA can be scaled up to increase the assay signal and, theoretically, decrease the LOD. Thus, the potential MVN has as a highly-selective capture reagent for *in vitro* ManLAM in urine was demonstrated, paving the way for the development of vital tools for the detection of *in vivo* ManLAM.

Acknowledgements

I would like to thank Dr. Westley Bauer and Dr. Leshern Karamchand for their contributions to this work. I would also like to thank Dr. Carole Bewley (Laboratory of Bioorganic Chemistry, NIDDK, National Institutes of Health) for gift of the MVN-pET15b plasmid, the Vanderbilt Antibody Protein Resource Core for the expression of MVN, Stephanie Pearlman for assistance with the characterization of MVN, and the Foundation for Innovative New Diagnostics for providing the anti-LAM antibodies. This chapter is based on work supported by the “A Prototype Diagnostic Device for Rapid, Sensitive and Direct Identification and Quantification of Mycobacterium Tuberculosis

at Point-of-Care in Low Resource Settings” grant from the University of Cape Town/South African Medical Research Council, the National Science Foundation Graduate Research Fellowship program under Grants DGE-1445197 and DGE-1937963, and the National Research Foundation of South Africa (NRF) under Grant SFP150729132726 and Grant 64760.

Chapter IV

Detection of the lipoarabinomannan mannose capping motif in clinical urine with microvirin-N

Introduction

Due to the low concentration of ManLAM in urine, various enrichment processes have been designed and implemented as sample preparation methods for detection tests. As previously discussed, the concentration of ManLAM in the urine of TB-infected, HIV-negative individuals varies from approximately 10 to 1000 pg/mL with higher reported concentrations of ManLAM in HIV-positive individuals.[41] These concentrations were determined using a copper complex reactive dye within a hydrogel nanocage to capture and concentrate ManLAM before detection with an immunoassay.[41] The copper dye was found to have a high affinity for ManLAM, with a dissociation constant of less than 7 nM.[41] Further, elution could be achieved easily with a combined yield of 95% over both steps.[41] Ultimately, the capture method resulted in a 100- to 1000-fold increase in sensitivity depending on the volume of urine available for the test and the concentration factor.[41] Specifically, for a starting volume of 1 mL and a 100-fold concentration factor, the LOD was 14 pg/mL.[41] This low LOD allowed ManLAM to be detected in HIV-negative urine samples with a sensitivity of 96% and a specificity of 81%.[41] Further, this method resulted in an increase of knowledge regarding the presence of ManLAM in urine, including that co-infection with

HIV is not necessary for detection of urinary ManLAM, which would have been impossible to learn without the use of a concentration method.[41]

Other studies developed sample preparation methods to work in conjunction with preexisting diagnostics, such as the Alere LFA. Garcia, *et al.* combined a delipidation procedure and treatment with an α-mannosidase to remove terminal 2-linked mannose residues and achieve a ten-fold detection improvement in detection with the Alere LFA.[117] Another study used Amicon Ultra-0.5 mL centrifugal filters with a 3 kDA nominal molecular weight cutoff to concentrate ManLAM in the urine of HIV-negative individuals for detection using an electrochemiluminescence method.[121] With this method, the urine samples were concentrated 7-fold for a sensitivity of 66.7% and a specificity of 98.1% compared to a microbiological reference standard.[121]

In this study, this Amicon centrifugation filter concentration method was applied for use with the MVN-based OB-ELISA to determine whether the mannose caps are detectable on *in vivo* ManLAM with MVN. Reports have shown that G3, an antibody specific for the mannose caps, was unable to bind to *in vivo* ManLAM, despite promising results with *in vitro* ManLAM.[73] However, My2F12, a different antibody that targets the mannose caps, was able to bind to *in vivo* ManLAM, albeit with low sensitivity.[53] As the mannose capping motif is specific to ManLAM and represents a promising target for the specific identification of ManLAM versus other variants of LAM, this study constitutes an essential preliminary investigation into the molecule's structure in clinical samples.

Materials and Methods

Clinical subjects and samples

For this study, 58 urine samples were procured from the Foundation for Innovative New Diagnostics (FIND). These samples were previously collected from adults presenting at primary care sites in Cambodia, Peru, South Africa, and Vietnam with clinical symptoms of TB who had not yet been treated. Approval by local ethics committees and informed patient consent were obtained before enrolling the patients. No personally identifiable information was available to FIND or to the researchers. Urine and blood samples were collected at first contact with the patient and then centrifuged (at 200 x*g* at 4°C for 10 minutes), aliquoted, and frozen (at -80°C) on the same day (typically within 4 hours). Due to reports of variation in the processing protocols for samples collected under different studies, the centrifugation step was repeated before analysis.[73] Sputum samples (typically two in the first 24 hours) were also collected from participants, decontaminated, and tested in up to six independent liquid cultures (MGIT; BD, Franklin Lakes, NJ, USA) and solid cultures (Lowenstein-Jensen medium). The presence of the *M. tb* complex in cultures was confirmed by Ziehl-Neelsen staining or auramine O fluorescence microscopy to identify acid-fast bacilli. HIV-status was determined by an HIV rapid test. The characteristics of the study population is summarized in **Table 6**.

Table 6. Sex, age, and country of origin information for the study population stratified by TB- and HIV-status.

		TB-positive		TB-negative	
Category	**Number**	**HIV-positive**	**HIV-negative**	**HIV-positive**	**HIV-negative**
All subjects	58	16	18	12	12
Sex:					
Female	25	7	2	9	7
Male	33	9	16	3	5
Age:					
20 - 29	13	5	5	1	2
30- 39	16	5	3	5	3
40 - 49	13	4	3	4	2
50 - 59	10	0	6	1	3
60+	6	2	1	1	2
Country:					
Cambodia	2	0	2	0	0
Peru	14	2	4	1	7
South Africa	26	12	1	11	2
Vietnam	16	2	11	0	3

Urine sample preparation and testing

FIND samples were thawed and centrifuged for 10 minutes at 2000 x*g* at 4°C. The liquid fraction was used moving forward. A positive (4 ng/mL) and negative ManLAM control were made from an aliquot of pooled human urine and centrifuged following the same procedure. All urine samples and controls were added to separate 3kDa nominal molecular weight limit Amicon Ultra-4 Centrifugal Filter Units (Millipore Sigma: Cat. No. UFC800324). The centrifugal filter units were centrifuged with a swinging bucket rotor for 40 minutes at 4000 x*g* and the concentrated sample was recovered with a pipette. The volume of the concentrated sample was then measured, and the sample was diluted with DI H_2O for a 14-fold concentration factor. Lastly, the diluted samples were heated at 85°C for 10 minutes and the MVN-based OB-ELISA was performed as described in Chapter III, with FIND Ab194 used for detection due to supply constraints. A training video of this procedure was developed for use with collaborators (**Figure 22**). For each sample, the measured absorbance was normalized to the full process positive control run simultaneously to account for plate-to-plate variation.

Figure 22. Training video showing the procedure of the MVN-based OB-ELISA with the Amicon centrifugation filter urine concentration method (playable with Adobe Acrobat).

Statistical analysis

All statistical analysis was performed using GraphPad Prism version 9.0.0 (86) for macOS, (GraphPad Software, San Diego, California USA, www.graphpad.com). Box-and-whisker plots were created to show the median and interquartile range for populations stratified by HIV-status, country of origin, and sex. One-tailed Mann Whitney tests were used to compare the mean absorbance values of TB-positive and TB-negative samples overall and in different sub-populations to determine if mannose caps are detectable on ManLAM in TB-positive samples with MVN. Spearman's correlation coefficient was calculated to study the correlation between absorbance and age for TB-positive and TB-negative samples. Approximate age was calculated from

the YOB and day of enrollment, as age and day of birth information was not provided. Of note, this means all ages reported are ±1 year, but it is unlikely that it would change the general results presented.

Lastly, a receiver operating characteristic curve was produced based on the data to determine a cutoff for the OB-ELISA. Youden's J statistic and the Euclidian distance to the top-left corner were calculated for all points of the curve to determine the optimal cutoff value. The maximum value for Youden's J statistic was calculated to be 0.2353 for a cutoff value of 0.2611. This cutoff corresponded to a sensitivity of 24% and a specificity of 100%. The minimum distance was determined to be 0.6309 for a cutoff of 0.08516. This cutoff corresponded to a sensitivity of 68% and a specificity of 46%. The top-left cutoff was used moving forward as it balanced the trade-off between sensitivity and specificity. Using this cutoff value, sensitivity and specificity were calculated in each sub-population (HIV status, country of origin) with a 95% confidence interval calculated using a hybrid Wilson/Brown method. Positive and negative predictive values were not calculated due to the variation in TB prevalence by country.[122] Positive and negative likelihood ratios, as well as the diagnostic odds ratio, were calculated for each sub-population.

Results

Clinical samples were tested with the MVN-based OB-ELISA. Due to the low concentrations of ManLAM in urine and the high background with the large-volume OB-ELISA, the samples were concentrated using Amicon Centrifugal filters. 2-fold, 7-fold, and 14-fold concentrated pooled human urine were compared (**Figure 23A**). A

14-fold concentration factor was selected based on signal-to-noise. Then, a standard curve of 14-fold concentrated ManLAM spiked into pooled human urine (n=8) was used to determine the LOD, which was found to be 274 pg/mL (**Figure 23B**).

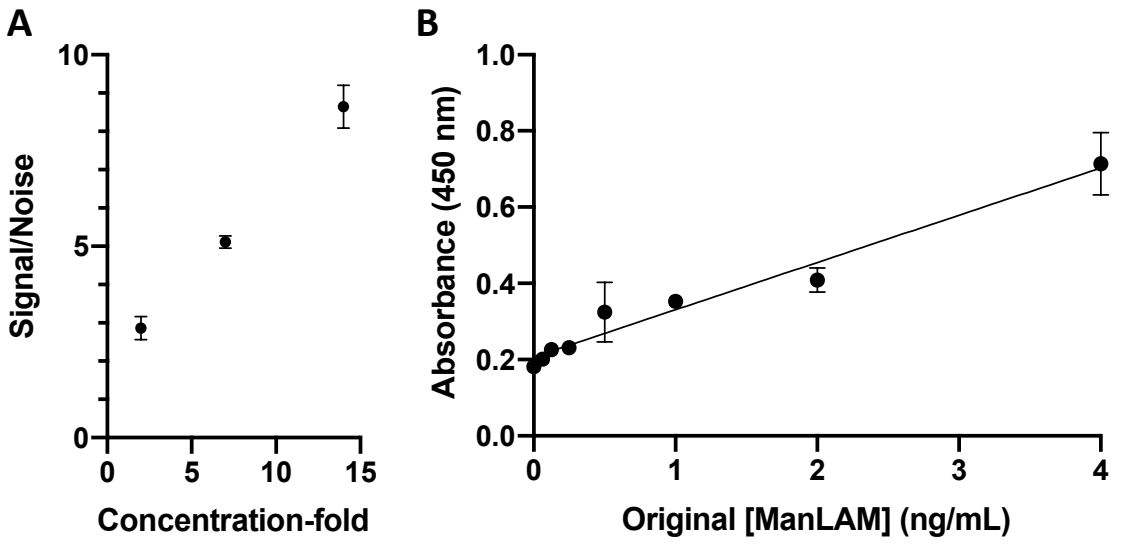

Figure 23. A) 2-fold, 7-fold, and 14-fold concentration factors were compared for the highest signal-to-noise. **B)** The LOD of the OB-ELISA on 14-fold concentrated mock urine samples was determined to be 274 pg/mL.

Next, clinical samples (n=58) were tested in 5 batches (**Table 6**). The samples originated from four countries: Cambodia (n=2), Peru (n=14), Vietnam (n=16), and Vietnam (n=16). Samples were defined as TB-positive if they had at least one positive culture. All of the TB-positive samples had positive microscopy results, as well. Additionally, samples were classified as HIV-positive (n=28) or HIV-negative (n=30) based on the result of an HIV rapid test. For each sample, the measured absorbance

was normalized to the full process positive control run simultaneously to account for plate-to-plate variation (**Figure 24**).

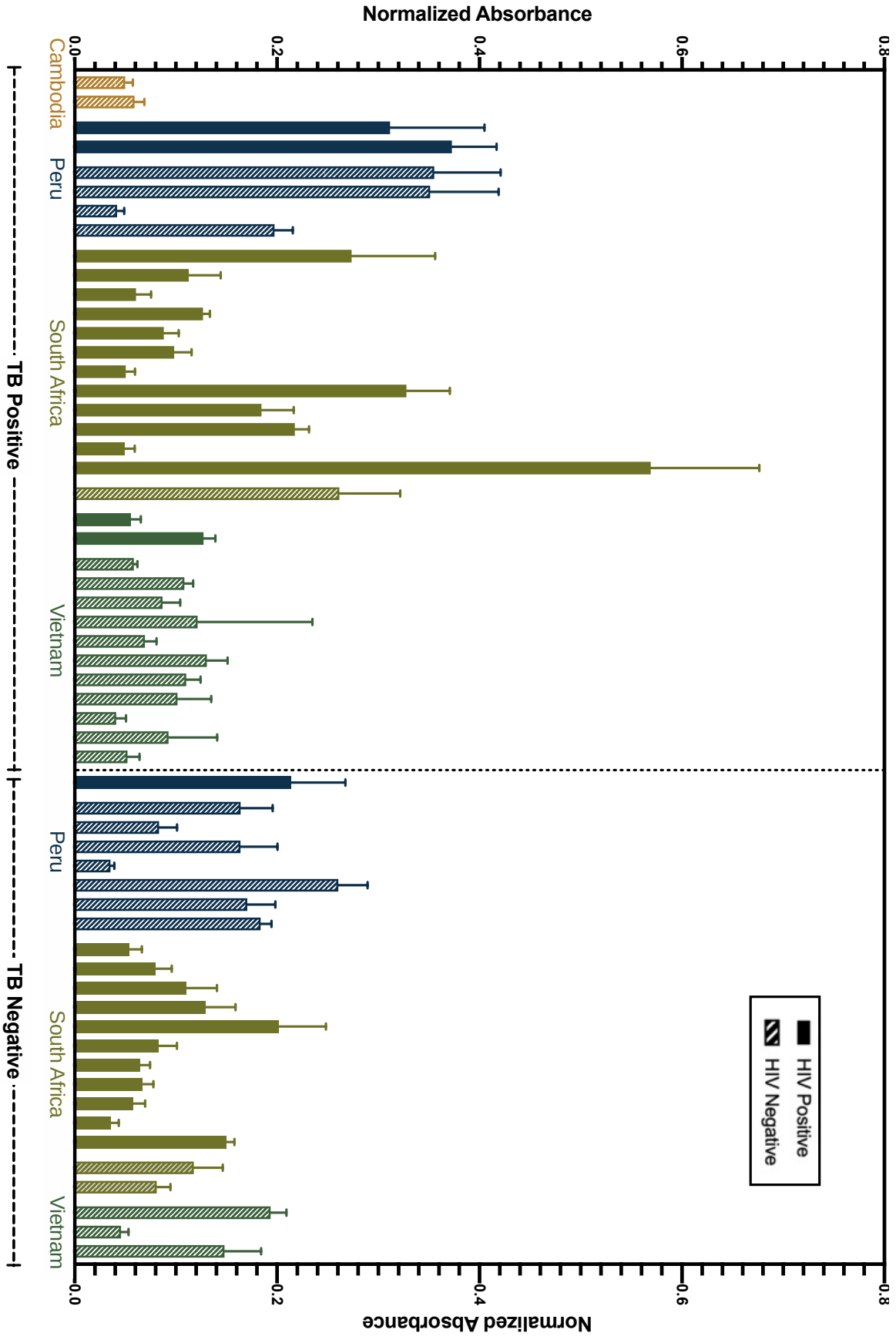

Figure 24. Normalized absorbance values for the 58 clinical urine samples.

Mann Whitney tests were performed to determine the difference between TB-positive samples and TB-negative samples (**Table 7**). First, TB-positive and TB-negative samples were compared, and no significant difference was found in the means (p value = 0.31). Then, the same analysis was performed on different sub-populations of the samples. There was also no significant difference between TB-positive and TB-negative samples for HIV-positive (p value = 0.080) or HIV-negative (p value = 0.22) samples. This was surprising as it is well-established that ManLAM concentrations are typically higher with HIV co-infection, resulting in increased detection ability in this sub-population.[41] However, a significant difference in the means of TB-positive and TB-negative samples from Peru was observed (p value = 0.030). No significant difference was observed in the means for samples from South Africa (p value = 0.051) or Vietnam (p value = 0.18). This analysis was not performed for samples from Cambodia as there were no TB-negative samples in that sub-population. Box-and-whisker plots were created to show the median and inter-quartile range for sub-populations by HIV-status and country of origin, as well (**Figure 25**)

Table 7. Mann Whitney test p values for the difference between the mean absorbance of TB-positive samples and TB-negative samples.

Population	n, TB-positive	n, TB-negative	P value
All	34	24	0.31
HIV-positive	16	12	0.080
HIV-negative	18	12	0.22
Peru	6	8	0.030
South Africa	13	13	0.051
Vietnam	13	3	0.18
Female	9	16	0.44
Male	25	8	0.35

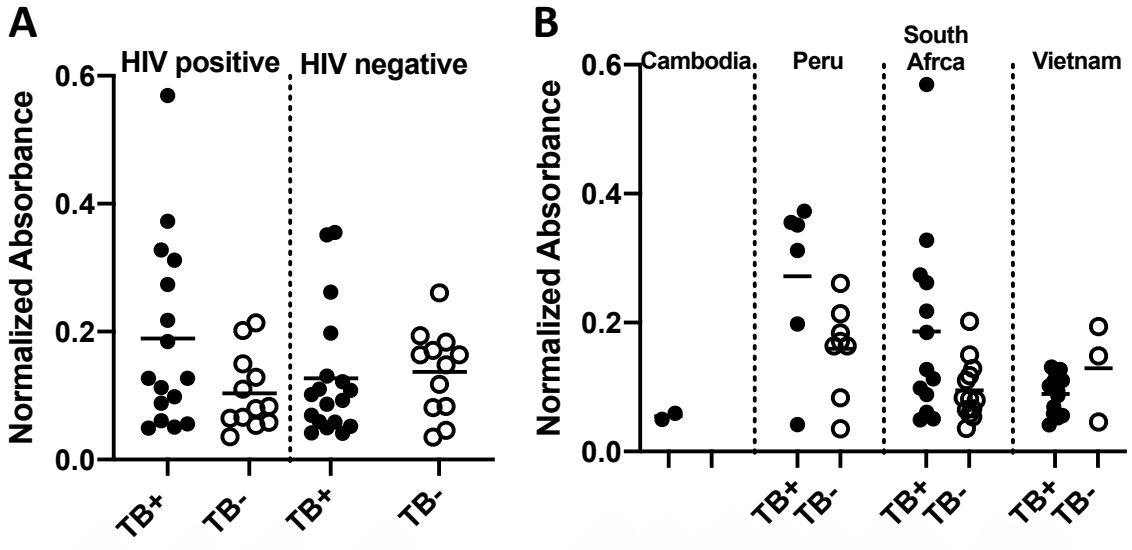

Figure 25. Box-and-whisker plots showing the median and interquartile range for different populations: **A)** HIV status and **B)** country of origin.

Association with biological sex and age was also tested. No significant difference was observed between TB-positive and TB-negative samples in female (p value = 0.44) and male (p value = 0.35) sub-populations by Mann-Whitney tests (**Figure 26A)**. Spearman's correlation coefficient was used to determine that there was no correlation between absorbance values and age for TB-positive (r = -0.10, p value = 0.57) and TB-negative (r = -0.044, p value = 0.84) samples (**Figure 26B**).

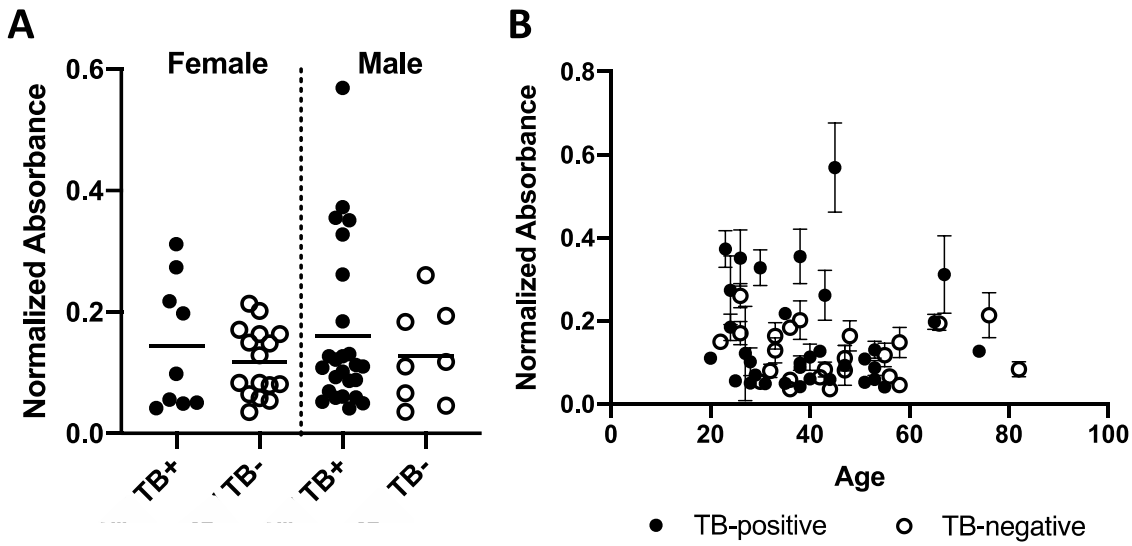

Figure 26. A) Box-and-whisker plots by TB-status and sex showing no association. **B)** Scatter plot showing no association between absorbance and age for TB-positive or TB-negative samples.

Lastly, the MVN-based OB-ELISA was studied as a diagnostic test for comparison to other methods. A receiver operating characteristic curve was produced based on all the samples and for each sub-population stratified by HIV-status and

country of origin (**Figure 27A**). For each of these curves, the area under the curve was determined as a measure of diagnostic performance; interestingly, the area under the curve was larger in every sub-population (**Figure 27B**).

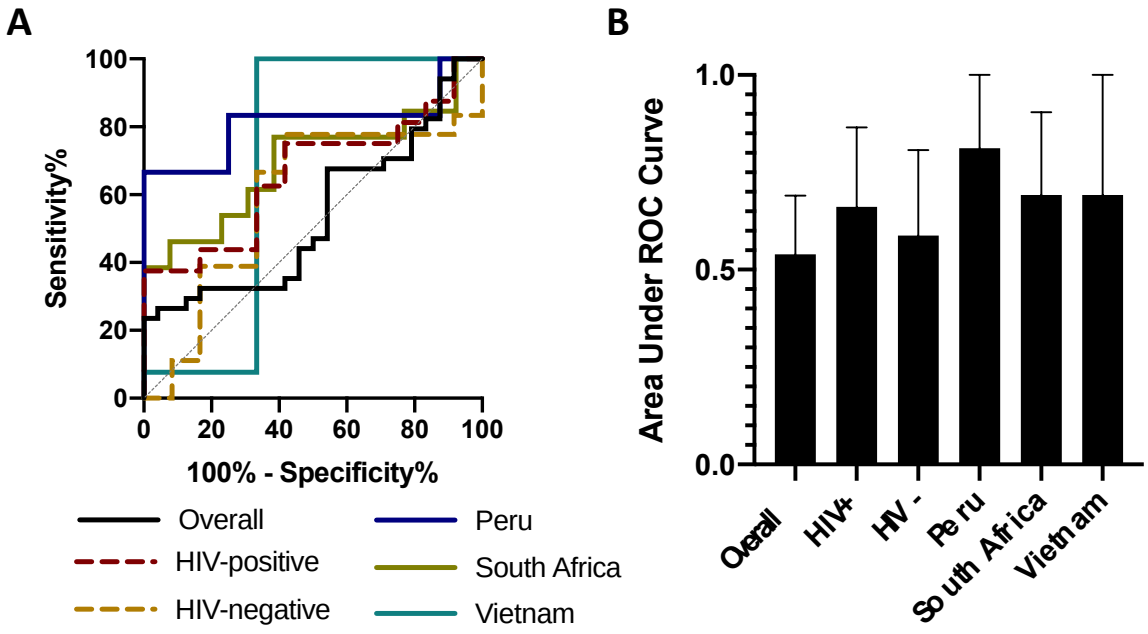

Figure 27. A) Receiver operating characteristic (ROC) curves for the clinical urine samples, overall and in sub-populations by HIV-status and country of origin. **B)** The area under the curve was determined for each ROC curve.

The overall receiver operating characteristic curve was used to determine a cutoff for the OB-ELISA, and a cutoff value of 0.08516 was selected Using this cutoff value, the sensitivity was determined to be 68% and the specificity was found to be 46% (**Table 8)**. In HIV-positive individuals, the sensitivity and specificity were slightly increased, while they were decreased in HIV-negative individuals. The sensitivity also

varied widely by country, with Peru having the highest value and Vietnam having the lowest. This trend was reversed for specificity. Lastly, the diagnostics odd ratio was calculated for each of these sub-populations as a means of comparing sensitivity and specificity simultaneously.[123] The overall diagnostic odds ratio was calculated to be 1.8. However, this value was increased in samples from South Africa (5.3) and in HIV-positive individuals (4.2). There was no significant difference in samples from Peru (1.7) and the diagnostics odd ratio was reduced in samples from Vietnam (0.80) and in HIV-negative individuals (0.79).

Table 8. Sensitivity, specificity, positive and negative likelihood ratios (LRs), and diagnostic odds ratio for all samples and sub-populations stratified by HIV-status and country of origin.

Population	Sensitivity	Specificity	Positive LR	Negative LR	Diagnostic odds ratio
Overall	68	46	1.2	0.71	1.8
HIV+	75	58	1.8	0.43	4.2
HIV-	61	33	0.92	1.2	0.79
Peru	83	25	1.1	0.67	1.7
South Africa	77	62	2.0	0.38	5.3
Vietnam	62	33	0.92	1.2	0.80

Discussion

Due to the low concentration of ManLAM in urine, an enrichment procedure

was developed and optimized before analyzing clinical samples. The LOD deceased from 1.14 ng/mL to 274 pg/mL, a 4-fold improvement. However, this did not meet the expectation of a 14-fold improvement in the LOD in line with the concentration factor. It is hypothesized that this moderate increase is partially due to biomarker loss during the centrifugation step. Despite this, it was reasoned that ManLAM could be detected in over 50% of TB-positive samples, regardless of HIV-status, based on this LOD and prior studies.[41] However, no significant difference was observed between mean absorbance values of TB-positive and TB-negative clinical samples.

There are many potential explanations for these results which will be explored from least to greatest impact. First, it is possible that MVN, like the mannose cap targeting antibody G3, is unable to detect *in vivo* ManLAM.[73] However, MVN is predicted to be more similar to the My2F12 antibody in terms on binding epitope.[74,82] As previously mentioned, both G3 and My2F12 were found to bind strongly to di-mannose capping motifs, but G3 exhibited a weak affinity for mono-mannose caps and My2F12 showed a weak affinity for tri-mannose caps.[74] MVN was found to bind to both di-mannose and tri-mannose structures, with a higher affinity for larger structures like the HIV glycan Man_9.[82] However, MVN has not been tested in a glycan array with LAM-specific structures, limiting further comparisons.

A second hypothesis is that the difference in binding results between the three molecular recognition elements is due to the clinical samples being tested. This study and the G3 antibody study both utilized urine samples from the Foundation for Innovative New Diagnostics. (FIND).[73] Further, the G3 study mainly tested samples from Peru, South Africa, and Vietnam, with a minor contribution of samples from Bangladesh.[73] Thus, there is likely considerable overlap in confounding factors

between the two studies. In contrast, the My2F12 study utilized samples from Georgia.[53] Specifically, the sample processing methods and storage conditions for these samples differ. The standard protocol for FIND is to centrifuge urine samples at 200 x*g* at 4°C for 10 minutes. In contrast, the samples used in the My2F12 study were heated at 95°C for 30 minutes in a drying oven.[53] However, in this study centrifugation was necessary to concentrate the samples to allow for ManLAM detection. Further, the arabinose backbone and MTX modifications have been detected after centrifugation weakening this hypothesis.[73] Another difference between the samples is storage temperature; FIND samples are frozen at -80°C, while the My2F12 samples were frozen at -20°C.[53] One study reported a roughly 50% loss of ManLAM detection by the Alere LFA after freezing for one day at -70°C.[124] A study with the Fuji-LAM test disagreed with this result, showing no loss after one month at -20°C.[125] However, it is possible that lower temperatures have a negative impact on ManLAM detection ability.

Additionally, the samples tested in this study, the G3 study, and the My2F2 study differed in geographic origin which could contribute to concentration differences in the ManLAM antigen. This hypothesis is supported by the observed variable results by country, with a significant difference in mean absorbance values only observed in Peruvian samples. Notably, this cannot be attributed to HIV as only 21% of all samples from Peru and 33% of TB-positive samples from Peru were HIV-positive. Previously reported differences in ManLAM concentration by geographic location, that cannot be explained by HIV status, were mainly attributed to the quality of the urine sample and glycosuria, which can be caused by diabetes..[126] However, information on diabetes status was not collected for these samples. Additionally, other risk factors – such as nutritional status, alcohol use, and tobacco use– have been shown to contribute to TB

progression, and thus ManLAM detectability.[127,128] Without more information, it is impossible to say whether these risk factors are causing the observed variation in ManLAM concentration.

Another explanation is that *in vivo* ManLAM could be endogenously modified in some populations contributing to geographic variation. De, *et al*. has hypothesized that "host enzymes either partially degrade the complex glycoform of ManLAM or modulate the structure of the sugars present at the caps that are characteristic of pathogenic strains of mycobacteria."[43] Human mannosidase enzymes in the endoplasmic reticulum and Golgi complex are capable of degrading the α-(1,2) mannose linkages in the HIV glycan Man_9.[129-135] Notably, the α-(1,2)-mannosidase-IA has been shown to preferentially degrade the Man_9 D1 mannose residue first, which corresponds to the MVN binding site on Man_9.[130,134] Further, these enzymes have been shown to be up- or down-regulated in response to disease state, including multiple sclerosis and various cancers.[136-138] However, no information was found regarding tuberculosis representing an area for further study. Interestingly, increased lysosomal α-mannosidase activity has been reported in people with diabetes, a common co-morbidity with TB.[139-141] Of the three countries of origin analyzed in this study, Vietnam has the highest prevalence of diabetes, which supports this reasoning.[142]

Lastly, epitope differences in ManLAM, particularly in the mannose caps or MTX residues, caused by pathogenic characteristics could explain the variable results by geography. Past results have shown that ManLAM epitopes vary in their discrimination performance by country.[126] One potential cause of ManLAM epitope differences is TB strain, which varies geographically.[121,143] Globally, the Euro-American lineage 4 is the most common, representing the dominant lineage in Georgia

(61.3%), Peru (79.6%), and South Africa (72.2%).[143] However, lineage 4 only represents 7.6% of the *M. tb* burden in Vietnam with the East Asian lineage 2 (37.4%) and Indo-Oceanic lineage 1 (24.9%) constituting the majority.[143] Reports from our collaborators have indicated significant variation in low molecular weight lipids between *in vitro M. tb* strains from lineages 2, 3, and 4 (J. Blackburn, personal communication, June 24, 2021). However, this lipidomic study did not attempt to detect ManLAM due the complexity of the molecule. In contrast, a separate mass spectrometry study of ManLAM was able to detect mannose caps and MTX modifications in a clinical sample from Peru and an *in vitro* lineage 2 strain; however, the relative abundance of various mannose cap structures varied between the two sources.[43] In my professional opinion, this hypothesis that the capping motifs or their relative abundance could vary by lineage is the most likely explanation of the observed geographic variation as ManLAM is known to be an extremely heterogenous molecule.[121] Further research into the exact binding site of MVN and the performance of the OB-ELISA by *M. tb* lineage is needed as this hypothesis could have important ramifications on the ability to diagnose TB with universal LAM detection tests.

Future Work

One area for future work is the development of an alternative sample preparation method. In this study, centrifugal filters were used to concentrate urine prior to analysis, but it is hypothesized that sample loss could be occurring during this step which could be limiting our detection ability in low concentration samples. However, this method demonstrated that it was possible to utilize a large volume urine sample without increased noise. This is attributed to filtration of molecules less than

3000 Da with the centrifugal filters. Thus, the goal of this future work will be to develop a method for removing small interferents that is compatible with the large-volume OB-ELISA method from Chapter III. Our lab has had great success with the use of immobilized metal affinity chromatography membranes to capture biomarkers from biological matrices.[144] In this method, a cellulose membrane is functionalized with divalent metal ions that bind to a His-tagged antibody.[144] In this case, the anti-LAM antibodies on the membrane would capture ManLAM in urine while allowing the interferents to flow through (**Figure 28**).[144] The antibody-ManLAM complex can then be eluted by competition with imidazole or chelation with EDTA.[144] MVN-functionalized beads will be added to the eluent to capture the antibody-ManLAM complex onto the surface of the bead, and the OB-ELISA would then be completed as normal. It is believed that this approach will enhance the sensitivity of the OB-ELISA to detect low concentration ManLAM urine samples, as well as ameliorate any potential centrifugation effects.

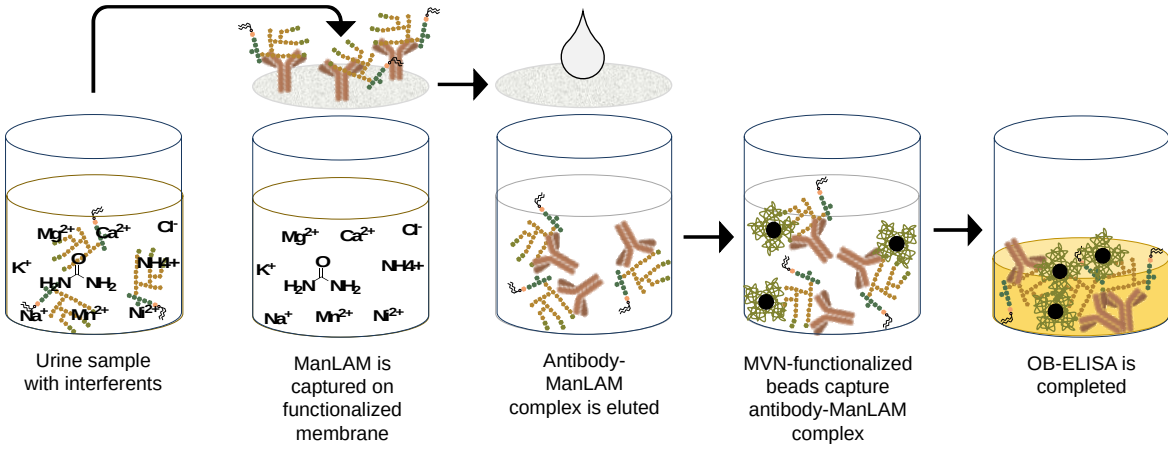

Figure 28. Workflow of the proposed membrane-based urine filtration method. An anti-LAM antibody functionalized membrane will be used to capture ManLAM from urine while the interferents flow through. The antibody-ManLAM complex can then be eluted from the membrane, captured with MVN-functionalized magnetic beads, and detected with the standard OB-ELISA protocol.

Secondly, the MVN binding epitopes on the ManLAM molecule will be thoroughly investigated with a glycan array study conducted by Dr. Todd Lowary at the University of Alberta.[74] The Lowary group is perfectly positioned to perform this study, as they have considerable experience synthesizing the complex structure of ManLAM and have previously developed a LAM-specific glycan array for studying the binding epitopes of anti-LAM antibodies.[74,145] Of particular interest will be the binding results with the mono, di, and tri-mannose capped tetra-arabinose structures with and without MTX modifications, as well as the mono- and di-mannose capped hexa-arabinose structures (**Figure 29**).[74] A more detailed understanding of MVN binding epitopes on ManLAM will allow the OB-ELISA to be utilized effectively as more

knowledge of the structure of *in vivo* ManLAM, generally and in specific groups, is obtained.

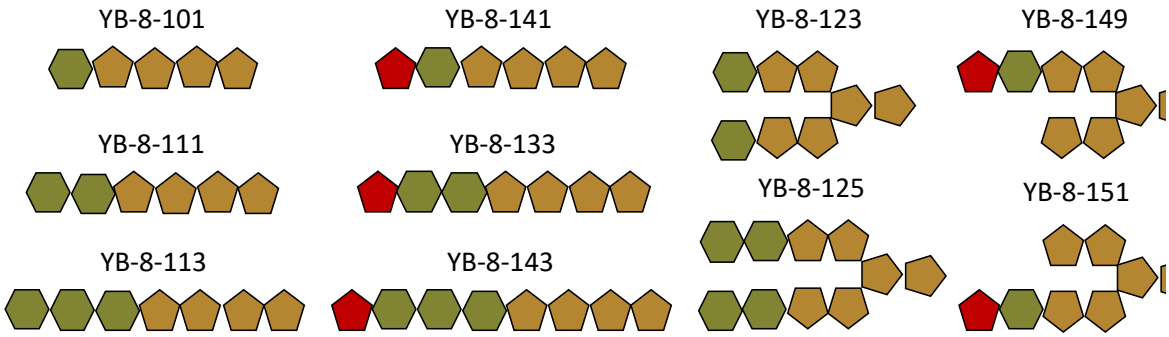

Figure 29. A subset of the ManLAM sub-structures that will be used to determine the MVN binding epitope in a glycan array study performed by Dr. Todd Lowary's group in Alberta, Canada. Figure adapted from Ref. 74.

Additional urine sample testing is needed to study the geographic variation hypotheses. This testing will be performed in conjunction with Drs. Valeria Rolla and Adriano Gomes at the Oswaldo Cruz Foundation in Rio de Janeiro and Dr. Jonathan Blackburn at the University of Cape Town, who have access to the primary patient samples needed to develop and evaluate the MVN-based OB-ELISA further. Based on the results of this pilot study, 18 samples per group are required to detect a significant difference between the groups at a 95% confidence interval with 80% power.[146] To allow further investigation of the effect of HIV-status on the results, we will stratify our groups for the Brazilian portion of the testing by HIV-status and CD4 count with 20 samples per sub-group (**Figure 30**). Additionally, we will test 20 urine

samples from non-tuberculosis mycobacteria infections to investigate the cross-reactivity of the assay. Originally, I was going to travel to Brazil to conduct a hands-on training session for the MVN-based OB-ELISA and to perform initial sample testing. However, this plan was modified due to the SARS-CoV-2 pandemic which resulted in global research shutdowns and travel bans. Training will now be conducted virtually, and the sample testing will be performed by researchers in the Gomes lab.

Further, Drs. Rolla and Gomes are part of the Regional Prospective Observational Research for Tuberculosis (RePORT) network with Vanderbilt University Medical Center. In addition to the Brazilian cohort, RePort has established cohorts in Indian and Indonesia. If testing in Brazil is successful, the MVN-based OB-ELISA could be tested in these other cohorts to study geographic variation. Further diversity will come from testing urine samples in South Africa. Dr. Blackburn has collected urine samples from Cape Town, Durban, and Johannesburg. These sites have different dominant *M. tb* lineages (lineage 2 in Cape Town, lineage 4 in Durban and Johannesburg) which will allow the performance of the assay by lineage to be studied. Expanding the geographic diversity of the samples tested will allow increased understanding of concentration and epitope differences.

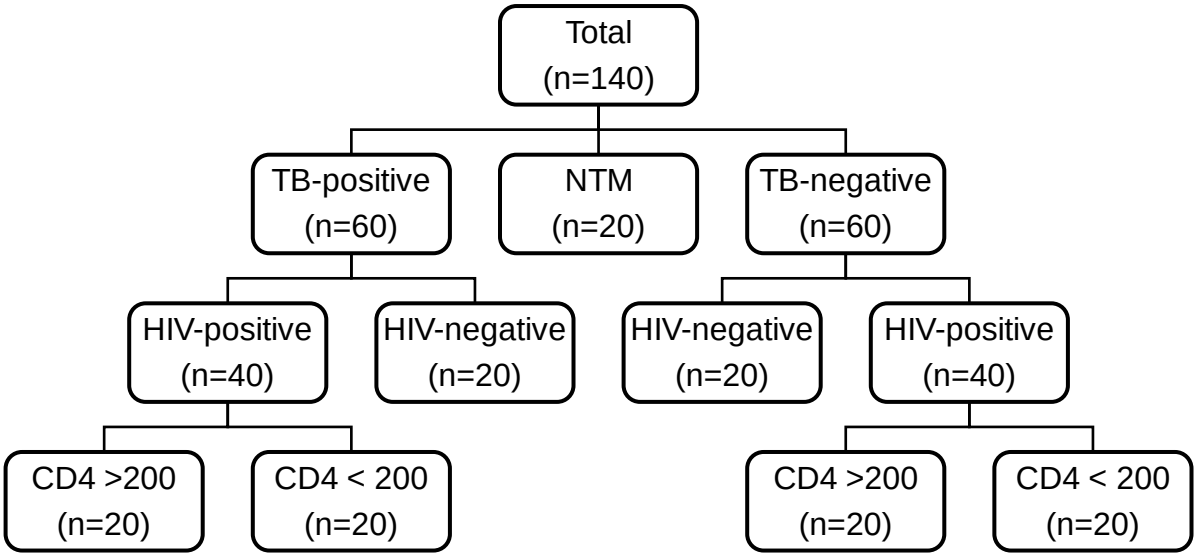

Figure 30. Tree diagram showing the groups and sample size for continued testing of the MVN-based OB-ELISA led by Drs. Valeria Rolla and Adriano Gomes in Rio de Janeiro, Brazil (NTM = non-TB mycobacterial infection).

Lastly, If it is determined that MVN cannot bind to mannose caps on *in vivo* ManLAM or to extend the reach of the OB-ELISA if geographic differences limit detection ability, the future work will be to optimize the assay for use in sputum samples. Mannose caps have previously been detected and studies have shown that there is a roughly 50-times higher concentration of ManLAM in sputum than in urine.[42,71] However, lower specificities have been reported for detected ManLAM in sputum, likely due to the cross-reactivity with molecules structurally similar to LAM.[57,147] The high selectivity of MVN for the mannose caps and prior success with magnetic bead-based LAM detection methods in sputum mark the MVN-based OB-ELISA as a promising avenue for the development of a more specific sputum-based

ManLAM detection test.[148] This work will be led by our collaborator, Drs. Jonathan Blackburn and Fezile Khumalo, at the University of Cape Town in South Africa. Dr. Blackburn has collected 120 sputum samples from TB suspects, plus matching urine samples for comparison. Dr. Khumalo will use these samples to test the performance of the OB-ELISA in sputum versus urine.

Conclusion

58 clinical urine samples were tested with the MVN-based OB-ELISA paired with a concentration sample preparation method using Amicon Ultra-4 Centrifugal Filter Units. No significant difference in mean absorbance values between TB-positive samples and TB-negative samples, so it is unclear if MVN is able to bind to the mannose caps on *in vivo* ManLAM. This result is in agreement with studies of the G3 antibody and in contrast with studies of the My2F12 antibody. One explanation for this is the samples utilized. Both this study and the G3 study utilized samples from the same biobank, while the My2F12 study utilized different samples. It's also possible that sample preparation or geographic concentration or epitope differences in urinary ManLAM could have contributed to these results. These theories will be examined by testing the OB-ELISA with additional urine samples at the University of South Africa and at the Oswaldo Cruz Foundation. Lastly, it is possible that MVN simply does not bind to *in vivo Man*LAM. A glycan array will be performed at the University of Alberta to determine the exact ManLAM binding epitope. In parallel, the OB-ELISA will be adapted for use with sputum samples by researchers at the University of Alberta to mitigate this problem.

Acknowledgements

I cannot thank Dalton Nelson enough for MVN-based OB-ELISA training video. I would like to recognize Dr. Westley Bauer and Dr. Leshern Karamchand for pioneering this work. I would also like to thank Dr. Carole Bewley (Laboratory of Bioorganic Chemistry, NIDDK, National Institutes of Health) for generously providing the MVN-pET15b plasmid, the Vanderbilt Antibody Protein Resource Core for the expression of MVN, Stephanie Pearlman for assistance with the characterization of MVN, and the Foundation for Innovative New Diagnostics for providing the anti-LAM antibodies and the clinical samples. Additionally, I would like to thank the Vanderbilt Biostatistics Clinic for their help with the study design and Dr. Christine Markwalter for help with analysis. Lastly, I would like to thank my collaborators at RePORT-Brazil, the University of South Africa Cape Town, and the Foundation for Innovative New Diagnostics for continuing this work. This chapter is based on work supported by the "A Prototype Diagnostic Device for Rapid, Sensitive and Direct Identification and Quantification of Mycobacterium Tuberculosis at Point-of-Care in Low Resource Settings" grant from the University of Cape Town/South African Medical Research Council, the National Science Foundation Graduate Research Fellowship program under Grants DGE-1445197 and DGE-1937963, and the National Research Foundation of South Africa (NRF) under Grant SFP150729132726 and Grant 64760.

Appendix I

Progress toward development of a low-resource diagnostic test for multidrug-resistant tuberculosis

Introduction

Nucleic acid amplification tests are becoming increasingly important for the detection of TB, particularly drug-resistant TB.[149] One example is the Cepheid Gene Xpert, which is used for the diagnosis of MDR-TB by detecting rifampin resistance-conferring mutations in the bacterial RNA polymerase gene.[26] Multi-drug resistance is defined by resistance to both isoniazid and rifampin; however, WHO guidelines state that all rifampin-resistant TB strains, regardless of isoniazid resistance, should be treated with a MDR-TB drug regimen.[150] Therefore, confirmation of rifampin resistance is all that is needed to inform treatment decisions. Importantly, almost all mutations that confer resistance to rifampin occur in a 81-base pair region of the bacterial RNA polymerase gene.[151] Additionally, any mutation in this region is sufficient for conferring resistance.[151] Gene Xpert takes advantage of this by using five probes that span the entire gene and are specific for the wildtype sequence.[152] Therefore, any mutation results in a loss of signal from at least one probe, indicating rifampin restistance.[152] Gene Xpert was found to be more sensitive and specific than microscopy and smear culture.[153] Unfortunately, Gene Xpert requires a high-resource laboratory and costs $10 per cartridge.[27] These disadvantages have prompted development of a low-

resource method for the detection of resistance.

The initial strategy explored for this goal used dendrimer-mediated silica precipitation as a detection method for rifampin resistance. A DNA probe would be conjugated to a polyamidoamine dendrimer forming a dendrimer nucleotide probe (**Figure 31**). The dendrimer nucleotide probe would recognize and bind to the resistance-conferring single-nucleotide polymorphism while simultaneously acting as a template for the precipitation of silicon dioxide from tetramethyl orthosilicate. This reaction occurs through the primary amine groups on the dendrimer, which can initiate a template-mediated silicon dioxide condensation reaction with tetramethyl orthosilicate to form silica nanoparticles. The silicon dioxide could then be visually detected as a white precipitate or quantified by measuring the light scattering. However, challenges with detection limits were quickly realized and necessitated the development of an alternative strategy for the goal of detecting resistance-conferring mutations.

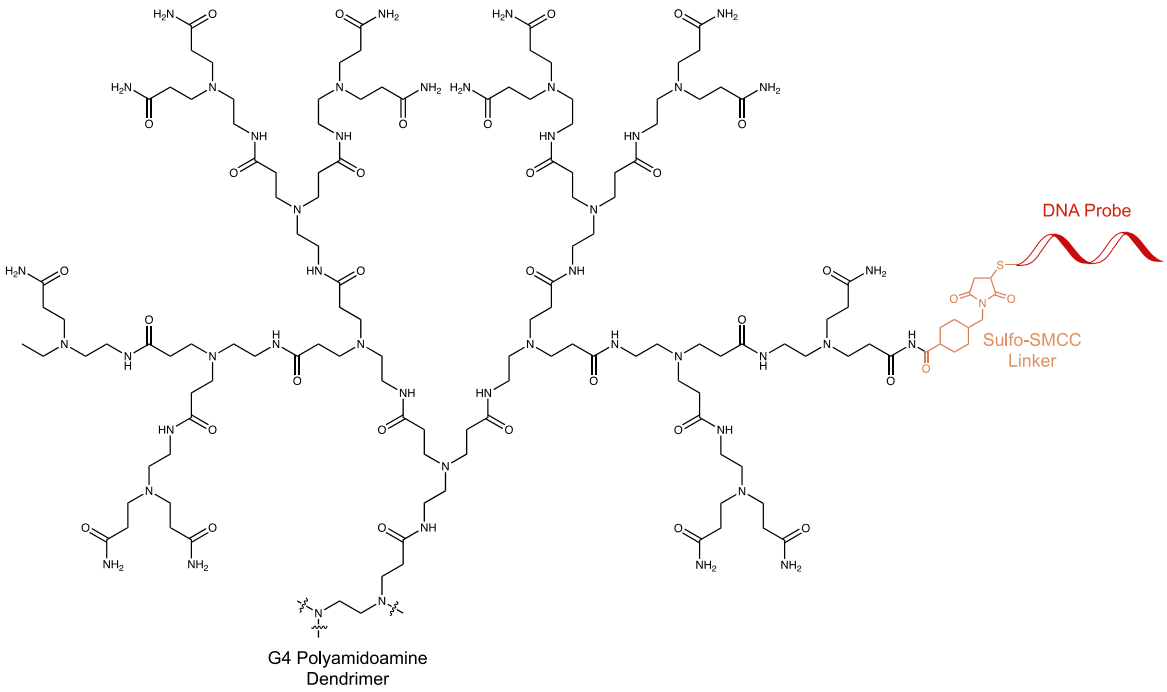

Figure 31. Schematic of the dendrimer nucleotide probe consisting of a G4 polyamidoamine dendrimer (1/4 of the dendrimer is shown in this figure) and a DNA probe specific for the mutation of interest. The DNA probe is connected to the dendrimer through a sulfo-SMCC linkage at a terminal amine group.

The second method explored employed an oligonucleotide ligation strategy.[154] For this assay, two DNA probes would be employed (**Figure 32A**). Probe A would be conjugated to a magnetic bead for isolation of the target DNA. The two probes would each bind to the target DNA, meeting at the site of the polymorphism. Probe B would be conjugated to a detection molecule, such as a gold nanoparticle or colored bead for colorimetric detection, or a fluorophore for fluorescent detection. In the presence of the mutant DNA, a ligase enzyme would ligate the two probes together forming a

continuous oligonucleotide. In the case of wildtype DNA, the mismatch between the target DNA and the probe will prevent ligation of the two probes. The beads would then be magnetically separated. In the presence of mutant DNA, the detection molecule would be attached to the magnetic bead due to the ligase linkage producing a detectable signal after separation. However, for the wildtype DNA, the detection molecule and magnetic bead would not be connected so no detectable signal would be produced after separation. For proof-of-concept experiments, the probes were attached to PCR primers, rather than detection molecules and magnetic beads (**Figure 32B**). After carrying out the ligation reaction, PCR was performed on the reaction mixture with SYBR Green fluorescence used for quantification of double-stranded DNA. In the presence of the mutation, the two probes were ligated together and could act as a PCR template, resulting in detectable signal. For proof-of-concept, this method was initially developed to detect the TCG to TTG mutation at codon 531, which is the most common mutation in the RNA polymerase gene, including in South Africa where this assay is to be tested.[155,156]

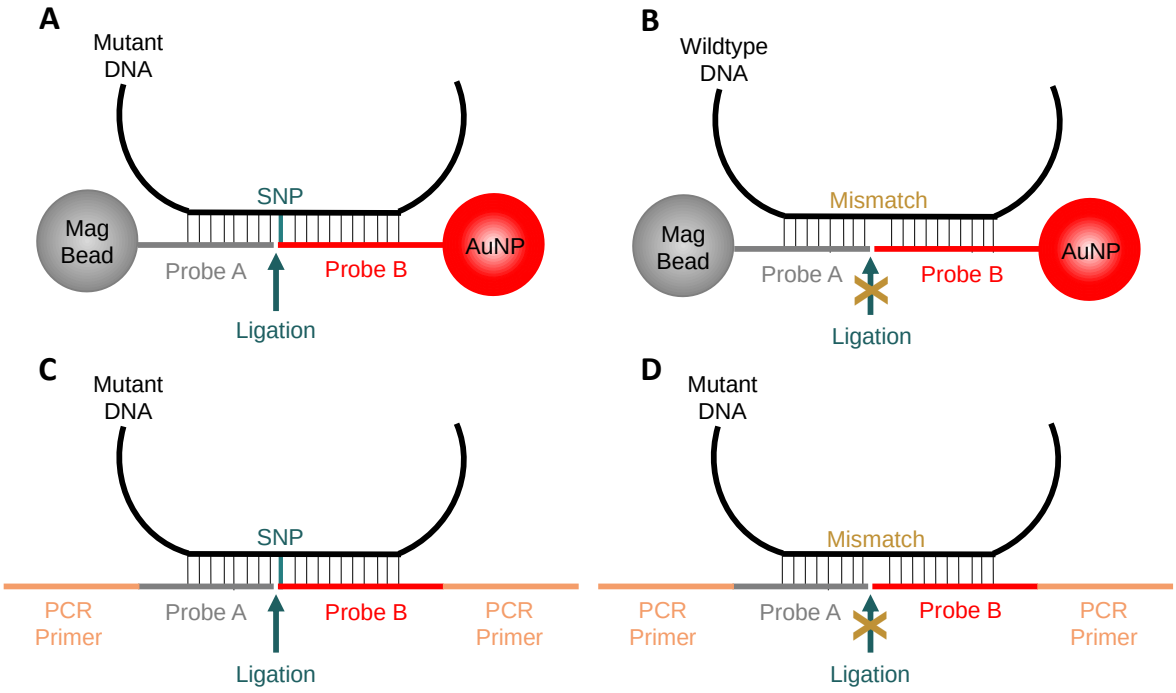

Figure 32. Schematic of the oligonucleotide reaction where two DNA probes would be employed to target a mutation of interest. The probes meet at the site of the mutation and are ligated together to form one linear strand. When the mutation is not present, ligation does not occur. **A)** Probe A is conjugated to a magnetic bead for isolation of the target DNA. Probe B is conjugated to a detection molecule, such as a gold nanoparticle or colored bead for colorimetric detection, or a fluorophore for fluorescent detection. After ligation and magnetic separation, signal would be detected only when the mutation is present. **B)** The probes are attached to PCR primers, rather than detection molecules and magnetic beads. After ligation, PCR is performed on the reaction mixture with SYBR Green fluorescence for quantification. In the presence of the mutation, the two probes are ligated together and can act as a PCR template, resulting in detectable signal.

Materials and Methods

Silica condensation reactions

1 M tetramethyl orthosilicate (Sigma-Aldrich: Cat. No 218472) in methanol (20 μL) was added to a solution (200 μL) of G4 polyamidoamine dendrimer (Sigma-Aldrich: Cat. No. 412449) or salmon-sperm DNA in 100 mM phosphate buffer (pH 7.5). The resulting mixture was allowed to incubate with shaking for 5 minutes at room temperature before centrifugation for 1 minute at 14,000 x*g*. Lastly, photos were taken of the product for qualitative results or light scattering was measured at 480 nm with a BioTek Synergy H4 plate reader.

Sulfo-SMCC conjugation with NMR quantification

G4 polyamidoamine dendrimer stock (25 μL) was added to solutions of sulfo-SMCC (Thermo Scientific: Cat. No 22622) in DI H_2O (780 μL). The reaction was allowed to incubate for 30 minutes at room temperature. The product was purified with Amicon Ultra-0.5 mL Centrifugal Filter Ultracel - 3K spin filters (Millipore Sigma: Cat. No. UFC500324) and centrifuged for 30 minutes at 14,000 x*g*. The spin filters were inverted into new collection tubes and centrifuged for 2 minutes at 1,000 x*g*. NMR samples were prepared in deuterated methanol. Proton NMR spectra were acquired with a 600 MHz instrument. The sulfo-SMCC aromatic proton peak (~7 ppm) was used for quantification by comparison to the dendrimer methylene peaks (~2.4-2.8 ppm), which are in a ratio of 2:1:1:2.

Oligonucleotides

All oligonucleotides were purchased from Integrated DNA Technologies with the standard desalting purification. The oligonucleotide sequences are listed below (**Table 9**). Upon arrival, oligonucleotides were re-suspended to 100 μM (1 μM for the positive control) in 10 mM tris hydrochloride, 0.1 mM ethylenediaminetetraacetic acid buffer.

Table 9. Oligonucleotide sequences used in Appendix I. The nucleotide corresponding to the mutation of interest is bolded and underlined in the mutant, wildtype, and Probe B sequences. The PCR primer sequences are italicized in the probe and positive control sequences.

Name	**Sequence (5'-> 3')**
Mutant	GGG TTG ACC CAC AAG CGC CGA CTG T**T**G GCG CTG GGG CCC GGC GGT CTG TC
Wildtype	GGG TTG ACC CAC AAG CGC CGA CTG T**C**G GCG CTG GGG CCC GGC GGT CTG TC
Probe A	/5Phos/AC AGT CGG CGC TTG TGG GTC AAC CCC GAC G*TT ATG AGA AAT CAA AGT CTT TGG GTT /3BioTEG/*
Probe B	*GTT AAG GGA GTG AAG ACG ATC AGA* GAC AGA CCG CCG GGC CCC AGC GCC **A**
Positive Control	*GTT AAG GGA GTG AAG ACG ATC AGA* GAC AGA CCG CCG GGC CCC AGC GCC **A**AC AGT CGG CGC TTG TGG GTC AAC CCC GAC G*TT ATG AGA AAT CAA AGT CTT TGG GTT*

Ligation and PCR reactions

The ligation reaction (20 μL) was performed with 1 nM Probe A, 10 nM Probe B, 1 pM “target” DNA, and 5% Hi Fi Taq DNA Ligase (New England BioLabs: Cat. No. M0647S). The ligation was performed in a Rotor-Gene Q PCR machine (Qiagen) with conditions described below. Following ligation, PCR was performed on each ligation product (2 μL). The PCR reactions (20 μL) were performed in Luna Universal qPCR Master Mix (New England BioLabs: Cat. No. M0647S) with SYBR Green detection and 200 nM of each primer. First, a 3-minute hold step was performed at 95°C. Then, 45 cycles of 15 seconds at 95°C and 15 seconds at 60°C were performed. Unless otherwise noted, ligation was performed with n=1 to conserve reagents and PCR was performed in duplicate for each ligation reaction. Lastly, the fluorescence was read on the green channel.

Results

A few select results corresponding to the initial strategy will be shown. First, a qualitative experiment was performed to determine whether DNA would be capable of acting as a template for silica condensation, in the same manner as the dendrimer. Preliminary results validated the dendrimer-directed reaction with G4 polyamidoamine dendrimer (**Figure 33A)** and demonstrated that DNA does not induce silica condensation (**Figure 33B**).

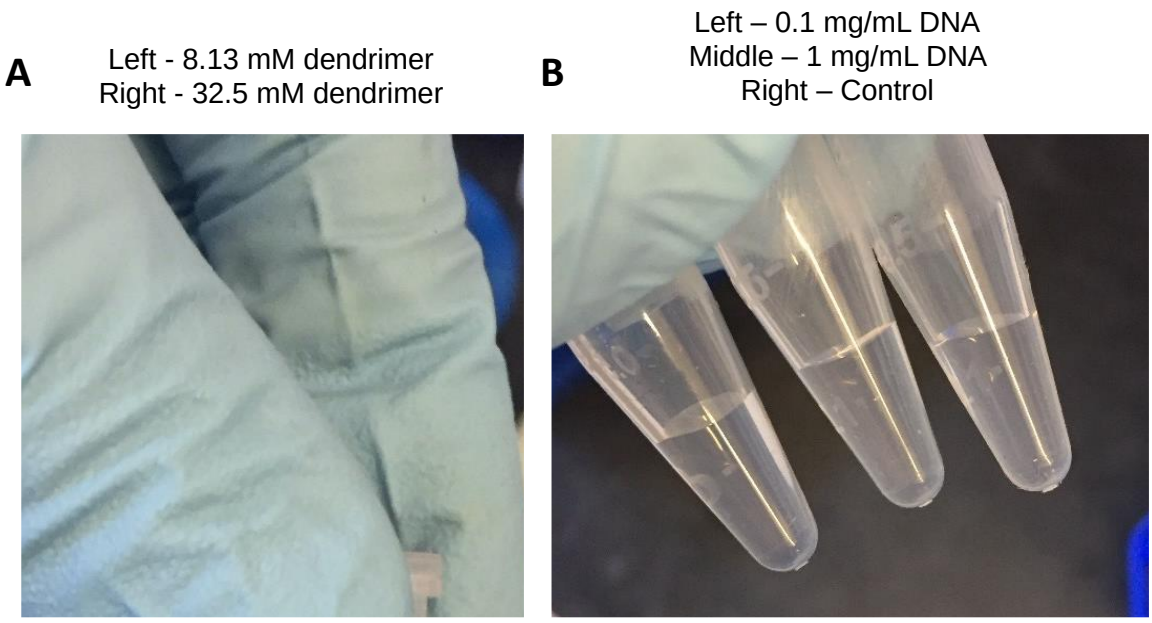

Figure 33. Proof-of-concept reactions validated the silica condensation system. **A**) G4 polyamidoamine dendrimer act as a template for silica condensation as indicating by the white precipitate. **B)** DNA does not act as a template for silica condensation as indicated by no precipitate. The reactions with DNA were indistinguishable from the control with no dendrimer or DNA present.

For the synthesis of the dendrimer nucleotide probes, the G4 polyamidoamine dendrimer was first conjugated to sulfo-SMCC, a bifunctional linker with an NHS-ester that reacts with the 64 terminal amine groups on the surface of the dendrimer. The number of molecules of sulfo-SMCC per dendrimer was determined by NMR. As expected, increasing the molar excess of sulfo-SMCC used increased the number of sulfo-SMCC molecules per dendrimer (**Table 10**). It was determined that a 96-fold molar excess of sulfo-SMCC yielded approximately 30 molecules of sulfo-SMCC per dendrimer. Thiol-terminated DNA sequences were reacted with the maleimide moiety

of the sulfo-SMCC linker; however, this reaction had low coupling efficiency. Future efforts were to be directed at using a biotin-streptavidin coupling strategy; however, simultaneous results regarding the detection limit changed the direction of this project before that strategy was employed.

Table 10. G4 polyamidoamine dendrimers with 64 terminal amine groups were conjugated to sulfo-SMCC. The number of sulfo-SMCC molecules per dendrimer (as determined by NMR) could be tailored by varying the molar excess of sulfo-SMCC used.

Dendrimer	Sulfo-SMCC Molar Excess	Sulfo-SMCC / Dendrimer
G4	32	1
G4	96	31
G4	200	45

The ability of the G4 polyamidoamine dendrimer to precipitate silica from tetramethyl orthosilicate was quantified by measuring the light scattering. The results showed that 0.817 μM dendrimer was required to produce a detectable signal (**Figure 34**). This detection limit was order of magnitudes higher than what is available for the detection of DNA. G5 polyamidoamine dendrimers were also investigated in the hope that the increased number of terminal amine groups (128 for G5 versus 64 for G4) would improve the detection limits. It was found that 0.529 μM G5 was required to produce a detectable signal. This result was expected based on a two-fold increase in

amine groups; however, it was not sufficient for the detection of DNA. These results prompted the switch to the oligonucleotide ligation assay.

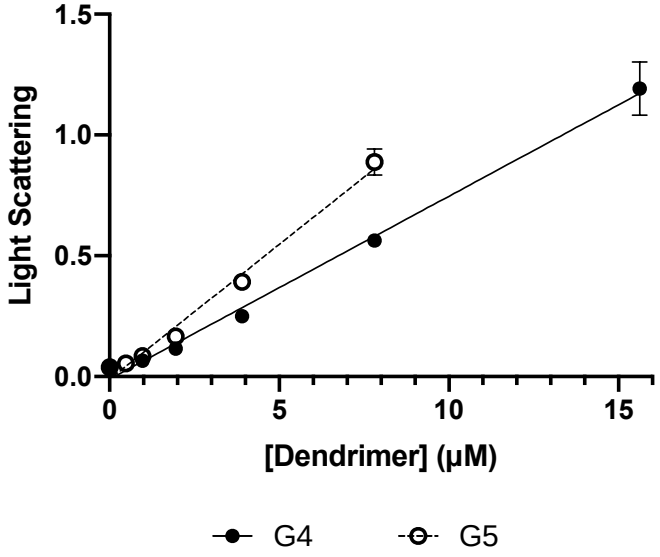

Figure 34. G4 (64 terminal amine groups) and G5 PAMAM dendrimers (128 terminal amine groups) were compared for their ability to precipitate silica from tertramethyl orthosilicate. The results were quantified by measuring the light scattering and showed that 0.817 μM G4 dendrimer or 0.529 μM G5 dendrimer was required to produce a detectable signal.

First, a proof-of-concept experiment was performed to confirm that PCR detection worked. For this experiment, reactions were performed with and without ligase to confirm that ligation was necessary for detection. For each condition, triplicate experiments were performed with 100 pM mutant “target” DNA, wildtype “target” DNA, or no “target” DNA (blank). The results plainly show a difference between reactions

containing ligase and without ligase for each type of “target” DNA (**Figure 35**). The results showed that the ligation product of the reaction with mutant DNA with the SNP of interest had a cycle threshold value of 6.94. The ligation product of the reaction with wildtype DNA had a cycle threshold value of 13.1, which was comparable to the value of 13.7 for the blank (**Table 11**). This indicated that the ligation reaction with mutant DNA had more copies of ligated product leading to higher PCR efficiency. Control reactions without ligase had a cycle threshold value of 17.7 for mutant DNA and 19.4 for wildtype DNA.

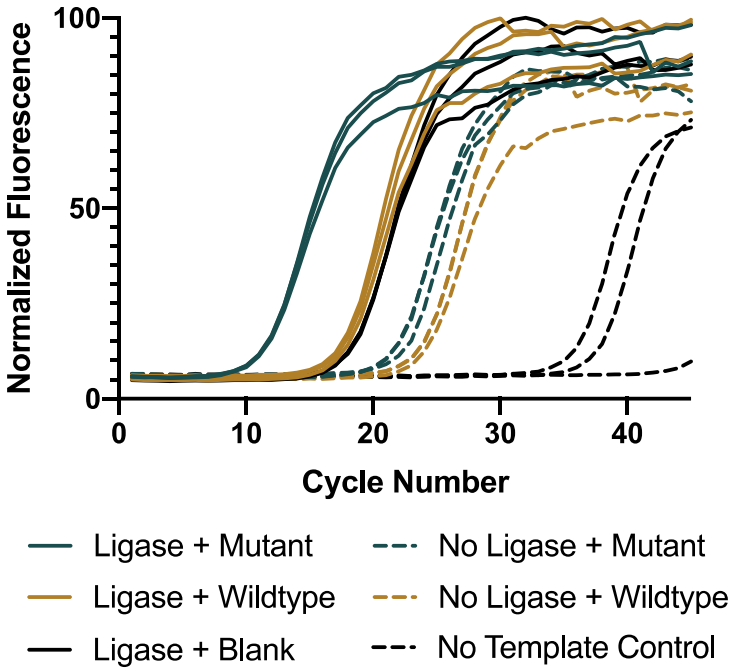

Figure 35. Proof-of-concept ligation and PCR experiment comparing ligase and no ligase conditions for mutant, wildtype, and no (blank) “target” DNA. The PCR reaction of the ligation product with mutant target DNA was the most efficient. There was no significant difference between the efficiency of the ligation product with wildtype or no target DNA confirming the specificity of the reaction. Lastly, PCR reactions on conditions without ligase were less efficient indicating fewer ligation products present.

Table 11. Cycle threshold value for a proof-of-concept ligation and PCR experiment comparing ligase and no ligase conditions for mutant, wildtype, and no (blank) “target” DNA.

Condition	Cycle threshold
Ligase + Mutant	6.94 ± 0.07
Ligase + Wildtype	13.1 ± 0.2
Ligase + Blank	13.7 ± 0.2
No Ligase + Mutant	17.1 ± 0.5
No Ligase + Wildtype	19.4 ± 0.2
No Ligase + Blank	36 ± 5

Next, the ligation temperature was investigated. The HiFi *Taq* DNA ligase enzyme has a reported maximum temperature of 75°C. However, the recommended ligation temperature based on the melting temperature of the probes was 83°C. Therefore, ligation reactions were performed with mutant or wildtype target DNA at both 75°C and 83°C. Additionally, a positive control consisting of the entire ligated product and a no-template control were implemented in the PCR reaction with all PCR reactions performed in triplicate. The results indicate that reactions in the presence of the mutant DNA perform better at 75°C than 83°C, likely due to decreased activity of the enzyme at the higher temperature (**Figure 36A**). This can be quantified by comparing the cycle threshold of each condition to the cycle threshold of the positive control (**Figure 36B**). The lower the difference in cycle threshold values, the more efficient the ligation reaction. Interestingly, the opposite seems to be true for the ligation reaction in the presence of wildtype DNA (**Figure 36A**). However, this is

beneficial as the goal is to maximize the separation between the mutant DNA reaction and the wildtype DNA reaction, which can be quantified by comparing the cycle threshold of the mutant to the cycle threshold of the wildtype at each temperature (**Figure 36C**). The greater the difference in cycle threshold values, the more specific the reaction. Therefore, it was determined that 75°C was the optimal temperature in terms of both efficiency and specificity.

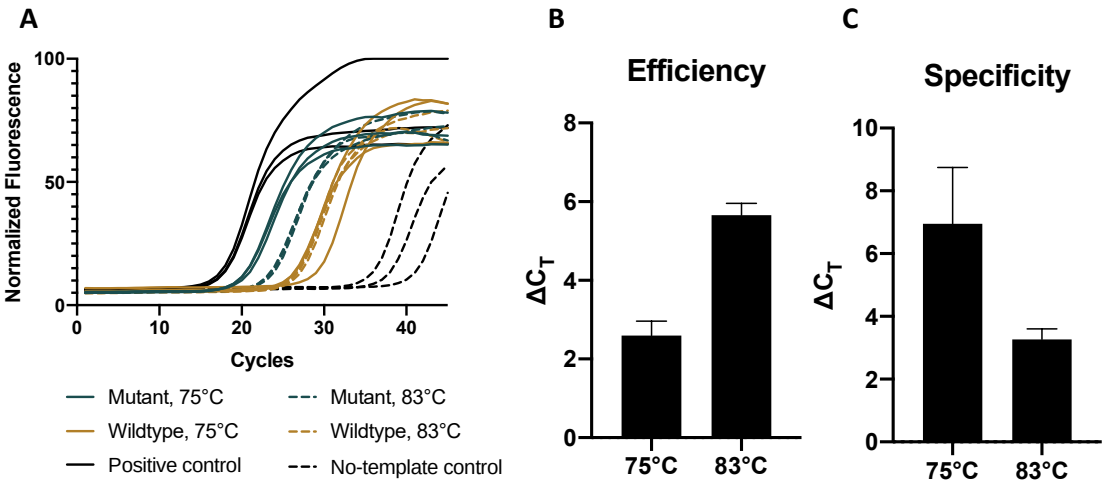

Figure 36. A) The performance of ligation reactions at 75°C and 83°C was investigated using PCR for detection and quantification. **B)** The cycle threshold value (C_T) for the PCR reactions on the products of the ligation reaction for each condition were calculated. The ligation efficiency at the two temperatures can be compared by subtracting the cycle threshold value of the positive control from the cycle threshold reaction with mutant target DNA. A smaller difference indicates a greater efficiency therefore 75°C is preferred. **C)** The specificity at each temperature can be determined by taking the difference of the cycle threshold values of the ligation reactions with mutant and wildtype target DNA. A greater difference indicates greater specificity therefore 75°C is the optimal temperature.

Following the optimization of the ligation temperature, cycling conditions were investigated. It was hypothesized that alternating ligation and melting would allow more ligation products to be produced, as each molecule of target DNA would be able to act as a template multiple times. For these experiments, ligation reactions with mutant or wildtype target DNA were performed with either a 30-minute hold at 75°C (what had previously been done), 15 cycles of 1 minute at 75°C and 1 minute at 95°C (total of 30 minutes), or 30 cycles of 1 minute at 75°C and 1 minute at 95°C (total of 30 minutes at 75°C). Of note, although the HiFi DNA *Taq* ligase enzyme has a maximum temperature for activity, it is a thermal-stable enzyme and thus, does not denature at higher temperatures. The results indicate that cycling improves the efficiency of the ligation reaction by reducing the cycle threshold value difference relative to the positive control (**Figure 37A**). In fact, the ligation reactions with cycling had a lower threshold value than the positive control resulting in a negative difference. No significant change in specificity (difference between wildtype and the mutant) was observed for any of the three conditions (**Figure 37B**).

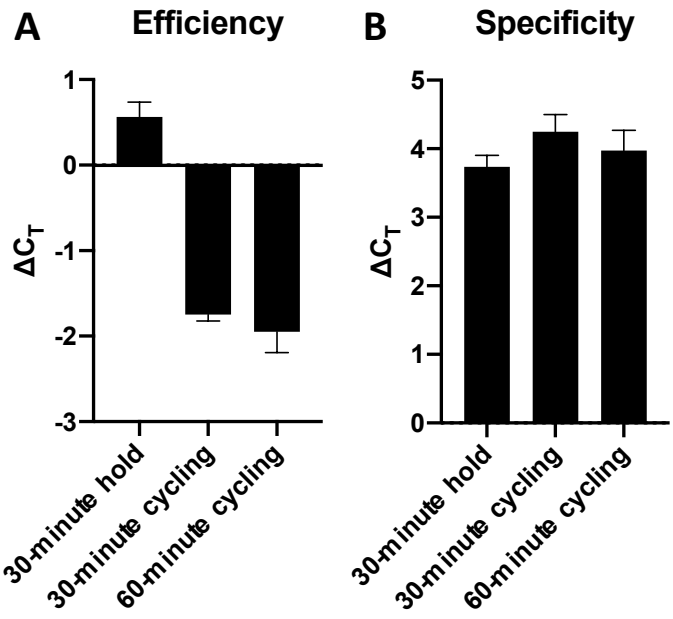

Figure 37. **A)** Cycling between 75°C for ligation and 95°C for melting improves the ligation efficiency for reactions with mutant target DNA relative to the PCR positive control. **B)** Cycling had no significant difference for specificity of the ligation reaction, as determined by comparing reactions with mutant and wildtype target DNA.

The cycling conditions were further investigated by performing a time study where a ligation experiment was performed with mutant target DNA for different lengths of time, up to 6 hours of cycling. The ligation efficiency for each length of time was compared to the positive control. Generally, ligation efficiency increased with increasing reaction time (**Figure 38**). However, this trend reached a plateau after 1 hour. Therefore, 1 hour was used moving forward.

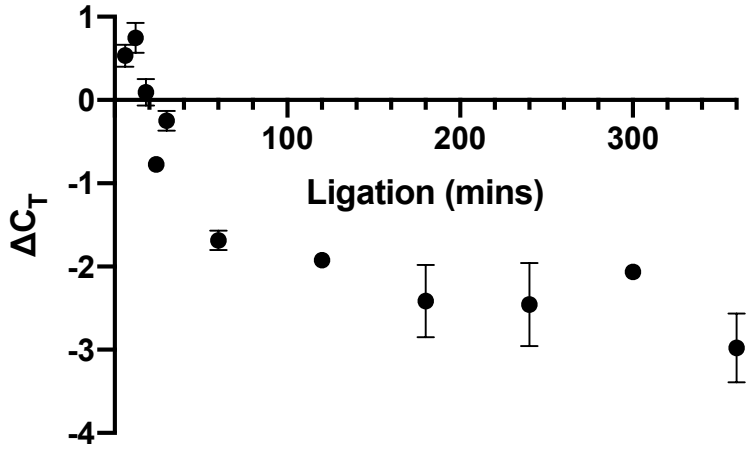

Figure 38. The total ligation reaction time was investigated for up to 6 hours of cycling. Increasing reaction time increased the ligation efficiency (in comparison to the PCR positive control) until 1 hour when the efficiency reached a plateau.

Lastly, the cycling conditions were optimized by investigating the time of the ligation step, the melt step, and the number of cycles. First, the length of time for the ligation step was compared at 20 seconds, 40 seconds, and 1 minute. It was determined that 40 seconds was the best time in terms of ligation efficiency (relative to the PCR positive control) and percent error (**Figure 39A**). Next, the length of time for the melt step was compared at 20 seconds and 60 seconds. No significance difference was found, so a 20-second melt step was used moving forward (**Figure 39B**). Lastly, the reaction time/number of cycles was investigated to determine whether 60 minutes or 30 cycles was optimal with the new step times. With the previous step times, 30 cycles resulted in a total reaction time of 60 minutes. However, under the new conditions, 30 cycles resulted in a total reaction time of only 30 minutes. The results indicated that 60 minutes was optimal (**Figure 38C**).

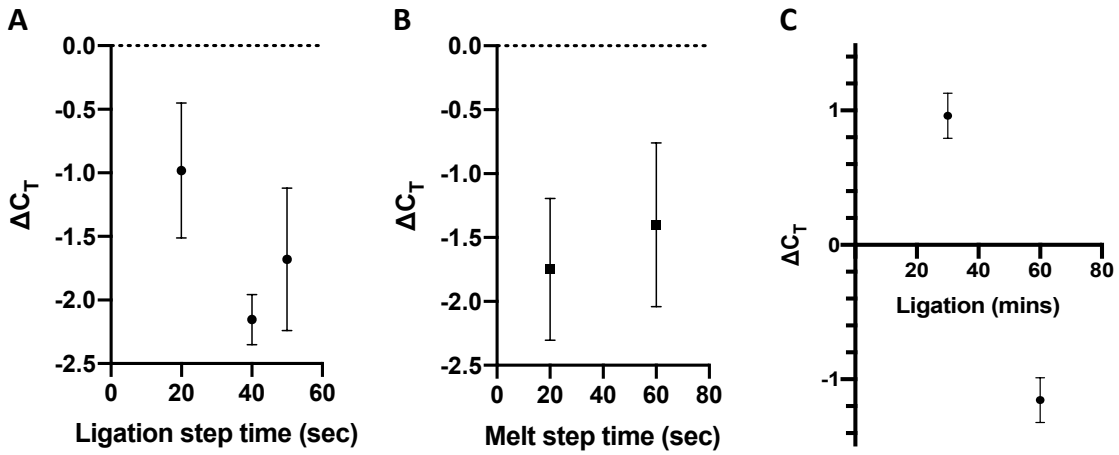

Figure 39. A) The length of the ligation step was investigated and 40 seconds was found to be optimal. **B)** Next, the length of the melt step was investigated. No significance difference was found and 20 seconds was used moving forward. Lastly, 60 cycles/minutes and 30 cycles/minutes were compared for the new conditions. 60 cycles/minutes was found to have increased ligation efficiency.

Discussion

The initial strategy that was proposed in this study used dendrimer-mediated silica precipitation as a detection method for rifampin resistance. In this strategy, a DNA probe was conjugated to a polyamidoamine dendrimer to form a dendrimer nucleotide probe, which would recognize and bind to the resistance-conferring single-nucleotide polymorphism. Simultaneously, the dendrimer nucleotide probe would act as a template for the precipitation of silicon dioxide from tetramethyl orthosilicate, which could be visually detected. Initial results were promising. The use of dendrimer as a template for silica condensation was validated and it was confirmed that DNA is not capable of acting as a template.

Then, the amine-terminated dendrimer was reacted with sulfo-SMCC to produce a maleimide-activated dendrimer. The product of this reaction would then be reacted with thiolated DNA to produce the conjugate. The first reaction was followed by NMR and it was determined that the number of sulfo-SMCC molecules per dendrimer varied depending on that ratio of sulfo-SMCC-to-dendrimer used. Specifically, a 96-fold molar excess resulted in approximately 30 sulfo-SMCC molecules out of the 64 amine groups on a G4 polyamidoamine dendrimer. It's important to note that these terminal amine groups serve two functions, as active sites for the silica condensation and as anchor points for the nucleotide sequences. Thus, a balance must be achieved between the number of amines conjugated to nucleotide probe sequences and the number of free amines remaining to drive the silica condensation. Next, the thiol-terminated DNA sequences were reacted with the maleimide moiety of the sulfo-SMCC linker; however, this reaction was found to have low coupling efficiency. Simultaneous results regarding the detection limit changed the direction of this project before the alternative methods could be investigated.

The ability of the dendrimer to precipitate silica was also investigated and the results were quantified by measuring the light scattering. Approximately 1 μM G4 dendrimer was required to produce a detectable signal. This is significantly higher than the amount of dendrimer that would be present after binding to DNA. The results were only marginally improved by the use of a G5 polyamidoamine dendrimer where approximately 0.5 μM dendrimer was required to produce a detectable signal. This result is explained by the 128 terminal amine groups of the G5 dendrimer, twice as many as the G4 dendrimer. Therefore, it was concluded that this method was not sufficient for the detection of rifampin resistance-conferring mutations in *M. tb*.

An alternative strategy was developed that did not rely on dendrimers for detection due to challenges with the detection limit. In this strategy, a modified oligonucleotide ligation assay would be used to detect the single nucleotide polymorphism. Preliminary experiments using PCR as a detection method, rather than magnetic bead separation and a spectrophotometric moiety, validated this system. Reactions with ligase resulted in more efficient PCR as indicated by a lower cycle threshold value. Additionally, the ligation reaction demonstrated a clear preference for mutant target DNA versus wildtype or no target DNA. Thus, the greatest signal was produced when mutant “target” DNA and ligase were present, as expected based on the development of the system.

Using this system, it was demonstrated that cycling ligation (75°C) and melting (95°C) enhances ligation efficiency compared to hold at 75°C. It is hypothesized that this is due to the strands de-hybridizing at the melting temperature of 95°C, which allows both the sample DNA to act as a template for ligation repeatedly, and each ligation product to act as template for ligation multiple times. Next, the total reaction time was investigated to determine if longer periods of time would increase the ligation efficiency. This hypothesis was confirmed for short periods of time; however, insignificant increases in efficiency were realized with times greater than 1 hour. The cycling conditions were further optimized to 60 minutes of 40 sec at 75°C, 20 sec at 96°C.

Conclusions

In this study, dendrimer nucleotide probes and an oligonucleotide ligation reaction were investigated for the detection of MDR-TB. Dendrimer-nucleotide probes were initially proposed as a low-resource method for detecting resistance-conferring mutations; however, challenges with detection limits prompted the switch to an oligonucleotide ligation assay. It was found that cycling between ligation and melting improved the efficiency of the ligation as measured by PCR cycle threshold value relative to a positive control.

Following the optimization of the cycling conditions, a system was developed that uses both a mutant and wildtype-specific probe. The mutant probe contains a sequence that is complimentary to a hybridization probe with a FAM fluorophore and the wildtype probe contains a sequence that is complimentary to a hybridization probe with a HEX fluorophore. This system allows the presence of both mutant and WT DNA to be detected on different channels (green and yellow, respectively). This system was designed to detect a different resistance-conferring mutation in the bacterial RNA polymerase gene, specifically the GAC to GGC mutation at codon 516.[156] However, initial experiments indicated that the reagents were contaminated and the COVID-19 pandemic prevented further development of this system. Other future work entails developing a low-resource method of cycling between ligation and melting/de-annealing steps that is compatible with magnetic bead separation and colorimetric detection, or with detection on a LFA.[157,158]

Acknowledgements

I would like to thank Dr. Donald Stec for his assistance with NMR quantification of the sulfo-SMCC conjugation reaction. I would also like to thank Dr. Mindy Leelawong for her invaluable guidance in the development of the oligonucleotide ligation assay and the use of PCR for detection. Lastly, I would like to thank the entire Haselton lab for generously allowing me to use their PCR machines. This chapter is based on work supported by the National Institutes of Health R01 AI135937 and the National Science Foundation Graduate Research Fellowship program under Grants DGE-1445197 and DGE-1937963.

References

(1) Lee, S. H. Tuberculosis Infection and Latent Tuberculosis. *Tuberc. Respir. Dis.* **2016**, *79* (4), 201–206. https://doi.org/10.4046/trd.2016.79.4.201.

(2) Cohen, A.; Mathiasen, V. D.; Schön, T.; Wejse, C. The Global Prevalence of Latent Tuberculosis: A Systematic Review and Meta-Analysis. *Eur. Respir. J.* **2019,** *54* (3). https://doi.org/10.1183/13993003.00655-2019.

(3) Kiazyk, S.; Ball, T. Latent Tuberculosis Infection: An Overview. *Can. Commun. Dis. Rep.* **2017**, *43* (3), 62–66.

(4) Behr, M. A.; Edelstein, P. H.; Ramakrishnan, L. Revisiting the Timetable of Tuberculosis. *BMJ* **2018**, *362*, k2738. https://doi.org/10.1136/bmj.k2738.

(5) World Health Organization. Global tuberculosis report 2020. World Health Organization: Geneva, 2020.

(6) Goletti, D.; Lee, M. R.; Wang, J. Y.; Walter, N.; Ottenhoff, T. H. M. Update on Tuberculosis Biomarkers: From Correlates of Risk, to Correlates of Active Disease and of Cure from Disease. *Respirology* **2018**, *23* (5), 455–466. https://doi.org/10.1111/resp.13272.

(7) Centers for Disease Control and Prevention. Basic TB Facts: Signs & Symptoms. https://www.cdc.gov/tb/topic/basics/signsandsymptoms.htm (accessed May 5, 2021).

(8) MacLean, E.; Saravu, K.; Pai, M. Diagnosing Active Tuberculosis in People Living with HIV: An Ongoing Challenge. *Curr. Opin. HIV AIDS* **2018,** *14* (1), 46-54. https://doi.org/10.1097/COH.0000000000000512.

(9) Kwan, C. K.; Ernst, J. D. HIV and Tuberculosis: A Deadly Human Syndemic. *Clin. Microbiol. Rev.* **2011**, *24* (2), 351–376. https://doi.org/10.1128/CMR.00042-10.

(10) Subbaraman, R.; Nathavitharana, R. R.; Mayer, K. H.; Satyanarayana, S.; Chadha, V. K.; Arinaminpathy, N.; Pai, M. Constructing Care Cascades for Active Tuberculosis: A Strategy for Program Monitoring and Identifying Gaps in Quality of Care. *PLoS Med.* **2019**, *16* (2), e1002754. https://doi.org/10.1371/journal.pmed.1002754.

(11) Subbaraman, R.; Nathavitharana, R. R.; Satyanarayana, S.; Pai, M.; Thomas, B. E.; Chadha, V. K.; Rade, K.; Swaminathan, S.; Mayer, K. H. The Tuberculosis Cascade of Care in India's Public Sector: A Systematic Review and Meta-Analysis. *PLoS Med.* **2016**, *13* (10), e1002149. https://doi.org/10.1371/journal.pmed.1002149.

(12) World Health Organization. Guidelines for treatment of drug-susceptible tuberculosis and patient care (2017 update). World Health Organization: Geneva, 2017

(13) Lin, P. L.; Flynn, J. L. Understanding Latent Tuberculosis: A Moving Target. *J. Immunol.* **2010**, *185* (1), 15–22. https://doi.org/10.4049/jimmunol.0903856.

(14) Naidoo, P.; Theron, G.; Rangaka, M. X.; Chihota, V. N.; Vaughan, L.; Brey, Z. O.; Pillay, Y. The South African Tuberculosis Care Cascade: Estimated Losses and Methodological Challenges. *J. Infect. Dis.* **2017**, *216* (Suppl 7), S702–S713. https://doi.org/10.1093/infdis/jix335.

(15) Harries, A. D.; Kumar, A. M. V. Challenges and Progress with Diagnosing Pulmonary Tuberculosis in Low- and Middle-Income Countries. *Diagnostics* **2018**, *8* (4). https://doi.org/10.3390/diagnostics8040078.

(16) World Health Organization. Chest radiography in tuberculosis detection. World Health Organization: Geneva, 2016.
(17) Pang, Y.; An, J.; Shu, W.; Huo, F.; Chu, N.; Gao, M.; Qin, S.; Huang, H.; Chen, X.; Xu, S. Epidemiology of Extrapulmonary Tuberculosis among Inpatients, China, 2008–2017. *Emerg. Infect. Dis.* **2019,** *25* (3), 457-464. https://doi.org/10.3201/eid2503.180572.
(18) Singhal, R.; Myneedu, V. P. Microscopy as a Diagnostic Tool in Pulmonary Tuberculosis. *Int. J. Mycobacteriol.* **2015**, *4* (1), 1–6. https://doi.org/10.1016/j.ijmyco.2014.12.006.
(19) Steingart, K. R.; Henry, M.; Ng, V.; Hopewell, P. C.; Ramsay, A.; Cunningham, J.; Urbanczik, R.; Perkins, M.; Aziz, M. A.; Pai, M. Fluorescence versus Conventional Sputum Smear Microscopy for Tuberculosis: A Systematic Review. *Lancet Infect. Dis.* **2006**, *6* (9), 570–581. https://doi.org/10.1016/S1473-3099(06)70578-3.
(20) Desikan, P. Sputum Smear Microscopy in Tuberculosis: Is It Still Relevant? *Indian J. Med. Res.* **2013**, *137* (3), 442–444. https://www.ijmr.org.in/article.asp?issn=0971-5916;year=2013;volume=137;issue=3;spage=442;epage=444;aulast=Desikan.
(21) Pai, M.; Nicol, M. P.; Boehme, C. C. Tuberculosis Diagnostics: State of the Art and Future Directions. *Microbiol. Spectr.* **2016**, *4* (5). https://doi.org/10.1128/microbiolspec.TBTB2-0019-2016.
(22) Phillips, P. P. J.; Mendel, C. M.; Nunn, A. J.; McHugh, T. D.; Crook, A. M.; Hunt, R.; Bateson, A.; Gillespie, S. H. A Comparison of Liquid and Solid Culture for Determining Relapse and Durable Cure in Phase III TB Trials for New Regimens. *BMC Med.* **2017**, *15* (1), 207. https://doi.org/10.1186/s12916-017-0955-9.
(23) Pfyffer, G. E.; Wittwer, F. Incubation Time of Mycobacterial Cultures: How Long Is Long Enough To Issue a Final Negative Report to the Clinician? *J. Clin. Microbiol.* **2012**, *50* (12), 4188–4189. https://doi.org/10.1128/JCM.02283-12.
(24) Peralta, G.; Barry, P.; Pascopella, L. Use of Nucleic Acid Amplification Tests in Tuberculosis Patients in California, 2010–2013. *Open Forum Infect. Dis.* **2016**, *3* (4). https://doi.org/10.1093/ofid/ofw230.
(25) Dunn, J. J.; Starke, J. R.; Revell, P. A. Laboratory Diagnosis of Mycobacterium Tuberculosis Infection and Disease in Children. *J. Clin. Microbiol.* **2016**, *54* (6), 1434–1441. https://doi.org/10.1128/JCM.03043-15.
(26) Helb, D.; Jones, M.; Story, E.; Boehme, C.; Wallace, E.; Ho, K.; Kop, J.; Owens, M. R.; Rodgers, R.; Banada, P.; Safi, H.; Blakemore, R.; Lan, N. T. N.; Jones-López, E. C.; Levi, M.; Burday, M.; Ayakaka, I.; Mugerwa, R. D.; McMillan, B.; Winn-Deen, E.; Christel, L.; Dailey, P.; Perkins, M. D.; Persing, D. H.; Alland, D. Rapid Detection of Mycobacterium Tuberculosis and Rifampin Resistance by Use of On-Demand, near-Patient Technology. *J. Clin. Microbiol.* **2010**, *48* (1), 229–237. https://doi.org/10.1128/JCM.01463-09.
(27) Sagili, K. D.; Muniyandi, M.; Nilgiriwala, K. S.; Shringarpure, K. S.; Satyanarayana, S.; Kirubakaran, R.; Chadha, S. S.; Tharyan, P. Cost-Effectiveness of GeneXpert and LED-FM for Diagnosis of Pulmonary Tuberculosis: A Systematic Review. *PLoS One* **2018**, *13* (10). https://doi.org/10.1371/journal.pone.0205233.
(28) MacLean, E.; Broger, T.; Yerlikaya, S.; Fernandez-Carballo, B. L.; Pai, M.; Denkinger, C. M. A Systematic Review of Biomarkers to Detect Active

Tuberculosis. *Nat. Microbiol.* **2019**, *4* (5), 748–758. https://doi.org/10.1038/s41564-019-0380-2.
(29) García-Basteiro, A. L.; DiNardo, A.; Saavedra, B.; Silva, D. R.; Palmero, D.; Gegia, M.; Migliori, G. B.; Duarte, R.; Mambuque, E.; Centis, R.; Cuevas, L. E.; Izco, S.; Theron, G. Point of Care Diagnostics for Tuberculosis. *Pulmonology* **2018**, *24* (2), 73–85. https://doi.org/10.1016/j.rppnen.2017.12.002.
(30) Lawn, S. D. Point-of-Care Detection of Lipoarabinomannan (LAM) in Urine for Diagnosis of HIV-Associated Tuberculosis: A State of the Art Review. *BMC Infect. Dis.* **2012**, *12*, 103. https://doi.org/10.1186/1471-2334-12-103.
(31) Goletti, D.; Petruccioli, E.; Joosten, S. A.; Ottenhoff, T. H. M. Tuberculosis Biomarkers: From Diagnosis to Protection. *Infect. Dis. Rep.* **2016**, *8* (2). https://doi.org/10.4081/idr.2016.6568.
(32) Sarkar, P.; Biswas, D.; Sindhwani, G.; Rawat, J.; Kotwal, A.; Kakati, B. Application of Lipoarabinomannan Antigen in Tuberculosis Diagnostics: Current Evidence. *Postgrad. Med. J.* **2014**, *90* (1061), 155–163. https://doi.org/10.1136/postgradmedj-2013-132053.
(33) Ricks, S.; Denkinger, C. M.; Schumacher, S. G.; Hallett, T. B.; Arinaminpathy, N. The Potential Impact of Urine-LAM Diagnostics on Tuberculosis Incidence and Mortality: A Modelling Analysis. *PLoS Med.* **2020**, *17* (12), e1003466. https://doi.org/10.1371/journal.pmed.1003466.
(34) Correia-Neves, M.; Fröberg, G.; Korshun, L.; Viegas, S.; Vaz, P.; Ramanlal, N.; Bruchfeld, J.; Hamasur, B.; Brennan, P.; Källenius, G. Biomarkers for Tuberculosis: The Case for Lipoarabinomannan. *ERJ Open Res.* **2019**, *5* (1). https://doi.org/10.1183/23120541.00115-2018.
(35) Cox, J. A.; Lukande, R. L.; Kalungi, S.; Van Marck, E.; Van de Vijver, K.; Kambugu, A.; Nelson, A. M.; Colebunders, R.; Manabe, Y. C. Is Urinary Lipoarabinomannan the Result of Renal Tuberculosis? Assessment of the Renal Histology in an Autopsy Cohort of Ugandan HIV-Infected Adults. *PLoS One* **2015**, *10* (4). https://doi.org/10.1371/journal.pone.0123323.
(36) Bhattacharya, A.; Ranadive, S. N.; Kale, M.; Bhattacharya, S. Antibody-Based Enzyme-Linked Immunosorbent Assay for Determination of Immune Complexes in Clinical Tuberculosis. *Am. Rev. Respir. Dis.* **1986**, *134* (2), 205–209. https://doi.org/10.1164/arrd.1986.134.2.205.
(37) Sada, E.; Aguilar, D.; Torres, M.; Herrera, T. Detection of Lipoarabinomannan as a Diagnostic Test for Tuberculosis. *J. Clin. Microbiol.* **1992**, *30* (9), 2415–2418.
(38) Sakamuri, R. M.; Price, D. N.; Lee, M.; Cho, S. N.; Barry, C. E.; Via, L. E.; Swanson, B. I.; Mukundan, H. Association of Lipoarabinomannan with Human High Density Lipoprotein in Blood: Implications for Bio-Distribution and Serum Diagnostics. *Tuberculosis (Edinb)* **2013**, *93* (3). https://doi.org/10.1016/j.tube.2013.02.015.
(39) Haraldsson, B.; Nyström, J.; Deen, W. M. Properties of the Glomerular Barrier and Mechanisms of Proteinuria. *Physiol. Rev.* **2008**, *88* (2), 451–487. https://doi.org/10.1152/physrev.00055.2006.
(40) Lawn, S. D.; Gupta-Wright, A. Detection of Lipoarabinomannan (LAM) in Urine Is Indicative of Disseminated TB with Renal Involvement in Patients Living with HIV and Advanced Immunodeficiency: Evidence and Implications. *Trans. R. Soc. Trop. Med. Hyg.* **2016**, *110* (3), 180–185. https://doi.org/10.1093/trstmh/trw008.

(41) Paris, L.; Magni, R.; Zaidi, F.; Araujo, R.; Saini, N.; Harpole, M.; Coronel, J.; Kirwan, D. E.; Steinberg, H.; Gilman, R. H.; Petricoin, E. F.; Nisini, R.; Luchini, A.; Liotta, L. Urine Lipoarabinomannan Glycan in HIV-Negative Patients with Pulmonary Tuberculosis Correlates with Disease Severity. *Sci. Transl. Med.* **2017**, *9* (420). https://doi.org/10.1126/scitranslmed.aal2807.

(42) Bulterys, M. A.; Wagner, B.; Redard-Jacot, M.; Suresh, A.; Pollock, N. R.; Moreau, E.; Denkinger, C. M.; Drain, P. K.; Broger, T. Point-Of-Care Urine LAM Tests for Tuberculosis Diagnosis: A Status Update. *J. C. Med.* **2020**, *9* (1), 111. https://doi.org/10.3390/jcm9010111.

(43) De, P.; Shi, L.; Boot, C.; Ordway, D.; McNeil, M.; Chatterjee, D. Comparative Structural Study of Terminal Ends of Lipoarabinomannan from Mice Infected Lung Tissues and Urine of a Tuberculosis Positive Patient. *ACS Infect. Dis.* **2020**, *6* (2), 291–301. https://doi.org/10.1021/acsinfecdis.9b00355.

(44) Mishra, A. K.; Driessen, N. N.; Appelmelk, B. J.; Besra, G. S. Lipoarabinomannan and Related Glycoconjugates: Structure, Biogenesis and Role in Mycobacterium Tuberculosis Physiology and Host–Pathogen Interaction. *FEMS Microbiol. Rev.* **2011**, *35* (6), 1126–1157. https://doi.org/10.1111/j.1574-6976.2011.00276.x.

(45) Petzold, C. J.; Stanton, L. H.; Leary, J. A. Structural Characterization of Lipoarabinomannans from Mycobacterium Tuberculosis and Mycobacterium Smegmatis by ESI Mass Spectrometry. *J. Am. Soc. Mass Spectrom.* **2005**, *16* (7), 1109–1116. https://doi.org/10.1016/j.jasms.2005.02.023.

(46) Nigou, J.; Gilleron, M.; Puzo, G. Lipoarabinomannans: From Structure to Biosynthesis. *Biochimie* **2003**, *85* (1–2), 153–166. https://doi.org/10.1016/s0300-9084(03)00048-8.

(47) Barnes, D. D.; Lundahl, M. L. E.; Lavelle, E. C.; Scanlan, E. M. The Emergence of Phenolic Glycans as Virulence Factors in Mycobacterium Tuberculosis. *ACS Chem. Biol.* **2017**, *12* (8), 1969–1979. https://doi.org/10.1021/acschembio.7b00394.

(48) Chatterjee, D.; Khoo, K.H. Mycobacterial Lipoarabinomannan: An Extraordinary Lipoheteroglycan with Profound Physiological Effects. *Glycobiology* **1998**, *8* (2), 113–120. https://doi.org/10.1093/glycob/8.2.113.

(49) Turner, J.; Torrelles, J. B. Mannose-Capped Lipoarabinomannan in Mycobacterium Tuberculosis Pathogenesis. *Pathog. Dis.* **2018**, *76* (4). https://doi.org/10.1093/femspd/fty026.

(50) Khoo, K.H.; Tang, J.B.; Chatterjee, D. Variation in Mannose-Capped Terminal Arabinan Motifs of Lipoarabinomannans from Clinical Isolates of Mycobacterium Tuberculosis and Mycobacterium Avium Complex. *J. Biol. Chem.* **2001**, *276* (6), 3863–3871. https://doi.org/10.1074/jbc.M004010200.

(51) Nigou, J.; Vercellone, A.; Puzo, G. New Structural Insights into the Molecular Deciphering of Mycobacterial Lipoglycan Binding to C-Type Lectins: Lipoarabinomannan Glycoform Characterization and Quantification by Capillary Electrophoresis at the Subnanomole Level. *J. Mol. Biol.* **2000**, *299* (5), 1353–1362. https://doi.org/10.1006/jmbi.2000.3821.

(52) Torrelles, J. B.; Khoo, K.H.; Sieling, P. A.; Modlin, R. L.; Zhang, N.; Marques, A. M.; Treumann, A.; Rithner, C. D.; Brennan, P. J.; Chatterjee, D. Truncated Structural Variants of Lipoarabinomannan in Mycobacterium Leprae and an Ethambutol-Resistant Strain of Mycobacterium Tuberculosis. *J. Biol. Chem.* **2004**, *279* (39), 41227–41239. https://doi.org/10.1074/jbc.M405180200.

(53) Chan, C. E.; Götze, S.; Seah, G. T.; Seeberger, P. H.; Tukvadze, N.; Wenk, M. R.; Hanson, B. J.; MacAry, P. A. The Diagnostic Targeting of a Carbohydrate Virulence Factor from M. Tuberculosis. *Sci. Rep.* **2015**, *5*, 10281. https://doi.org/10.1038/srep10281.
(54) Treumann, A.; Xidong, F.; McDonnell, L.; Derrick, P. J.; Ashcroft, A. E.; Chatterjee, D.; Homans, S. W. 5-Methylthiopentose: A New Substituent on Lipoarabinomannan in Mycobacterium Tuberculosis. *J. Mol. Biol.* **2002**, *316* (1), 89–100. https://doi.org/10.1006/jmbi.2001.5317.
(55) Turnbull, W. B.; Shimizu, K.; Chatterjee, D.; Homans, S. W.; Treumann, A. Identification of the 5-Methylthiopentosyl Substituent in Mycobacterium Tuberculosis Lipoarabinomannan. *Angew. Chem.: Int. Ed.* **2004**. https://doi.org/10.1002/anie.200454119.
(56) Hamasur, B.; Bruchfeld, J.; Haile, M.; Pawlowski, A.; Bjorvatn, B.; Källenius, G.; Svenson, S. B. Rapid Diagnosis of Tuberculosis by Detection of Mycobacterial Lipoarabinomannan in Urine. *J. Microbiol. Methods* **2001**, *45* (1), 41–52. https://doi.org/10.1016/S0167-7012(01)00239-1.
(57) Dheda, K.; Davids, V.; Lenders, L.; Roberts, T.; Meldau, R.; Ling, D.; Brunet, L.; van Zyl Smit, R.; Peter, J.; Green, C.; Badri, M.; Sechi, L.; Sharma, S.; Hoelscher, M.; Dawson, R.; Whitelaw, A.; Blackburn, J.; Pai, M.; Zumla, A. Clinical Utility of a Commercial LAM-ELISA Assay for TB Diagnosis in HIV-Infected Patients Using Urine and Sputum Samples. *PLoS One* **2010**, *5* (3), e9848. https://doi.org/10.1371/journal.pone.0009848.
(58) Minion, J.; Leung, E.; Talbot, E.; Dheda, K.; Pai, M.; Menzies, D. Diagnosing Tuberculosis with Urine Lipoarabinomannan: Systematic Review and Meta-Analysis. *Eur. Respir. J.* **2011**, *38* (6), 1398–1405. https://doi.org/10.1183/09031936.00025711.
(59) Wood, R.; Racow, K.; Bekker, L.G.; Middelkoop, K.; Vogt, M.; Kreiswirth, B. N.; Lawn, S. D. Lipoarabinomannan in Urine during Tuberculosis Treatment: Association with Host and Pathogen Factors and Mycobacteriuria. *BMC Infect. Dis.* **2012**, *12*, 47. https://doi.org/10.1186/1471-2334-12-47.
(60) World Health Organization. Global Tuberculosis Report 2018. World Health Organization: Geneva, 2018.
(61) Boehme, C.; Molokova, E.; Minja, F.; Geis, S.; Loscher, T.; Maboko, L.; Koulchin, V.; Hoelscher, M. Detection of Mycobacterial Lipoarabinomannan with an Antigen-Capture ELISA in Unprocessed Urine of Tanzanian Patients with Suspected Tuberculosis. *Trans. R. Soc. Trop. Med. Hyg.* **2005**, *99* (12), 893–900. https://doi.org/10.1016/j.trstmh.2005.04.014.
(62) Zhou, K.L.; Li, X.; Zhang, X.L.; Pan, Q. Mycobacterial Mannose-Capped Lipoarabinomannan: A Modulator Bridging Innate and Adaptive Immunity. *Emerg. Microbes. Infect.* **2019**, *8* (1), 1168–1177. https://doi.org/10.1080/22221751.2019.1649097.
(63) Songkhla, M. N.; Tantipong, H.; Tongsai, S.; Angkasekwinai, N. Lateral Flow Urine Lipoarabinomannan Assay for Diagnosis of Active Tuberculosis in Adults With Human Immunodeficiency Virus Infection: A Prospective Cohort Study. *Open Forum Infect. Dis.* **2019**, *6* (ofz132). https://doi.org/10.1093/ofid/ofz132.
(64) Nel, J. S.; Lippincott, C. K.; Berhanu, R.; Spencer, D. C.; Sanne, I. M.; Ive, P. Does Disseminated Nontuberculous Mycobacterial Disease Cause False-Positive Determine TB-LAM Lateral Flow Assay Results? A Retrospective Review. *Clin. Infect. Dis.* **2017**, *65* (7), 1226–1228. https://doi.org/10.1093/cid/cix513.

(65) Benjamin, A.; Cavalcante, S. C.; Jamal, L. F.; Arakaki-Sanchez, D.; Lima, J. N. de; Pilotto, J. H.; Oliveira, F. I. de, Jr.; Souza, T. N. L.; Lourenço, M. C.; Mello, M. B. de; Brasil, P. E. A. A. do; Barreira, D.; Rolla, V. Accuracy of Determine TB-LAM Ag to Detect TB in HIV Infected Patients Associated with Diagnostic Methods Used in Brazilian Public Health Units. *PLoS One* **2019**, *14* (9), e0221038. https://doi.org/10.1371/journal.pone.0221038.

(66) Nyamogoba, H. D. N.; Mbuthia, G.; Kikuvi, G.; Mpoke, S.; Obala, A.; Obel, M.; Menya, D.; Waiyaki, P. G. Misdiagnosis and Clinical Significance of Non-Tuberculous Mycobacteria in Western Kenya in the Era of Human Immunodeficiency Virus Epidemic. *East Afr. Med.l J.* **2011**, *88* (9), 298–303. https://doi.org/10.4314/eamj.v88i9.

(67) Snydman, D. R.; Redelman-Sidi, G.; Sepkowitz, K. A. Rapidly Growing Mycobacteria Infection in Patients with Cancer. *Clin. Inf. Dis.* **2010**, *51* (4), 422–434. https://doi.org/10.1086/655140.

(68) Abubakar, I.; Gupta, R. K.; Rangaka, M. X.; Lipman, M. Update in Tuberculosis and Nontuberculous Mycobacteria 2017. *Am. J. Respir. Crit. Care Med.* **2018**, *197* (10), 1248–1253. https://doi.org/10.1164/rccm.201801-0106UP.

(69) Gopinath, K.; Singh, S. Non-Tuberculous Mycobacteria in TB-Endemic Countries: Are We Neglecting the Danger? *PLoS Negl. Trop. Dis.* **2010**, *4* (4). https://doi.org/10.1371/journal.pntd.0000615.

(70) Hoefsloot, W.; Ingen, J. van; Andrejak, C.; Ängeby, K.; Bauriaud, R.; Bemer, P.; Beylis, N.; Boeree, M. J.; Cacho, J.; Chihota, V.; Chimara, E.; Churchyard, G.; Cias, R.; Daza, R.; Daley, C. L.; Dekhuijzen, P. N. R.; Domingo, D.; Drobniewski, F.; Esteban, J.; Fauville-Dufaux, M.; Folkvardsen, D. B.; Gibbons, N.; Gómez-Mampaso, E.; Gonzalez, R.; Hoffmann, H.; Hsueh, P.-R.; Indra, A.; Jagielski, T.; Jamieson, F.; Jankovic, M.; Jong, E.; Keane, J.; Koh, W.-J.; Lange, B.; Leao, S.; Macedo, R.; Mannsåker, T.; Marras, T. K.; Maugein, J.; Milburn, H. J.; Mlinkó, T.; Morcillo, N.; Morimoto, K.; Papaventsis, D.; Palenque, E.; Paez-Peña, M.; Piersimoni, C.; Polanová, M.; Rastogi, N.; Richter, E.; Ruiz-Serrano, M. J.; Silva, A.; Silva, M. P. da; Simsek, H.; Soolingen, D. van; Szabó, N.; Thomson, R.; Fernandez, T. T.; Tortoli, E.; Totten, S. E.; Tyrrell, G.; Vasankari, T.; Villar, M.; Walkiewicz, R.; Winthrop, K. L.; Wagner, D. The Geographic Diversity of Nontuberculous Mycobacteria Isolated from Pulmonary Samples: An NTM-NET Collaborative Study. *Eur. Respir. J.* **2013**, *42* (6), 1604–1613. https://doi.org/10.1183/09031936.00149212.

(71) Kawasaki, M.; Echiverri, C.; Raymond, L.; Cadena, E.; Reside, E.; Gler, M. T.; Oda, T.; Ito, R.; Higashiyama, R.; Katsuragi, K.; Liu, Y. Lipoarabinomannan in Sputum to Detect Bacterial Load and Treatment Response in Patients with Pulmonary Tuberculosis: Analytic Validation and Evaluation in Two Cohorts. *PLoS Med.* **2019**, *16* (4), e1002780. https://doi.org/10.1371/journal.pmed.1002780.

(72) Broger, T.; Sossen, B.; Toit, E. du; Kerkhoff, A. D.; Schutz, C.; Reipold, E. I.; Ward, A.; Barr, D. A.; Macé, A.; Trollip, A.; Burton, R.; Ongarello, S.; Pinter, A.; Lowary, T. L.; Boehme, C.; Nicol, M. P.; Meintjes, G.; Denkinger, C. M. Novel Lipoarabinomannan Point-of-Care Tuberculosis Test for People with HIV: A Diagnostic Accuracy Study. *Lancet Infect. Dis.* **2019**, *19* (8), 852–861. https://doi.org/10.1016/S1473-3099(19)30001-5.

(73) Sigal, G. B.; Pinter, A.; Lowary, T. L.; Kawasaki, M.; Li, A.; Mathew, A.; Tsionsky, M.; Zheng, R. B.; Plisova, T.; Shen, K.; Katsuragi, K.; Choudhary, A.; Honnen, W. J.; Nahid, P.; Denkinger, C. M.; Broger, T. A Novel Sensitive Immunoassay

Targeting the 5-Methylthio-d-Xylofuranose–Lipoarabinomannan Epitope Meets the WHO's Performance Target for Tuberculosis Diagnosis. *J. Clin. Microbiol.* **2018**, *56* (12). https://doi.org/10.1128/JCM.01338-18.

(74) Choudhary, A.; Patel, D.; Honnen, W.; Lai, Z.; Prattipati, R. S.; Zheng, R. B.; Hsueh, Y.-C.; Gennaro, M. L.; Lardizabal, A.; Restrepo, B. I.; Garcia-Viveros, M.; Joe, M.; Bai, Y.; Shen, K.; Sahloul, K.; Spencer, J. S.; Chatterjee, D.; Broger, T.; Lowary, T. L.; Pinter, A. Characterization of the Antigenic Heterogeneity of Lipoarabinomannan, the Major Surface Glycolipid of Mycobacterium Tuberculosis, and Complexity of Antibody Specificities toward This Antigen. *J. Immunol.* **2018**, *200* (9), 3053–3066. https://doi.org/10.4049/jimmunol.1701673.

(75) Kehr, J.C.; Zilliges, Y.; Springer, A.; Disney, M. D.; Ratner, D. D.; Bouchier, C.; Seeberger, P. H.; de Marsac, N. T.; Dittmann, E. A Mannan Binding Lectin Is Involved in Cell-Cell Attachment in a Toxic Strain of Microcystis Aeruginosa. *Mol. Microbiol.* **2006**, *59* (3), 893–906. https://doi.org/10.1111/j.1365-2958.2005.05001.x.

(76) Tanabe, Y.; Hodoki, Y.; Sano, T.; Tada, K.; Watanabe, M. M. Adaptation of the Freshwater Bloom-Forming Cyanobacterium Microcystis Aeruginosa to Brackish Water Is Driven by Recent Horizontal Transfer of Sucrose Genes. *Front. Microbiol.* **2018**, *9*. https://doi.org/10.3389/fmicb.2018.01150.

(77) Yamaguchi, M.; Ogawa, T.; Muramoto, K.; Kamio, Y.; Jimbo, M.; Kamiya, H. Isolation and Characterization of a Mannan-Binding Lectin from the Freshwater Cyanobacterium (Blue-Green Algae) Microcystis Viridis. *Biochem. Biophys. Res. Commun.* **1999**, *265* (3), 703–708. https://doi.org/10.1006/bbrc.1999.1749.

(78) Bewley, C. A.; Cai, M.; Ray, S.; Ghirlando, R.; Yamaguchi, M.; Muramoto, K. New Carbohydrate Specificity and HIV-1 Fusion Blocking Activity of the Cyanobacterial Protein MVL: NMR, ITC and Sedimentation Equilibrium Studies. *J. Mol. Biol.* **2004**, *339* (4), 901–914. https://doi.org/10.1016/j.jmb.2004.04.019.

(79) Jimbo, M.; Yamaguchi, M.; Muramoto, K.; Kamiya, H. Cloning of the Microcystis Aeruginosa M228 Lectin (MAL) Gene. *Biochem. Biophys. Res. Commun.* **2000**, *273* (2), 499–504. https://doi.org/10.1006/bbrc.2000.2961.

(80) Boyd, M. R.; Gustafson, K. R.; McMahon, J. B.; Shoemaker, R. H.; O'Keefe, B. R.; Mori, T.; Gulakowski, R. J.; Wu, L.; Rivera, M. I.; Laurencot, C. M.; Currens, M. J.; Cardellina, J. H.; Buckheit, R. W.; Nara, P. L.; Pannell, L. K.; Sowder, R. C.; Henderson, L. E. Discovery of Cyanovirin-N, a Novel Human Immunodeficiency Virus-Inactivating Protein That Binds Viral Surface Envelope Glycoprotein Gp120: Potential Applications to Microbicide Development. *Antimicrob. Agents. Chemother.* **1997**, *41* (7), 1521–1530. https://doi.org/10.1128/AAC.41.7.1521.

(81) Bewley, C. A.; Otero-Quintero, S. The Potent Anti-HIV Protein Cyanovirin-N Contains Two Novel Carbohydrate Binding Sites That Selectively Bind to Man(8) D1D3 and Man(9) with Nanomolar Affinity: Implications for Binding to the HIV Envelope Protein Gp120. *J. Am. Chem. Soc.* **2001**, *123* (17), 3892–3902. https://doi.org/10.1021/ja004040e.

(82) Shahzad-ul-Hussan, S.; Gustchina, E.; Ghirlando, R.; Clore, G. M.; Bewley, C. A. Solution Structure of the Monovalent Lectin Microvirin in Complex with Manα(1–2)Man Provides a Basis for Anti-HIV Activity with Low Toxicity. *J. Biol. Chem.* **2011,** 286 (23), 20788-96. https://doi.org/10.1074/jbc.M111.232678.

(83) Bewley, C. A.; Hussan, S. (2010) Microvirin lectin DOI: 10.2210/pdb2Y1S/pdb

(84) Fan, X. Wang, J., Lei, J. L., Wang, H. W. Biotin-bound streptavidin DOI: 10.2210/pdb6J6J/pdb

(85) Fan, X.; Wang, J.; Zhang, X.; Yang, Z.; Zhang, J. C.; Zhao, L.; Peng, H. L.; Lei, J.; Wang, H.W. Single Particle Cryo-EM Reconstruction of 52 KDa Streptavidin at 3.2 Angstrom Resolution. *Nat. Commun.* **2019**, *10* (1), 2386. https://doi.org/10.1038/s41467-019-10368-w.
(86) Harris, L. J.; McPherson, A. Structure of Immunoglobulin DOI: 10.2210/pdb1IGY/pdb
(87) Harris, L. J.; Skaletsky, E.; McPherson, A. Crystallographic Structure of an Intact IgG1 Monoclonal Antibody. *J. Mol. Biol.* **1998**, *275* (5), 861–872. https://doi.org/10.1006/jmbi.1997.1508.
(88) Huskens, D.; Ferir, G.; Vermeire, K.; Kehr, J. C.; Balzarini, J.; Dittmann, E.; Schols, D. Microvirin, a Novel (1,2)-Mannose-Specific Lectin Isolated from Microcystis Aeruginosa, Has Anti-HIV-1 Activity Comparable with That of Cyanovirin-N but a Much Higher Safety Profile. *J. Biol. Chem.* **2010**, *285* (32), 24845–24854. https://doi.org/10.1074/jbc.M110.128546.
(89) Férir, G.; Vermeire, K.; Huskens, D.; Balzarini, J.; Van Damme, E. J. M.; Kehr, J.C.; Dittmann, E.; Swanson, M. D.; Markovitz, D. M.; Schols, D. Synergistic in Vitro Anti-HIV Type 1 Activity of Tenofovir with Carbohydrate-Binding Agents (CBAs). *Antivir. Res.* **2011**, *90* (3), 200–204. https://doi.org/10.1016/j.antiviral.2011.03.188.
(90) Férir, G.; Huskens, D.; Palmer, K. E.; Boudreaux, D. M.; Swanson, M. D.; Markovitz, D. M.; Balzarini, J.; Schols, D. Combinations of Griffithsin with Other Carbohydrate-Binding Agents Demonstrate Superior Activity Against HIV Type 1, HIV Type 2, and Selected Carbohydrate-Binding Agent-Resistant HIV Type 1 Strains. *AIDS Res. Hum. Retrovir.* **2012**, *28* (11), 1513–1523. https://doi.org/10.1089/aid.2012.0026.
(91) Conceição de Souza, R.; de Medeiros Muniz, G.; Siqueira, A. S.; de Melo Lima, A.; da Silva, A. P.; Gonçalves, E. C.; da Silva Gonçalves Vianez Júnior, J. L. Investigating the Effects of Point Mutations on the Affinity between the Cyanobacterial Lectin Microvirin and High Mannose-Type Glycans Present on the HIV Envelope Glycoprotein. *J. Mol. Model* **2016**, *22* (11), 269. https://doi.org/10.1007/s00894-016-3137-3.
(92) Manivannan, P.; Muralitharan, G. Probing Potent Interfacial Residues in Microvirin before Complexation with Glycoproteins: Visualizing Anti-HIV Activity in Silico. *J. Marine Sci. Res. Dev.* **2017**, *07* (05). https://doi.org/10.4172/2155-9910.1000241.
(93) Parajuli, B.; Acharya, K.; Nangarlia, A.; Zhang, S.; Parajuli, B.; Dick, A.; Ngo, B.; Abrams, C. F.; Chaiken, I. Identification of a Glycan Cluster in Gp120 Essential for Irreversible HIV-1 Lytic Inactivation by a Lectin-Based Recombinantly Engineered Protein Conjugate. *Biochem.* **2020**, *477* (21), 4263–4280. https://doi.org/10.1042/BCJ20200495.
(94) Min, Y.Q.; Duan, X.C.; Zhou, Y.D.; Kulinich, A.; Meng, W.; Cai, Z.P.; Ma, H.Y.; Liu, L.; Zhang, X.L.; Voglmeir, J. Effects of Microvirin Monomers and Oligomers on Hepatitis C Virus. *Biosci. Rep.* **2017**, *37* (3). https://doi.org/10.1042/BSR20170015.
(95) Shahid, M.; Qadir, A.; Yang, J.; Ahmad, I.; Zahid, H.; Mirza, S.; Windisch, M. P.; Shahzad-ul-Hussan, S. An Engineered Microvirin Variant with Identical Structural Domains Potently Inhibits Human Immunodeficiency Virus and Hepatitis C Virus Cellular Entry. *Viruses* **2020**, *12* (2), 199. https://doi.org/10.3390/v12020199.

(96) Driessen, N. N.; Boshoff, H. I. M.; Maaskant, J. J.; Gilissen, S. A. C.; Vink, S.; Sar, A. M. van der; Vandenbroucke-Grauls, C. M. J. E.; Bewley, C. A.; Appelmelk, B. J.; Geurtsen, J. Cyanovirin-N Inhibits Mannose-Dependent Mycobacterium–C-Type Lectin Interactions but Does Not Protect against Murine Tuberculosis. *J. Immunol.* **2012**, *189* (7), 3585–3592. https://doi.org/10.4049/jimmunol.1102408.

(97) Shahzad-Ul-Hussan, S.; Sastry, M.; Lemmin, T.; Soto, C.; Loesgen, S.; Scott, D. A.; Davison, J. R.; Lohith, K.; O'Connor, R.; Kwong, P. D.; Bewley, C. A. Insights from NMR Spectroscopy into the Conformational Properties of Man-9 and Its Recognition by Two HIV Binding Proteins. *Chembiochem.* **2017**, *18* (8), 764–771. https://doi.org/10.1002/cbic.201600665.

(98) Lipman, N. S.; Jackson, L. R.; Trudel, L. J.; Weis-Garcia, F. Monoclonal versus Polyclonal Antibodies: Distinguishing Characteristics, Applications, and Information Resources. *ILAR J.* **2005**, *46* (3), 258–268. https://doi.org/10.1093/ilar.46.3.258.

(99) Glatman-Freedman, A.; Martin, J. M.; Riska, P. F.; Bloom, B. R.; Casedevall, A. Monoclonal Antibodies to Surface Antigens of Mycobacterium Tuberculosis and Their Use in a Modified Enzyme-Linked Immunosorbent Spot Assay for Detection of Mycobacteria. *J. Clin. Microbiol.* **1996**, *34* (11), 2795–2802.

(100) Hamasur, B.; Haile, M.; Pawlowski, A.; Schroder, U.; Kallenius, G.; Svenson, S. B. A Mycobacterial Lipoarabinomannan Specific Monoclonal Antibody and Its F(Ab') Fragment Prolong Survival of Mice Infected with Mycobacterium Tuberculosis. *Clin. Exp. Immunol.* **2004**, *138* (1), 30–38. https://doi.org/10.1111/j.1365-2249.2004.02593.x.

(101) Murase, T.; Zheng, R. B.; Joe, M.; Bai, Y.; Marcus, S. L.; Lowary, T. L.; Ng, K. K. S. Structural Insights into Antibody Recognition of Mycobacterial Polysaccharides. *J. Mol. Biol.* **2009**, *392* (2), 381–392. https://doi.org/10.1016/j.jmb.2009.06.074.

(102) Amin, A. G.; De, P.; Spencer, J. S.; Brennan, P. J.; Daum, J.; Andre, B. G.; Joe, M.; Bai, Y.; Laurentius, L.; Porter, M. D.; Honnen, W. J.; Choudhary, A.; Lowary, T. L.; Pinter, A.; Chatterjee, D. Detection of Lipoarabinomannan in Urine and Serum of HIV-Positive and HIV-Negative TB Suspects Using an Improved Capture-Enzyme Linked Immuno Absorbent Assay and Gas Chromatography/Mass Spectrometry. *Tuberculosis (Edinb)* **2018**, *111*, 178–187. https://doi.org/10.1016/j.tube.2018.06.004.

(103) Kaur, D.; Lowary, T. L.; Vissa, V. D.; Crick, D. C.; Brennan, P. J. Characterization of the Epitope of Anti-Lipoarabinomannan Antibodies as the Terminal Hexaarabinofuranosyl Motif of Mycobacterial Arabinans. *Microbiology (Reading, Engl.)* **2002**, *148* (Pt 10), 3049–3057. https://doi.org/10.1099/00221287-148-10-3049.

(104) Concepcion, J.; Witte, K.; Wartchow, C.; Choo, S.; Yao, D.; Persson, H.; Wei, J.; Li, P.; Heidecker, B.; Ma, W.; Varma, R.; Zhao, L.-S.; Perillat, D.; Carricato, G.; Recknor, M.; Du, K.; Ho, H.; Ellis, T.; Gamez, J.; Howes, M.; Phi-Wilson, J.; Lockard, S.; Zuk, R.; Tan, H. Label-Free Detection of Biomolecular Interactions Using BioLayer Interferometry for Kinetic Characterization. *Comb. Chem. High Throughput Screen.* **2009**, *12* (8), 791–800. https://doi.org/10.2174/138620709789104915.

(105) van der Horst, M.; Karamchand, L.; Bauer, W. S.; Nel, A. J. M.; Blackburn, J. M.; Wright, D. W. The Cyanobacterial Lectin, Microvirin-N, Enhances the Specificity

and Sensitivity of Lipoarabinomannan-Based TB Diagnostic Tests. *Analyst* **2021**, *146* (4), 1207–1215. https://doi.org/10.1039/d0an01725f.
(106) Centers for Disease Control and Prevention. Mycobacterium bovis (Bovine Tuberculosis) in Humans. https://www.cdc.gov/tb/publications/factsheets/general/mbovis.htm (accessed July 15, 2019).
(107) Koniev, O.; Wagner, A. Developments and Recent Advancements in the Field of Endogenous Amino Acid Selective Bond Forming Reactions for Bioconjugation. *Chem. Soc. Rev.* **2015**, *44* (15), 5495–5551. https://doi.org/10.1039/C5CS00048C.
(108) Sabur, N. F.; Esmail, A.; Brar, M. S.; Dheda, K. Diagnosing Tuberculosis in Hospitalized HIV-Infected Individuals Who Cannot Produce Sputum: Is Urine Lipoarabinomannan Testing the Answer? *BMC Infect. Dis.* **2017**, *17*. https://doi.org/10.1186/s12879-017-2914-7.
(109) The Immunoassay Handbook, Fourth Edition; Wild, D., Eds.; Elsevier: 2013.
(110) Hsieh, H. V.; Dantzler, J. L.; Weigl, B. H. Analytical Tools to Improve Optimization Procedures for Lateral Flow Assays. *Diagnostics* **2017**, *7* (2). https://doi.org/10.3390/diagnostics7020029.
(111) Wu, J.; Zhu, J.; Yin, H.; Buckanovich, R. J.; Lubman, D. M. Analysis of Glycan Variation on Glycoproteins from Serum by the Reverse Lectin-Based ELISA Assay. *J. Proteome Res.* **2014**, *13* (4), 2197–2204. https://doi.org/10.1021/pr401061c.
(112) Åström, E.; Stål, P.; Zenlander, R.; Edenvik, P.; Alexandersson, C.; Haglund, M.; Rydén, I.; Påhlsson, P. Reverse Lectin ELISA for Detecting Fucosylated Forms of A1-Acid Glycoprotein Associated with Hepatocellular Carcinoma. *PLoS One* **2017**, *12* (3), e0173897. https://doi.org/10.1371/journal.pone.0173897.
(113) Immunoassay Plate Guide. ThermoFisher.
(114) Damborský, P.; Koczula, K. M.; Gallotta, A.; Katrlík, J. Lectin-Based Lateral Flow Assay: Proof-of-Concept. *Analyst* **2016**, *141* (23), 6444–6448. https://doi.org/10.1039/C6AN01746K.
(115) Markwalter, C. F.; Ricks, K. M.; Bitting, A. L.; Mudenda, L.; Wright, D. W. Simultaneous Capture and Sequential Detection of Two Malarial Biomarkers on Magnetic Microparticles. *Talanta* **2016**, *161*, 443–449. https://doi.org/10.1016/j.talanta.2016.08.078.
(116) MacLean, E.; Pai, M. Urine Lipoarabinomannan for Tuberculosis Diagnosis: Evolution and Prospects. *Clin. Chem.* **2018**, *64* (8), 1133–1135. https://doi.org/10.1373/clinchem.2018.286625.
(117) García, J. I.; Kelley, H. V.; Meléndez, J.; de León, R. A. A.; Castillo, A.; Sidiki, S.; Yusoof, K. A.; Nunes, E.; Téllez, C. L.; Mejía-Villatoro, C. R.; Ikeda, J.; García-Basteiro, A. L.; Wang, S.-H.; Torrelles, J. B. Improved Alere Determine Lipoarabinomannan Antigen Detection Test for the Diagnosis of Human and Bovine Tuberculosis by Manipulating Urine and Milk. *Sci. Rep.* **2019**, *9* (1), 1–6. https://doi.org/10.1038/s41598-019-54537-9.
(118) Alere Determine TB LAM Ag Package Insert. Alere Connected Health Ltd.
(119) Hamasur, B.; Bruchfeld, J.; van Helden, P.; Källenius, G.; Svenson, S. A Sensitive Urinary Lipoarabinomannan Test for Tuberculosis. *PLoS One* **2015**, *10* (4), e0123457. https://doi.org/10.1371/journal.pone.0123457.
(120) Markwalter, C. F.; Corstjens, P. L. A. M.; Mammoser, C. M.; Camps, G.; Dam, G. J. van; Wright, D. W. Poly(Amidoamine)-Coated Magnetic Particles for

Enhanced Detection of Schistosoma Circulating Anodic Antigen in Endemic Urine Samples. *Analyst* **2018**, *144* (1), 212–219. https://doi.org/10.1039/C8AN00941D.
(121) Broger, T.; Nicol, M.; Sigal, G.; Gotuzzo, E.; Zimmer, A. J.; Surtie, S.; Caceres-Nakiche, T.; Mantsoki, A.; Reipold, E. I.; Székely, R.; Tsionsky, M.; Heerden, J. van; Plisova, T.; Chikamatsu, K.; Lowary, T. L.; Pinter, A.; Mitarai, S.; Moreau, E.; Schumacher, S. G.; Denkinger, C. M. Diagnostic Accuracy of Three Urine Lipoarabinomannan Tuberculosis Assays in HIV-Negative Outpatients. *J. Clin. Invest.* **2020**. https://doi.org/10.1172/JCI140461.
(122) Dye, C.; Scheele, S.; >Dolin, P.; Pathania, V.; Raviglione, M. C.; for the WHO Global Surveillance and Monitoring Project. Global Burden of Tuberculosis: Estimated Incidence, Prevalence, and Mortality by Country. *JAMA* **1999**, *282* (7), 677–686. https://doi.org/10.1001/jama.282.7.677.
(123) Fischer, J. E.; Bachmann, L. M.; Jaeschke, R. A Readers' Guide to the Interpretation of Diagnostic Test Properties: Clinical Example of Sepsis. *Intensive Care Med.* **2003**, *29* (7), 1043–1051. https://doi.org/10.1007/s00134-003-1761-8.
(124) Connelly, J. T.; Grant, B.; Munsamy, V.; Pym, A.; Somoskovi, A. Lipoarabinomannan Point-of-Care Tests: Evaluation with Fresh Samples Needed. *Lancet Infect. Dis.* **2019**, *19* (10), 1053. https://doi.org/10.1016/S1473-3099(19)30475-X.
(125) Broger, T.; Muyoyeta, M.; Kerkhoff, A. D.; Denkinger, C. M.; Moreau, E. Tuberculosis Test Results Using Fresh versus Biobanked Urine Samples with FujiLAM. *Lancet Infect. Dis.* **2020**, *20* (1), 22–23. https://doi.org/10.1016/S1473-3099(19)30684-X.
(126) Magni, R.; Rruga, F.; Alsaab, F.; Sharif, S.; Howard, M.; Espina, V.; Kim, B.; Lepene, B.; Lee, G.; Alayouni, M. A.; Steinberg, H.; Araujo, R.; Kashanchi, F.; Riccardi, F.; Morreira, S.; Araujo, A.; Poli, F.; Jaganath, D.; Semitala, F. C.; Worodria, W.; Andama, A.; Choudhary, A.; Honnen, W. J.; Petricoin, E. F.; Cattamanchi, A.; Colombatti, R.; de Waard, J. H.; Oberhelman, R.; Pinter, A.; Gilman, R. H.; Liotta, L. A.; Luchini, A. Lipoarabinomannan Antigenic Epitope Differences in Tuberculosis Disease Subtypes. *Sci. Rep.* **2020**, *10* (1), 13944. https://doi.org/10.1038/s41598-020-70669-9.
(127) Narasimhan, P.; Wood, J.; MacIntyre, C. R.; Mathai, D. Risk Factors for Tuberculosis. *Pulm. Med.* **2013**, *2013*. https://doi.org/10.1155/2013/828939.
(128) Martins-Melo, F. R.; Bezerra, J. M. T.; Barbosa, D. S.; Carneiro, M.; Andrade, K. B.; Ribeiro, A. L. P.; Naghavi, M.; Werneck, G. L. The Burden of Tuberculosis and Attributable Risk Factors in Brazil, 1990–2017: Results from the Global Burden of Disease Study 2017. *Popul. Health Metr.* **2020**, *18* (1), 10. https://doi.org/10.1186/s12963-020-00203-6.
(129) al Daher, S.; de Gasperi, R.; Daniel, P.; Hall, N.; Warren, C. D.; Winchester, B. The Substrate-Specificity of Human Lysosomal Alpha-D-Mannosidase in Relation to Genetic Alpha-Mannosidosis. *Biochem. J.* **1991**, *277 (Pt 3)*, 743–751. https://doi.org/10.1042/bj2770743.
(130) Lal, A.; Pang, P.; Kalelkar, S.; Romero, P. A.; Herscovics, A.; Moremen, K. W. Substrate Specificities of Recombinant Murine Golgi Alpha1, 2-Mannosidases IA and IB and Comparison with Endoplasmic Reticulum and Golgi Processing Alpha1,2-Mannosidases. *Glycobiology* **1998**, *8* (10), 981–995. https://doi.org/10.1093/glycob/8.10.981.

(131) Tremblay, L. O.; Herscovics, A. Characterization of a CDNA Encoding a Novel Human Golgi A1,2-Mannosidase (IC) Involved in N-Glycan Biosynthesis. *J. Biol. Chem.* **2000**, *275* (41), 31655–31660. https://doi.org/10.1074/jbc.M004935200.
(132) Zhou, T.; Frabutt, D. A.; Moremen, K. W.; Zheng, Y.-H. ERManI (Endoplasmic Reticulum Class I α-Mannosidase) Is Required for HIV-1 Envelope Glycoprotein Degradation via Endoplasmic Reticulum-Associated Protein Degradation Pathway. *J. Biol. Chem.* **2015**, *290* (36), 22184–22192. https://doi.org/10.1074/jbc.M115.675207.
(133) Crispin, M.; Aricescu, A. R.; Chang, V. T.; Jones, E. Y.; Stuart, D. I.; Dwek, R. A.; Davis, S. J.; Harvey, D. J. Disruption of α-Mannosidase Processing Induces Non-Canonical Hybrid-Type Glycosylation. *FEBS Letters* **2007**, *581* (10), 1963–1968. https://doi.org/10.1016/j.febslet.2007.04.020.
(134) Jan, M.; Upadhyay, C.; Hioe, C. E. HIV-1 Envelope Glycan Composition as a Key Determinant of Efficient Virus Transmission via DC-SIGN and Resistance to Inhibitory Lectins. *iScience* **2019**, *21*, 413–427. https://doi.org/10.1016/j.isci.2019.10.030.
(135) Sobala, Ł. F.; Fernandes, P. Z.; Hakki, Z.; Thompson, A. J.; Howe, J. D.; Hill, M.; Zitzmann, N.; Davies, S.; Stamataki, Z.; Butters, T. D.; Alonzi, D. S.; Williams, S. J.; Davies, G. J. Structure of Human Endo-α-1,2-Mannosidase (MANEA), an Antiviral Host-Glycosylation Target. *Proc. Natl. Acad. Sci.* **2020**, *117* (47), 29595–29601. https://doi.org/10.1073/pnas.2013620117.
(136) Mkhikian, H.; Grigorian, A.; Li, C. F.; Chen, H.L.; Newton, B.; Zhou, R. W.; Beeton, C.; Torossian, S.; Tatarian, G. G.; Lee, S.U.; Lau, K.; Walker, E.; Siminovitch, K. A.; Chandy, K. G.; Yu, Z.; Dennis, J. W.; Demetriou, M. Genetics and the Environment Converge to Dysregulate N-Glycosylation in Multiple Sclerosis. *Nat. Commun.* **2011**, *2*, 334. https://doi.org/10.1038/ncomms1333.
(137) Tu, H.; Hsiao, Y.C.; Yang, W.Y.; Tsai, S.L.; Lin, H.K.; Liao, C.Y.; Lu, J.W.; Chou, Y.T.; Wang, H.D.; Yuh, C.H. Up-Regulation of Golgi α-Mannosidase IA and down-Regulation of Golgi α-Mannosidase IC Activates Unfolded Protein Response during Hepatocarcinogenesis. *Hepatol. Commun.* **2017**, *1* (3), 230–247. https://doi.org/10.1002/hep4.1032.
(138) Legler, K.; Rosprim, R.; Karius, T.; Eylmann, K.; Rossberg, M.; Wirtz, R. M.; Müller, V.; Witzel, I.; Schmalfeldt, B.; Milde-Langosch, K.; Oliveira-Ferrer, L. Reduced Mannosidase MAN1A1 Expression Leads to Aberrant N-Glycosylation and Impaired Survival in Breast Cancer. *Br. J. Cancer* **2018**, *118* (6), 847–856. https://doi.org/10.1038/bjc.2017.472.
(139) Goi, G.; Lombardo, A.; Fabi, A.; Burlina, A. B.; Segalini, G.; Guagnellini, E.; Tettamanti, G. Serum Enzymes of Lysosomal Origin as Indicators of the Metabolic Control in Non-Insulin-Dependent Diabetics. *Acta Diabetol. Lat/* **1987**, *24* (4), 331–340. https://doi.org/10.1007/BF02742966.
(140) Waters, P. J.; Flynn, M. D.; Corrall, R. J.; Pennock, C. A. Increases in Plasma Lysosomal Enzymes in Type 1 (Insulin-Dependent) Diabetes Mellitus: Relationship to Diabetic Complications and Glycaemic Control. *Diabetologia* **1992**, *35* (10), 991–995. https://doi.org/10.1007/BF00401431.
(141) Harries, A. D.; Satyanarayana, S.; Kumar, A. M. V.; Nagaraja, S. B.; Isaakidis, P.; Malhotra, S.; Achanta, S.; Naik, B.; Wilson, N.; Zachariah, R.; Lönnroth, K.; Kapur, A. Epidemiology and Interaction of Diabetes Mellitus and Tuberculosis and Challenges for Care: A Review. *Public Health Action* **2013**, *3* (1), 3–9. https://doi.org/10.5588/pha.13.0024.

(142) Lin, X.; Xu, Y.; Pan, X.; Xu, J.; Ding, Y.; Sun, X.; Song, X.; Ren, Y.; Shan, P.-F. Global, Regional, and National Burden and Trend of Diabetes in 195 Countries and Territories: An Analysis from 1990 to 2025. *Sci. Rep.* **2020**, *10* (1), 14790. https://doi.org/10.1038/s41598-020-71908-9.
(143) Wiens, K. E.; Woyczynski, L. P.; Ledesma, J. R.; Ross, J. M.; Zenteno-Cuevas, R.; Goodridge, A.; Ullah, I.; Mathema, B.; Djoba Siawaya, J. F.; Biehl, M. H.; Ray, S. E.; Bhattacharjee, N. V.; Henry, N. J.; Reiner, R. C.; Kyu, H. H.; Murray, C. J. L.; Hay, S. I. Global Variation in Bacterial Strains That Cause Tuberculosis Disease: A Systematic Review and Meta-Analysis. *BMC Med.* **2018**, *16* (1), 196. https://doi.org/10.1186/s12916-018-1180-x.
(144) Moore, C. P., Pieterson, K. P., DeSousa, J. M. Gibson, L. E., Wright, D. W. Characterization and utility of immobilized metal affinity-functionalized cellulose membranes for point-of-care malaria diagnostics. In preparation for submission to *J. Chromatog. B.* Expected publication date: August 2021.
(145) Lowary, T. L. Twenty Years of Mycobacterial Glycans: Furanosides and Beyond. *Accounts of Chemical Research* **2016**, *49* (7), 1379–1388. https://doi.org/10.1021/acs.accounts.6b00164.
(146) Rosner, B. *Fundamentals of Biostatistics*, 8th ed.; Cengage Learning: U.S., 2015.
(147) Peter, J. G.; Cashmore, T. J.; Meldau, R.; Theron, G.; van Zyl-Smit, R.; Dheda, K. Diagnostic Accuracy of Induced Sputum LAM ELISA for Tuberculosis Diagnosis in Sputum-Scarce Patients. *Int. J. Tuberc. Lung Dis.* **2012**, *16* (8), 1108–1112. https://doi.org/10.5588/ijtld.11.0614.
(148) Wilson, S.; Lane, A.; Rosedale, R.; Stanley, C. Concentration of Mycobacterium Tuberculosis from Sputum Using Ligand-Coated Magnetic Beads. *Int. J. Tuberc. Lung Dis.* **2010**, *14* (9), 1164–1168.
(149) Lawn, S. D.; Mwaba, P.; Bates, M.; Piatek, A.; Alexander, H.; Marais, B. J.; Cuevas, L. E.; McHugh, T. D.; Zijenah, L.; Kapata, N.; Abubakar, I.; McNerney, R.; Hoelscher, M.; Memish, Z. A.; Migliori, G. B.; Kim, P.; Maeurer, M.; Schito, M.; Zumla, A. Advances in Tuberculosis Diagnostics: The Xpert MTB/RIF Assay and Future Prospects for a Point-of-Care Test. *Lancet Infect. Dis.* **2013**, *13* (4), 349–361. https://doi.org/10.1016/S1473-3099(13)70008-2.
(150) World Health Organization. WHO Treatment Guidelines for Drug-Resistant Tuberculosis: 2016 Update. World Health Organization: Geneva, 2016.
(151) Musser, J. M. Antimicrobial Agent Resistance in Mycobacteria: Molecular Genetic Insights. *Clin. Microbiol. Rev.* **1995**, *8* (4), 496–514. https://doi.org/10.1128/CMR.8.4.496-514.1995.
(152) El-Hajj, H. H.; Marras, S. A. E.; Tyagi, S.; Kramer, F. R.; Alland, D. Detection of Rifampin Resistance InMycobacterium Tuberculosis in a Single Tube with Molecular Beacons. *J. Clin. Microbiol.* **2001**, *39* (11), 4131–4137. https://doi.org/10.1128/JCM.39.11.4131-4137.2001.
(153) Kaur, R.; Kachroo, K.; Sharma, J. K.; Vatturi, S. M.; Dang, A. Diagnostic Accuracy of Xpert Test in Tuberculosis Detection: A Systematic Review and Meta-Analysis. *J. Glob. Infect. Dis.* **2016**, *8* (1), 32–40. https://doi.org/10.4103/0974-777X.176143.
(154) Landegren, U.; Kaiser, R.; Sanders, J.; Hood, L. A Ligase-Mediated Gene Detection Technique. *Science* **1988**, *241* (4869), 1077–1080. https://doi.org/10.1126/science.3413476.
(155) Zaw, M. T.; Emran, N. A.; Lin, Z. Mutations inside Rifampicin-Resistance Determining Region of RpoB Gene Associated with Rifampicin-Resistance in

Mycobacterium Tuberculosis. *J. Infect. Public Health* **2018**, *11* (5), 605–610. https://doi.org/10.1016/j.jiph.2018.04.005.
(156) Hoshide, M.; Qian, L.; Rodrigues, C.; Warren, R.; Victor, T.; Evasco, H. B.; Tupasi, T.; Crudu, V.; Douglas, J. T. Geographical Differences Associated with Single-Nucleotide Polymorphisms (SNPs) in Nine Gene Targets among Resistant Clinical Isolates of Mycobacterium Tuberculosis. *J. Clin. Microbiol.* **2014**, *52* (5), 1322–1329. https://doi.org/10.1128/JCM.00857-13.
(157) Panpradist, N.; Beck, I. A.; Chung, M. H.; Kiarie, J. N.; Frenkel, L. M.; Lutz, B. R. Simplified Paper Format for Detecting HIV Drug Resistance in Clinical Specimens by Oligonucleotide Ligation. *PLoS One* **2016**, *11* (1), e0145962. https://doi.org/10.1371/journal.pone.0145962.
(158) Ma, Q.; Liu, H.; Ye, F.; Xiang, G.; Shan, W.; Xing, W. Rapid and Visual Detection of Mycobacterium Tuberculosis Complex Using Recombinase Polymerase Amplification Combined with Lateral Flow Strips. *Mol. Cell. Probes*. https://doi.org/10.1016/j.mcp.2017.08.004.